Trinity College Dublin
Coláiste na Tríonóide, Baile Átha Cliath
The University of Dublin

Characterising the progression of haemophilic arthropathy in knee joints of a novel mouse model of severe haemophilia A

This thesis is submitted to Trinity College Dublin, University of Dublin, as requirement for the degree of Doctor in Philosophy (PhD) in Clinical Medicine

2024

Aoife Yeow B.A. (Hons)

Under the supervision and direction of

Professor Padraic Fallon

School of Medicine

Declaration of Authorship

I declare that this thesis has not been submitted as an exercise for a degree at this or any other university and it is entirely my own work.

I agree to allow the Library to do so on my behalf, subject to Irish Copyright Legislation and Trinity College Library conditions of use and acknowledgement.

I do not consent to the examiner retaining a copy of the thesis beyond the examining period, should they so wish (EU GDPR May 2018).

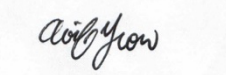

Aoife Yeow

Acknowledgements

Firstly, I would like to thank my supervisor, Professor Padraic Fallon, for his continued support, mentoring, and guidance. The past few years have had many challenges come our way, but your leadership has been at the forefront of everything, guiding myself and other lab members alike. Thank you for all the time you have put in and this thesis would not have been possible without your support.

I would like to thank my lab colleagues, both past and present, but particularly Heike Hawerkamp, Anne Chevalier, Laura Matarazzo, Emily Hams, Keelin O'Shanahan, Silvia Talavera, Niamh O'Dowd, and Neha Patil. A specific big thank you to Joseph Roberts and Ciara Byrne whom without their constant encouragement and support I would not have had such an enjoyable experience and whom have had a big impact on both my PhD and this part of my life. I'm forever grateful for all the lab members for being there for me.

Thank you to Science Foundation Ireland, without this support my PhD would not have been possible, and the Irish Personalised Approach to the Treatment of Haemophilia (iPATH) programme and all the colleagues working in this programme as well, who I've had the pleasure to meet and work alongside with during my time.

To my kind and supportive partner, Matas, I cannot thank you enough. The time during my PhD, both the good and the bad, has been made that much brighter with your love and support and I look forward to our future together.

Finally, thank you to my family. My mum, Alison, and dad, Ricky, who have supported me my entire life but especially more these past five years. For being patient and kind with me through all the hard times and supporting all my choices. And of course, my dearest sister, Ivana, whom I look up to in life for almost everything. Your guidance from your own PhD experience has helped me immensely but moreover, your love and support, even from afar, has carried me through all the hard and long days I have had. Thank you for everything you do for me.

Summary

Haemophilia A is an X-linked blood clotting disorder, where clotting factor, Factor VIII, is unable to induce the coagulation cascade. Thus, the lack of this clotting factor prevents efficient clotting of blood during injuries such as open wounds. While treatable with a number of methods, most commonly with clotting factor replacement, patients with severe haemophilia A can develop a plethora of co-morbidities, including osteoporosis, inhibitor development, and haemarthrosis. With haemophilia A subdivided into varying severities, mild, moderate, and severe, the probability of comorbidities also varies with that. The development of haemophilic arthropathy is a natural occurrence that normally coincides with bleeds into the joint in patients with severe haemophilia A. The increased instances of haemarthrosis can lead to joint deformation and a reduced quality of life for patients affected by this. However, the development of the joint disease is dependent on several factors, of which are yet to be fully elucidated. While there have been strides made in the investigations of immunological impact in haemophilic arthropathy, there has yet to be a clearly established number of specific genes that may predispose one to the development of haemophilic arthropathy. Adolescence, including adolescence leading into adulthood, is a crucial time for bone development and while treatments for haemophilia have developed significantly, chronic arthropathy is still of concern for patients with severe haemophilia A.

Investigating required a model of haemophilic arthropathy to first be established in the lab. The creation of a novel mouse model of severe haemophilia A, that exhibited similar characteristics such as spontaneous bleeding, by a previous lab member allowed me to establish a working model of haemophilia arthropathy in the lab and identify several genes involved in the development and progression of the disease. As expected, post-injury induction altered the expression of pro-inflammatory genes dramatically as immune cells were recruited to the site of injury, such as *Tnf*, *Il1β*, and *Il6*, suggesting perhaps a potential osteoclastogenic mechanism by which a key feature in haemophilic arthropathy, osteoporosis, may develop during haemarthrosis. With multiple bleeds overtime, the increased risk of developing osteoporosis may lead to other negative impacts on quality of life like increased risk of bone fractures.

Concretely identifying genes involved in the development of haemophilic arthropathy, I used dual-knockout mice to my advantage to further elucidate the roles of a number of upregulated genes found during the progression of haemophilic arthropathy. While some had no notable effects on the development and progression of haemophilic arthropathy, there was some significance specifically in the *F8*$^{em1-/-}$/*Il1rl1*$^{-/-}$ mouse model, where the severity as seen by measuring the size of the joint, was greatly reduced. A significant difference was also seen in patient plasma samples, where levels of soluble ST2 protein were significantly elevated in comparison to healthy plasma control samples as well. As previously mentioned, specific cytokines are known to be inducers of osteoclastogenesis, while some, like IL-33, act as alarmins and inhibit osteoclastogenesis. With the finding that the IL-33/ST2 axis may be involved in the development and progression of haemophilic arthropathy, this axis could potentially be a useful starting point for the development of or use of therapeutics to attenuate haemophilic arthropathy development.

Similarly, while specific pro-/anti-inflammatory genes have been identified as crucial in the process of haemophilic arthropathy, the effects of genetic background have proven to yield significant results in our novel mouse model of severe haemophilia A. Two other strains of mice aside from the C57BL/6J mice were used, BALB/c and A/J, with the exact same single nucleotide polymorphism in exon 1 of the *F8* gene that created the model of severe haemophilia A, thus allowing investigations between the effect of varied genetic backgrounds. There was no notable difference between the C57BL/6J strain and the A/J strain. However, the mice on the BALB/c background had significantly lower joint measurements throughout the time course of the experiment. Studies have shown one major difference between the C57BL/6J and BALB/c strains, and that is the adaptive immune response, particularly the Th1 and Th2 responses. Th1 in C57BL/6J mice plays a key role in the immune response, whereas Th2 plays a more vital role in BALB/c mice. Again, referring back to the development of haemophilic arthropathy, there is evidence that the IL-33/ST2 axis may play a key element in the development of haemophilia arthropathy, with IL-33 enhancing Th2 cell cytokine production and thus, having a more anti-osteoclastogenic effect.

The findings in this thesis have proven that there may be a potential role of the IL-33-ST2 axis in the development and progression in haemophilic arthropathy. By exploiting this knowledge, therapeutic interventions may potentially be used alongside replacement of coagulation factors in order to attenuate the effects of haemarthroses. Thus, potentially preventing development and/or progression of haemophilic arthropathy.

Publications

Bone R, Fennell, BJ, Tam A, Sheldon R, Nocka, K, Varghese S, Chang CS, Hawerkamp HC, **Yeow A**, Saunders SP, Hams E, Walsh PT, Cunningham O and Fallon PG (2022). Discovery and multi-parametric optimization of a high-affinity antibody against interleukin-25 with neutralizing activity in a mouse model of skin inflammation. *Antib Ther.* 5(4):258-267. doi: 10.1093/abt/tbac022.

List of abbreviations used

APC	Antigen presenting cell
aPTT	Activated partial thromboplastin time
AUC	Area under the curve
BSA	Bovine serum albumin
CAIA	Collagen antibody-induced arthritis
CD	Cluster of differentiation
cDNA	Complimentary deoxyribonucleic acid
CIA	Collagen-induced arthritis
CLP	Common lymphoid progenitor
CMP	Common myeloid progenitor
COX-2	Cyclooxygenase-2
CRISPR/Cas9	Clustered regularly interspaced short palindromic repeats/CRISPR-associated protein 9
DAMP	Damage associated molecular pattern
DMARD	Disease-modifying antirheumatic drug
DNA	Deoxyribonucleic acid
dNTPs	Deoxynucleoside triphosphates
DPX	Dibutylphthalate polystyrene xylene
EDTA	Ethylenediaminetetraacetic acid
ELISA	Enzyme-linked immunosorbent assay
ES	Embryonic stem
FACS	Fluorescence-activated cell sorting
FSC	Forward scatter
FVIII	Factor VIII protein
gDNA	Genomic deoxyribonucleic acid
GMP	Granulocyte/macrophage progenitor
H&E	Haematoxylin and eosin
HA	Haemophilic arthropathy
Hemi	Hemizygous
Het	Heterozygous
HJHS	Haemophilia joint health score

Hom	Homozygous
HPRA	Health Products and Regulatory Authority
HRP	Horse radish peroxidase
IMS	Industrial methylated spirits
iPATH	Irish Personalised Approach to the Treatment of Haemophilia
IVCs	Individually ventilated cages
LCN-2	Lipocalin-2
mCT	Micro-computed tomography
mgHA	Magnesium-hydroxyapatite
MHC	Major histocompatibility complex
mRNA	Messenger ribonucleic acid
MSD	Meso scale discovery
OA	Osteoarthritis
PAMP	Pathogen associated molecular pattern
PBS	Phosphate buffered saline
PBST	Phosphate buffered saline-Tween 20
PCR	Polymerase chain reaction
PwH	People with haemophilia
PwsH	People with severe haemophilia
RA	Rheumatoid arthritis
RNA	Ribonucleic acid
RPMI	Roswell Park Memorial Institute medium
RT	Reverse transcriptase
RT-qPCR	Quantitative reverse transcription polymerase chain reaction
SD	Standard deviation
SEM	Standard error of margin
SPF	Specific pathogen free
SSC	Side scatter
TBE	Tris borate ethylenediaminetetraacetic acid
TF	Tissue factor
Th	Helper T
Treg	Regulatory T
vWF	Von Willebrand factor
WT	Wildtype

Table of Contents

Chapter 1 – Introduction

1.1. The Immune System

The immune system is at the forefront of the fight of foreign substances within our body. The highly adaptive system comprises of a balance between organs, cells, and cytokines working together to form such a sensitive system. This defence mechanism is highly specified to prevent a host of agents from entering the body, as well as maintaining a delicate balance within the body itself. However, should this homeostasis be broken, and the scales tipped to one side, too long anti-inflammatory could lead to the development of tumours, while too long pro-inflammatory can lead to autoimmune diseases. Thus, the fine balance of the immune system must be maintained to prevent it becoming too anti-inflammatory or too pro-inflammatory.

1.1.1. Cells of the Immune system

The cells of the immune system can be roughly divided into two systems, the innate immune system, comprising of cells derived from a common myeloid progenitor (CMP) cell, and the adaptive immune system, comprising of cells derived from a common lymphoid progenitor (CLP) cell, as seen in Figure 1.1.

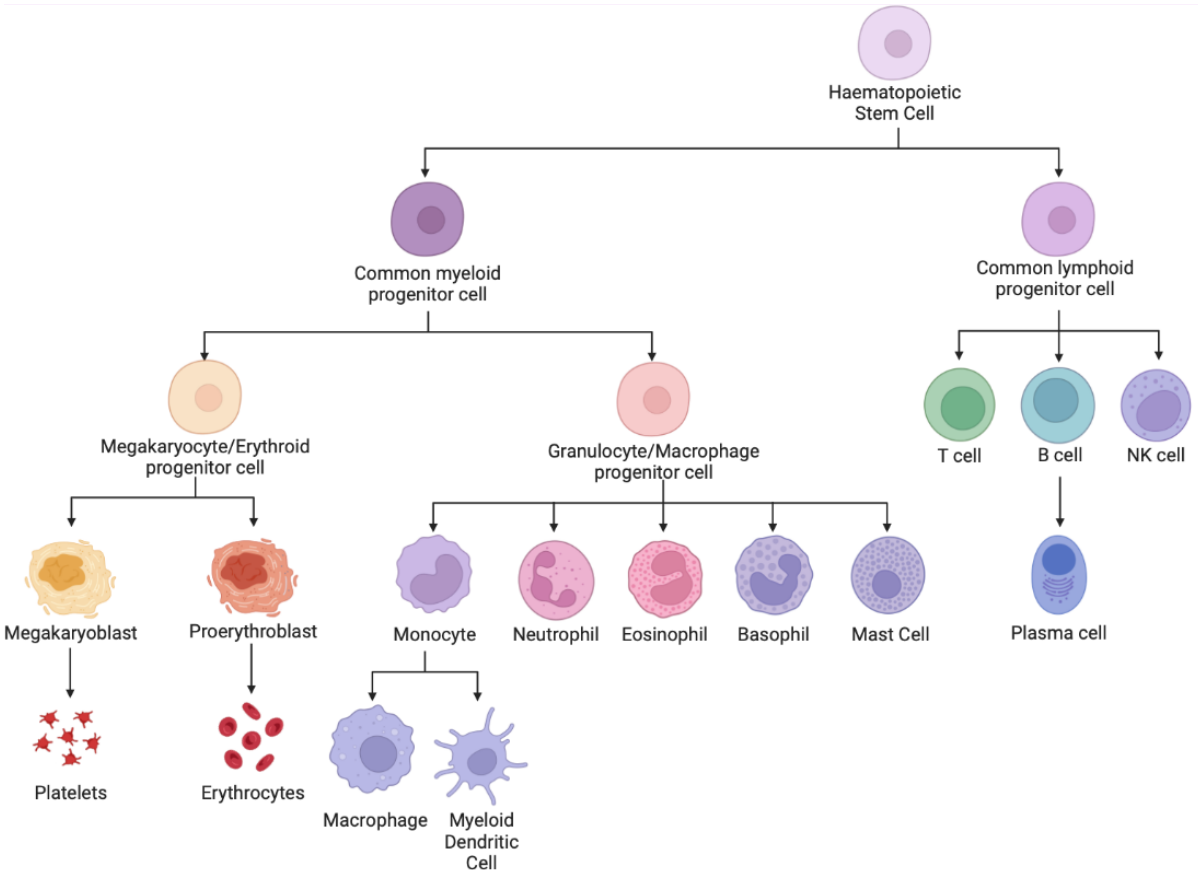

Figure 1.1. General hierarchal depiction of cells of the immune system. Each immune cell is derived from the haematopoietic stem cell and roughly falls into one of two categories: myeloid cells or lymphoid cells. Figure created in Biorender and adapted from (Torang et al., 2019).

1.1.2. The innate immune system

The innate immune system is known to be the first line of defence in the immune system and responds to pathogen associated molecular patterns (PAMPs) and damage associated molecular patterns (DAMPs). The cell responses are general and not specific, including cellular and humoral responses. The cellular response includes the innate immune cells, macrophages, dendritic cells, neutrophils, eosinophils, basophils, and mast cells. While the humoral response includes natural antibodies, complement proteins, C-reactive proteins, and coagulation factors. Here I will briefly cover only a handful of innate immune cells stemming from the CMP cell.

1.1.2.1. Monocytes – Macrophages

Macrophages are derived from monocytes stemming from granulocyte/macrophage progenitor (GMP) cells. They are antigen presenting cells (APCs) that work as the first line of defence against PAMPs and DAMPs, but also serve as a "link" between the innate and adaptive immune systems. While these innate immune cells can act as APCs, they also phagocytose pathogens and apoptotic cells, as well as recruit other immune cells through secretion of cytokines and chemokines. While not further characterised in Figure 1.1, macrophages have historically been subdivided into two phenotypes: M1 macrophages and M2 macrophages (Wynn et al., 2013). These two phenotypes are also known as "classically activated" and "alternatively activated", respectively. M1 "classically activated" macrophages are, generally, functionally more pro-inflammatory compared to M2 macrophages. Thus, they have a critical role in the immune response in eliminating pathogens and certain cells (e.g., cells infected with viruses). M2 "alternatively activated" macrophages are, generally, functionally more anti-inflammatory compared to M1 macrophages. Thus, rather than having a vital role in eliminating pathogens and virus-infected cells, the M2 macrophages tend towards promotion of tissue repair and wound healing. These alternatively activated macrophages play an important role in type 2 immune responses in allergy disease, asthma, and helminth infections (Joseph et al., 2019). In the context of this thesis, M1 macrophages have shown to be increased during the first week post-joint bleeding in FVIII-deficient mice. This was then followed by an increase in M2 macrophages, approximately from the second week onwards post-joint bleeding. The polarisation of macrophages contributes to the clearance of the blood in the joint. M1 macrophages produce pro-inflammatory cytokines, including IL-1b, TNFa, IL-6, that stimulate catabolic activity and hydrogen peroxide production by cartilage chondrocytes, which leads to cartilage destruction and poor elimination of iron from the joint (Nieuwenhuizen et al., 2014, Roosendaal et al., 1998b). M2 macrophages, with its secretion of growth factors colony stimulating factor and vascular endothelial growth factor, in the joint can lead to higher vascularisation and remodelling in the joint space (Cooke et al., 2018).

1.1.2.2. Neutrophils

Neutrophils are one of the many granulocytes forming part of the innate immune system. These innate immune cells comprise of approximately 50 – 70% of circulating leukocytes in humans, but only 10 – 25% in mice (Mestas and Hughes, 2004). Neutrophils are also derived from GMP cells and the primary function of these innate immune cells involves the recognition, phagocytosis, and elimination of invading microbe, but can also act as a link between the innate and adaptive immune system (Rosales, 2020). These cells can be identified morphologically by the lobed nucleus and by the expression of CD11b and Ly6G surface markers (Misharin et al., 2013). Circulating neutrophils are attracted to a site of infection or injury from cytokines and chemokines released during damaged tissues or activated immune cells, including TNFa, IL-1b, IL-6, and IL-8 (Rosales, 2018). Once at the sight of infection or injury, neutrophils can rapidly migrate into the tissue and begin to phagocytose the invading microbes, as well as recruiting other granulocytes, monocytes, and T cells. While having only a short half-life of 6 – 8 hours, neutrophils can still damage healthy tissues at the site of recruitment, which occurs in various inflammatory diseases like rheumatoid arthritis and inflammatory bowel disease (Summers et al., 2010, Zhang et al., 2019). With many commonalities between rheumatoid arthritis and haemophilic arthropathy, another is the increased presence of neutrophil extracellular traps in the promotion of joint destruction in both diseases (Kaminski et al., 2020, O'Neil et al., 2023).

1.1.2.3. Eosinophils

Similar to neutrophils, eosinophils are also granulocytes derived from GMP cells. They are effector cells and heavily involved in the type 2 immune response, as well as providing protection against viruses and bacteria. The innate immune cells are well characterised by the presence of large, granular structures in their cytoplasm, and identifiable by the expression of CD11b, F4/80, and SiglecF in mice (Misharin et al., 2013). While primarily involved in defence against parasitic infections, eosinophils are also involved in the immune response to allergies and asthma, potentially exacerbating the response in these diseases (Nakagome and Nagata, 2018, Fulkerson and Rothenberg, 2013). On top of this, eosinophils also play a role in the regulation of the antibody response (Jacobsen et al., 2012). Immunoregulations by

eosinophils as an APC for B cells and through cytokine secretion for T cells (Akuthota et al., 2008, Wechsler et al., 2021).

1.1.3. The adaptive immune system

While we have the innate immune system that acts as a first line of defence, the adaptive immune system is more specific in its response. In juxtaposition to the innate immune system, the adaptive immune system is pathogen-specific and relies on B and T lymphocytes that are antigen specific. The specificity from the adaptive immune system is dependent on APCs, for example macrophages. Unlike the innate immune system that acts immediately, the adaptive immune response requires several days to respond effectively to a primary infection. This is due to the APCs digesting pathogens, presenting the major histocompatibility complex (MHC) to the naïve T cells to activate and expand them. Antibodies from B cells can be membrane bound and secreted antibodies. Similar to the innate immune response, the adaptive immune response can be generally categorised into a cellular response, T cells, and a humoral response, B cells. Here I will only cover two of the cells stemming from the CLP cell.

1.1.3.1. B cells

B cells, or B lymphocytes, play a crucial role in the humoral response of the adaptive immune system. B cells are responsible for producing antibodies, which can then identify and bind to specific antigens, such as bacteria or viruses. Originating from the bone marrow, B lymphocytes migrate to the lymph nodes and other lymphoid tissues, where they mature and exposure from APCs and T cells allow the B lymphocytes to activate. Once activated, B cells undergo clonal expansion, where the lymphocytes rapidly divide and differentiate into plasma cells, thus producing a large number of antibodies specific to the antigen that initiated the response. B cells may also develop into memory B cells, remaining in the body after the initial immune response. Thus, a large amount of antibodies can be produced upon subsequent exposure to the same antigen, allowing a more rapid response (Clark and Ledbetter, 1989, Tanaka and Baba, 2020). In haemophilia A mouse models, anti-B cell activating factor, along with anti-CD20, has been shown to help improve the levels of inhibitors in patients with haemophilia A (Doshi et al., 2021). Targeting B cell differentiation could be key in

ensuring that all patients are able to receive factor treatment without complications. Without the treatment, patients are highly susceptible to a lot more complications.

1.1.3.2. T cells

T cells, or T lymphocytes, are also produced in the bone marrow but mature specifically in the thymus gland. These cells can be classified into two main subtypes based on specific surface proteins: $CD4^+$ T cells and $CD8^+$ T cells. $CD4^+$ T cells, or T helper (Th) cells, recognise and bind to foreign antigens presented by APCs. Subsequently, cytokine release from the $CD4^+$ T cells from the binding of surface receptors leads to the activation of other immune cells, such as B cells and $CD8^+$ T cells. $CD8^+$ T cells, also known as cytotoxic T cells, directly eliminate infected cells. Additionally, T cells also play a role in regulating immune responses. Regulatory T cells (Tregs) are a specific subset of $CD4^+$ T cells that suppress immune responses and prevent autoimmunity. This role is particularly important to prevent illnesses like overactive immune systems that may lead to autoimmunity. In arthropathies, T cells have been confirmed to play a role in the early stages of long-term pathology post-injury as well as infiltrating into the joint space during synovitis (Moradi et al., 2019, Tran et al., 2005). Thus, T cells could play a key role in the pathology of other joint diseases as well.

1.2. Haemophilia A

1.2.1. Background

Haemophilia A is an X-linked blood clotting disorder that affects mostly males. With haemophilia A, Factor VIII (FVIII) clotting factor is unable to induce the coagulation cascade, thus preventing efficient blood clotting and leading to a prolonged activated partial thromboplastin time (aPTT) (Mannucci and Tuddenham, 2001, Kitchens, 2005). The predominantly male-affected disorder, due to the X-linked recessive disease, affects approximately 1 in 5,000 male births (Iorio et al., 2019). The disease can be classified into three categories based on the FVIII activity; mild, moderate, and severe (Coppola et al., 2010, Knobe and Berntorp, 2011). As seen in the coagulation cascade in Figure 1.2, FVIII is required as a cofactor in the intrinsic pathway to activate Factor X (tenase) to form a fibrin clot as part of the common pathway (Smith et al., 2015). Without the ability to efficiently form a clot, patients with severe haemophilia (PwsH)

are at a much higher risk of bleeding into the skin or soft tissues like muscle, haemarthrosis, or bleeding into the joints, frequent nosebleeds, and in extreme cases death due to excessive bleeding (Konkle and Nakaya Fletcher, 1993, Berntorp et al., 2021). There are a number of treatments available to people with haemophilia (PwH) that have different dosages and treatment regimens, but overall improve the quality of life for PwH (Blumberg et al., 2018, Bhardwaj et al., 2018, Castaldo et al., 2007). However, even with treatments being used, breakthrough bleeds may still occur (Gruppo et al., 2004, Tiede et al., 2021).

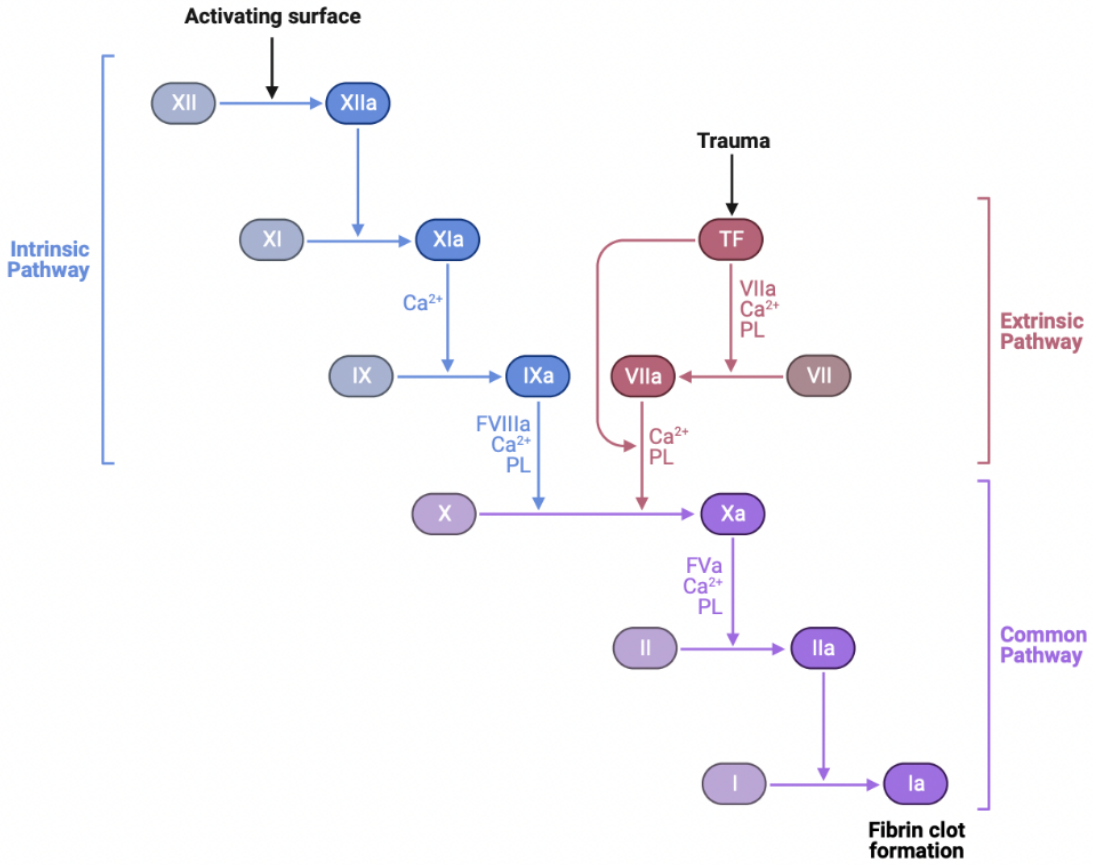

Figure 1.2. Coagulation cascade showing the intrinsic and extrinsic pathways as well as the common pathway to form a fibrin clot formation. Factor VIII is required as a cofactor in the intrinsic pathway to activate the common pathway, to eventually lead to a fibrin clot formation. Figure created in Biorender and adapted from (Perez-Pujol et al., 2012).

1.2.2. Severities of Haemophilia A

While haemophilia A is classified as the lack of or decrease in clotting factor FVIII, it can be further subdivided into three general categories. Firstly, patients with mild haemophilia A have a FVIII activity ranging from 5% to 40%. No spontaneous bleeding occurs in these individuals however, during certain circumstances, such as surgery, excessive bleeding may occur if no pre- or post-treatment is considered. Diagnosis of mild haemophilia A is generally only later in life. Moderate haemophilia A is classified as FVIII activity between 1% and 5%. While spontaneous bleeding can occur in these individuals, it is not common and varies from individual to individual. Frequency of bleeding occurs more often than in mild haemophilia A, with bleeds occurring between approximately once a month to once a year. Diagnosis of moderate haemophilia A generally occurs before the ages of five to six years. Severe haemophilia is categorised as individuals with less than 1% FVIII activity. Diagnosis is usually made in the first two years of life. The jump from moderate to severe is quite drastic with lack of treatment leading to up to two to five spontaneous bleeding incidences monthly. These bleeding episodes can occur anywhere including into the joint or as deep-muscle haematomas (Konkle and Nakaya Fletcher, 1993, Coppola et al., 2010, Bolton-Maggs and Pasi, 2003).

1.2.3. Comorbidities

In haemophilia A, particularly severe haemophilia A, the risk of bleeding is very high but there are also other risk factors associated with haemophilia A. Bleeding into joints, or haemarthrosis, can lead to chronic haemophilic arthropathy as the number of bleeds and frequency of the bleeds increases. Other risk factors related to haemophilia A include low bone mineral density, which increases the risk of bone fractures, intracranial haemorrhage, which increases the risk of stroke amongst other symptoms, and reduced mobility, dexterity, and acuity, overall reducing the quality of life of the individual (Kempton et al., 2021, Chu et al., 2018). Prophylactic treatment may be preferred to on demand factor replacement, however, while it does improve quality of life, this does not completely ameliorate the number of bleeds into joints (Aledort et al., 1994, Bhardwaj et al., 2018, Mejia-Carvajal et al., 2008, Rehill et al., 2021). Research has also shown potential negative effects in terms of haemarthrosis in plasma-derived

FVIII compared to recombinant products (Bertling et al., 2017). Thus, further research is needed to elucidate the exact mechanisms of this comorbidity.

1.3. The Knee Joint

The knee joint is the largest joint in the body (Gupton et al., 2023). The knee joint is made up of three bones for the articular joint: the femur, the fibula, and the tibia. Within the knee structure, as seen in Figure 1.3, resides the all-important synovial capsule, a space within the joint that fills with synovial fluid and provides important components such as hyaluronan, lubricin, and collagenases, surrounded by the synovium (Seidman and Limaiem, 2023). The knee joint can become a target joint in PwsH, as identified by the individual's healthcare professional, but usually when more than three bleeds have occurred within a six-month period (Mulder and Llinas, 2004, Kiialainen et al., 2022). The knee is susceptible to development of arthritis in not only PwsH, but in patients that have mechanical changes or trauma, are overweight, as well as those that have developed age-related cartilage degradation (Sinusas, 2012). With increasing severity and unresponsiveness to drug treatments, patients may turn to alternatives such as total knee replacement, where suitable, to restore the normal functions of the knee joint (Vaienti et al., 2017). Within the knee joint, the synovial membrane (synovium) can become a major target during arthritis in the knee, making it an ideal tissue to analyse in research to elucidate the pathways of the arthritic disease (Van Landuyt et al., 2010). The bone structure of the knee joint, namely bone erosion and cartilage degradation, may also be affected due to osteoclastogenesis as previous research has shown (Pettit et al., 2001).

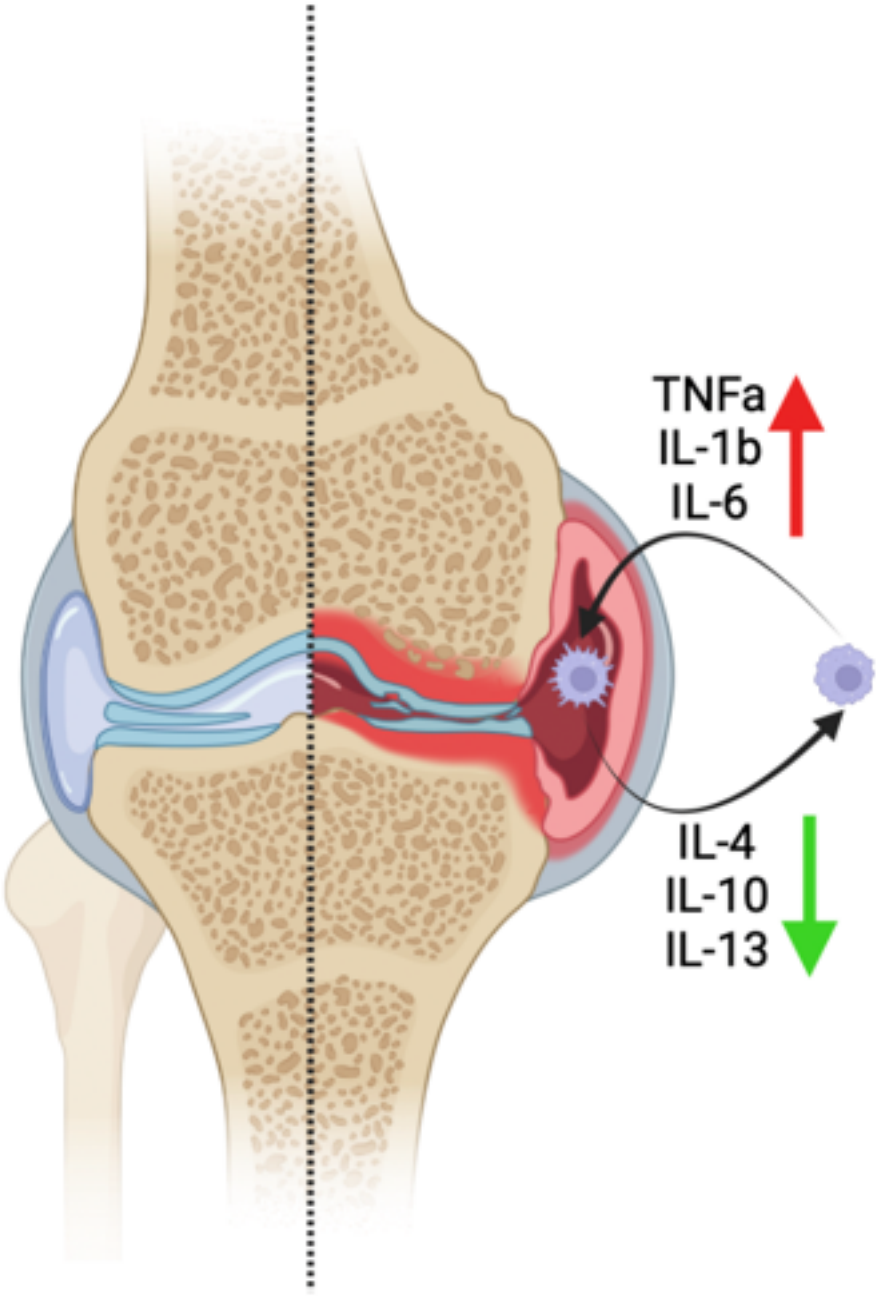

Figure 1.3. The knee joint in both steady state condition and during arthropathy. The knee joint is usually in a steady state (left side of the figure) where there is a delicate balance in the involvement of immune cells as well as any cells, such as osteoclasts and osteoblasts, involved in maintaining bone structure. The right side of the photo depicts the knee joint in an inflamed state during arthropathy, with increased cell activation in what is usually only filled with synovial fluid. Some known cytokines involved in the pathogenesis of arthropathy are listed as well. Figure created in Biorender and adapted from (Berntorp et al., 2021).

1.3.1. The synovial capsule

Within the synovial capsule, the synovial fluid is contained by fibroblast like synoviocytes. The synovium covers the intra-articular tendons and ligaments as well as the fat pads, but not the cartilage or meniscus (Veale and Firestein, 2017). While formed of non-immune cells, the synovium is vital in the production of necessary components for the healthy functioning of the joint, including hyaluronan, lubricin, and collagenases, amongst other components (Seidman and Limaiem, 2023). However, dysregulation of this sterile environment in the joint can cause a number of issues to the joint, as seen in Figure 1.4 (Muirden and Senator, 1968, Sculco, 1998, Lee and Weinblatt, 2001, Scott et al., 2010, Kapoor et al., 2011).

1.3.2. Diseases associated with (knee) joints

1.3.2.1. Osteoarthritis

Osteoarthritis (OA) is a degenerative bone disease that affects the joint cartilage and the underlying bone below it, affecting millions of people worldwide (Karsdal et al., 2014). The disease is generally progressed with age and can also be termed as “wear and tear” degeneration of the joint but other risk factors for the disease include obesity, joint injury, and genetic predisposition (Litwic et al., 2013, Ashford and Williard, 2014, Barnett, 2018, Dulay et al., 2015). While well characterised by the presence of cartilage and bone degradation, the whole joint is affected and can also affect the synovial membrane, specifically synovitis may occur (Sharma, 2021). The treatment of OA can include intervention using exercise, weight management, physiotherapy, as well as pharmacologic treatments, ranging between analgesics and anti-inflammatory drugs to biologics (Hochberg et al., 2012, Loeser et al., 2012, Glyn-Jones et al., 2015). In some cases, where the severity of OA has progressed significantly, total joint replacement surgery is required (Singh et al., 2015).

1.3.2.2. Rheumatoid arthritis

Rheumatoid arthritis (RA) is a systemic autoimmune inflammatory disease affecting the joint, with characteristics of synovitis being prominent in the pathogenesis of the disease (Scott et al., 2010, Buckley et al., 2021, Wasserman, 2011). Similar to OA, RA develops symptoms of cartilage and bone degradation in the pathogenesis of the disease. The pathogenesis of RA involves complex interplay between not only genetic

factors but also environmental factors, that ultimately lead to destruction of the synovial joint (McInnes and Schett, 2011). The disease has been well-characterised with many drug therapeutics having been developed, such as TNF inhibitors and IL-6 inhibitors (Gibbons et al., 2023, Singh et al., 2016, Joshi et al., 2018). However, the first biologic treatment that is usually recommend are disease-modifying antirheumatic drugs (DMARDs) to improve outcomes and prevent joint damage (Singh et al., 2016).

1.4. Haemophilic Arthropathy (HA)

1.4.1. Background and Clinical Background

HA is one of the comorbidities of severe haemophilia A and can develop from bleeding into the joints, or haemarthrosis (Christensen et al., 2019). The occurrence of haemarthrosis begins from birth, but the high cost and need for venous access devices complicates the treatment in young children. Thus, methods such as serological biomarker identification for personalised treatment would help identify and prevent target joints occurring, and subsequent musculoskeletal complications (Rodriguez-Merchan, 2012). When a target joint, a joint where more than three episodes of haemarthrosis has occurred in the span of six months, is identified, the likelihood of HA developing is increased significantly (Mulder and Llinas, 2004). The occurrence of spontaneous bleeding is not present in mild haemophilia A, is rare (between once a month to once a year) in moderate haemophilia A, and can occur quite often if left without treatment in severe haemophilia A (Konkle and Nakaya Fletcher, 1993, Coppola et al., 2010). To measure the impairment of the joint, one of the methods is the haemophilia joint health score (HJHS). The HJHS is analysed by taking into account multiple factors, such as swelling, muscle atrophy, and crepitus on motion. PwsH may also present symptomatic to medical professionals which can lead to the identification of HA (Ng et al., 2005). Some characteristics of HA, as seen in Figure 1.4, include synovitis, cartilage degradation, and bone remodelling, along with elevation of certain biomarkers, and are shared with OA and RA (Hua et al., 2017, Kotela et al., 2019, Lafeber et al., 2008, Melchiorre et al., 2017, Roosendaal et al., 1998a, Roosendaal et al., 1999a). Blood-induced joint damage has been clearly seen both *in vitro* and *in vivo*, particularly affecting immature cartilage when compared to mature cartilage, but without any other mechanical or biological disturbances, improvements in the joint integrity can occur (Hooiveld et al., 2003a, Hooiveld et al.,

2003b, Hooiveld et al., 2003d, Jansen et al., 2007, Roosendaal and Lafeber, 2003, Roosendaal and Lafeber, 2006, Roosendaal et al., 1999b).

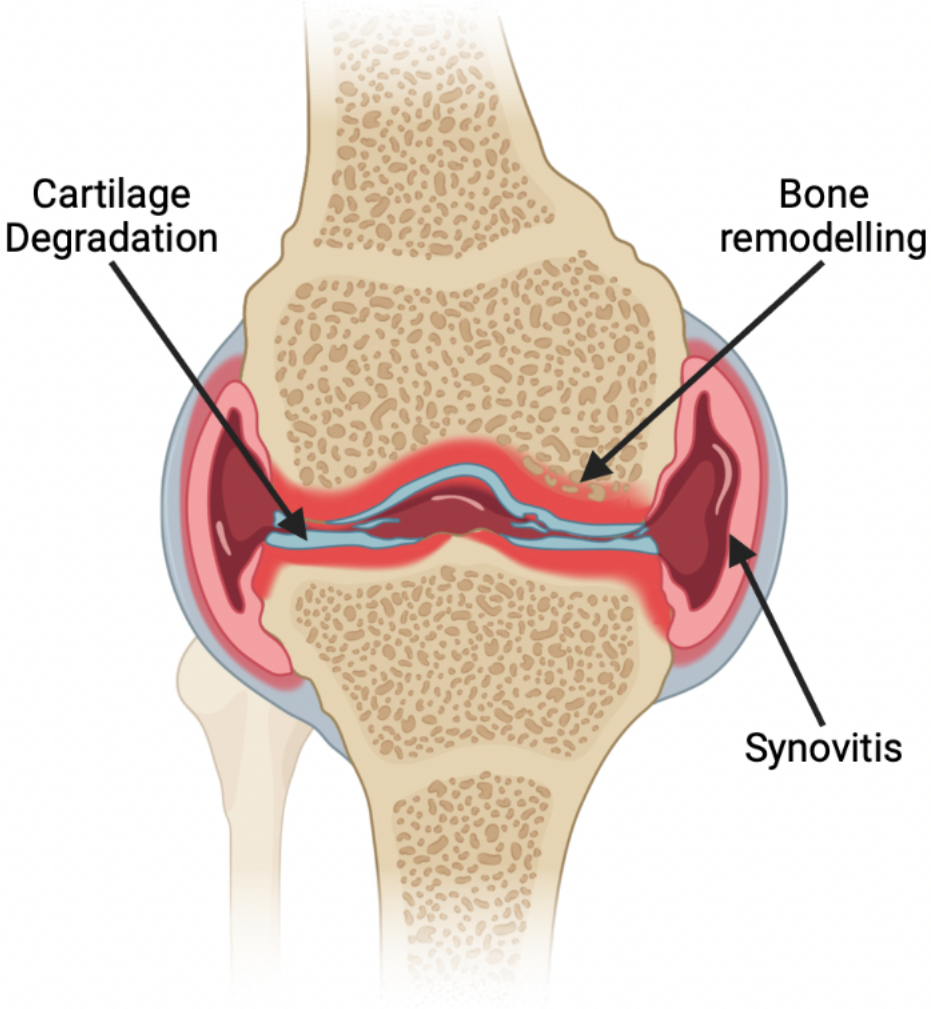

Figure 1.4. Depiction of an arthritic knee joint. Inflamed synovial membrane is one of the key characteristics found in chronic HA, OA, and RA cases. Other features that can be seen are cartilage degradation as well as presence of bone remodelling in some cases. Figure created in Biorender and adapted from (Berntorp et al., 2021).

1.4.2. Current knowledge of treatments

In HA, there are a number of treatments available, including painkillers, biologics, and surgical methods. Aspirin and non-steroidal anti-inflammatory drugs are generally

advised to be avoided in patients with haemarthrosis due to the risk of bleeding. However, in instances where haemarthrosis is acute, cyclooxygenase-2 (COX-2) inhibitors may be prescribed to the patient (Nacca et al., 2017). Examples of COX-2 inhibitors include celecoxib and etoricoxib. In more recent years, biologics such as emicizumab have been prescribed in treatment of severe haemophilia A, with efficacy of lowering the risk of haemarthroses and the subsequential development of HA (Kiialainen et al., 2022, Gualtierotti et al., 2021). However, particularly in patients with chronic HA, procedures such as synovectomies, arthrodesis, where cartilage of two bones in a joint is removed and the two bones stabilised to heal, or total joint replacement may be required (Chin et al., 2022, Pulles et al., 2017, Raffini and Manno, 2007).

1.5. Role of Immunity in HA

The mechanisms of development and progression of HA have yet to be clearly elucidated. Various immune cells and genes have been implicated but a clear mechanism or specific pathway has yet to be elucidated. It is known that the innate response is important in the pathogenesis of HA, with responses from different cell types occurring as the disease progressed (Cooke et al., 2018, Nieuwenhuizen et al., 2014). Naturally, we see key cytokines playing a major role in the inflammatory processes of the disease when bleeding into the joint has occurred, including TNFa, IL-1b, and IL-6 (Wojdasiewicz et al., 2018, Valentino et al., 2004, van Vulpen et al., 2015, Haxaire et al., 2018), amongst other factors (Valentino et al., 2007). But not only this, there have been studies showing the similar responses in HA that are found in OA and RA, indicating potential common pathways may be linked between the arthropathies (Cooke et al., 2019, Nieuwenhuizen et al., 2013).

1.5.1. Immunology of Arthritis

Joint diseases, namely OA and RA, are multifactorial but the immune system is without a doubt a key factor in both arthritides. OA, as mentioned in section 1.3.2.1, is a degenerative bone disease that causes “wear and tear” of the cartilage and underlying bone (Karsdal et al., 2014). While mechanical distress affects the progression of OA, there are a number of cytokines involved as well. RA, as mentioned in section 1.3.2.2, is a systemic autoimmune inflammatory disease affecting the joint (Scott et al., 2010).

In both OA and RA, key inflammatory cytokines that are involved include TNFa, IL-1b, and IL-6 (Farrugia and Baron, 2016, Loef et al., 2018, Abramson and Amin, 2002, Vincent, 2019, Akeson and Malemud, 2017). The signalling pathways can be balanced with the production in anti-inflammatory cytokines, including IL-4 and IL-10 (Dong et al., 2018, Katsikis et al., 1994). While all these cytokines are implicated in inflammatory diseases in general, IL-33 has also been implicated in RA pathogenesis (Xu et al., 2010a). IL-33, an IL-1 alarmin, could potentially be an indicator for severity of progression in RA (Hong et al., 2011).

1.5.2. Immunology of HA

As mentioned previously, key cytokines involved in HA pathogenesis include TNFa, IL-1b, and IL-6. Anti-inflammatory cytokines also play an antagonistic role, for example IL-4 and IL-10, in HA (Wojdasiewicz et al., 2018). These signalling pathways, while implicated in HA progression, have yet to be fully elucidated. The activation of TNFa, IL-1b, and IL-6 cytokines, has already been shown to be increased in HA compared to OA and RA (Zhang et al., 2015, Roosendaal et al., 1999a, Roosendaal et al., 1998b). The expression of IL-4 during HA not only normalises proteoglycans through increased production through chondrocytes, but the cytokine also reduces the expression of IL-1b and TNFa, two key inflammatory cytokines in HA (van Meegeren et al., 2012). In the same study, IL-10 was shown to limit production of pro-inflammatory cytokines in blood-induced cartilage damage, a critical factor in HA.

1.6. Mouse Models

1.6.1. Current mouse models in haemophilia A

F8^{tm1kaz} (*F8*$^{tm1-/-}$) and *F8*^{tm2kaz} mice are two widely used models of severe haemophilia A. Aside from lack of plasma FVIII activity, the mouse models are otherwise healthy mice with no signs of spontaneous bleeding. The *F8*$^{tm1-/-}$ mouse model is a knockout model affecting the FVIII mRNA on exon 16. While the *F8*^{tm2kaz} mouse model is also a knockout model, it affects exon 17 instead. Both knockout models produce a truncated, non-functional FVIII protein, but with the exon 17 mouse model it may also be due to partially delete protein (Bi et al., 1996, Bi et al., 1995). The mouse model used in this project for comparison is the *F8*$^{tm1-/-}$ mouse model.

1.6.2. Limitations of current models

As mentioned above, one of the most widely used mouse model of severe haemophilia A that is used is the *F8*$^{tm1-/-}$ mouse model. While a suitable model that displays prolonged aPTT and FVIII activity levels that are not detectable, the mouse model still has circulated truncated, non-functional proteins of FVIII which can still potentially tolerise the system (Bril et al., 2006). When the immune system has been introduced to foreign FVIII, like rFVIII, the body can begin to produce antibodies against the FVIII products. These antibodies, in turn, then prevent FVIII from acting on the coagulation pathway to help form clots during treatment or prevent the prophylaxis from acting when needed. Tolerisation against FVIII, i.e., inhibitor development, can cause significant issues, such as breakthrough or spontaneous bleeds (Bril et al., 2006). Breakthrough bleeds can occur anywhere but are found quite often in the joint spaces when inhibitors have formed in the immune system to FVIII. Thus, appropriate treatment and monitoring is extremely important in patients who are receiving FVIII replacement. In severe haemophilia A, immune tolerance, is induced in increments so patients do not mount anti-FVIII antibodies, occurring in approximately 30% of patients, which would result in redundancy of rFVIII replacement (Schep et al., 2018). Tolerance of the immune system in haemophilia A, where the model cannot respond to the rFVIII dose prophylactically nor on demand, can cause issues with experimental studies using rFVIII, i.e., the factor replacement therapy is rendered redundant. While this also may seem like merely an observation, this creates an environment that may not be completely naïve to the FVIII protein. In the case of HA, should the immune system be already tolerised then rFVIII would be ineffective in treatment prevention. To fully elucidate the exact mechanism, I chose a microenvironment where this would not be an issue, hence the use of a mouse model that presents with a total deletion of the FVIII gene to prevent truncated proteins from translating and tolerising the immune system. The development of the *F8*$^{tm1-/-}$ mouse model was also through injection of targeted embryonic stem (ES) cells, that were 129S4/SvJae derived, into C57BL/6 blastocysts (Bi et al., 1996). Passenger mutations can occur this way, where the ES cells used are of one genetic background, while the genetic background of the backcross used is of another genetic background, in short, a genetically engineered mouse model of mixed genetic background. While suitable as a model for research, it does not reflect the population of those affected by severe haemophilia A, where

spontaneous bleeds is something that can occur up to five times in every month (Konkle and Nakaya Fletcher, 1993, Berntorp et al., 2021).

1.6.3. Current mouse models of experimental HA

From the current literature for induced experimental HA, there are two main methods found that are used. Firstly, a spring-loaded instrument can be used to induce a blunt force trauma to the knee joint to induce the injury (Valentino et al., 2004, Valentino et al., 2007, Hakobyan et al., 2004). In this method, as seen in Figure 1.5. (A), the mice have a reproducible blunt force applied to the knee joint, without damage to the cartilage or the bone as the impact of the device is cushioned. Another method is to induce a needle puncture injury below the patella of the knee joint, which has been done in many studies as well (Ovlisen et al., 2008, Vols et al., 2019, Hakobyan et al., 2008). This method, as seen in Figure 1.5 (B), produces an external blood spot on extraction of the 30 G needle. Research using these models has provided more knowledge on the pathogenesis of HA, but also potential treatments that have shown amelioration of the disease in these mouse models (Kashiwakura et al., 2012). The needle-injury method is less invasive and highly reproducible and thus preferred.

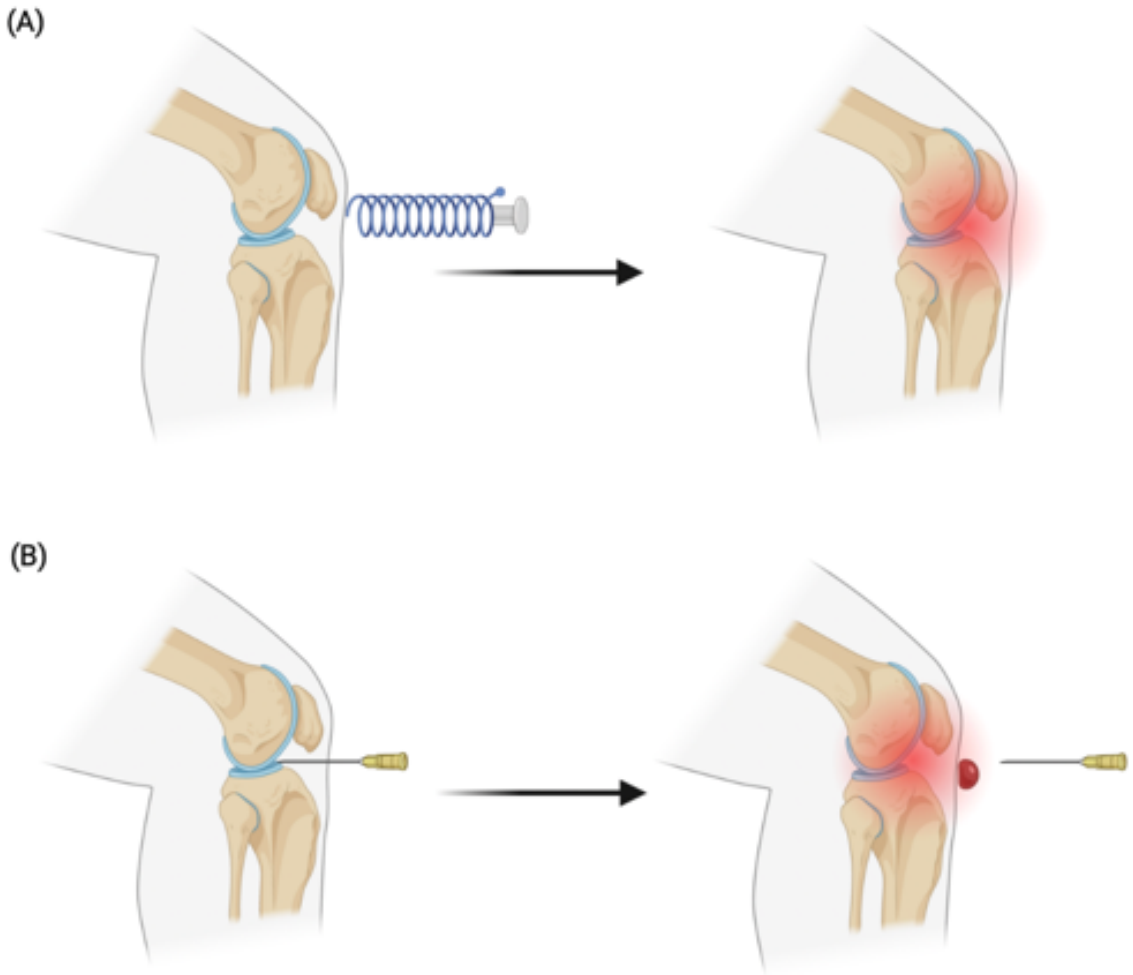

Figure 1.5. Induction of experimental HA in mice. (A) Blunt force trauma induces haemarthrosis without external bleeding. **(B)** Needle-induced injury induces haemarthrosis, with an external blood spot appearing on confirmation of the injury. Figure created in Biorender.

1.7. Mouse strains

1.7.1. Heterogeneity and predisposition

Within the lab, there are various strains of mice to choose from but amongst these, some of the most common strains are C57BL/6J and BALB/c backgrounds. BALB/c mice, however, possess a more Th2-mediated immunity which juxtaposes that seen in the more Th1-mediated immune response in C57BL/6J mice (Fukushima et al., 2006). Thus, comparing two immune environments that are genetically differently predisposed to the development of diseases. However, we will also look at the A/J

mouse strain in this thesis to see the effects of genetic predisposition, as seen in Figure 1.6, on the development of HA. With age, A/J mice develop muscular dystrophy, and thus muscle strength is weakened (Ho et al., 2004). The loss of muscle strength is a characteristic found also in PwsH and it is known that atrophy of muscle develops post-haemarthrosis, thus reducing quality of life (Wojdasiewicz et al., 2018). However, if a model is already predisposed to weakened muscles, would this have a knock-on effect on the severity of HA?

1.7.1.1. C57BL/6J

C57BL/6J mice are an inbred strain of mice that share nearly an identical genotype and one of the most widely used strains in research (Bryant, 2011). These mice are fantastic models for research as they breed frequently. The C57BL/6J strain has a more Th1-mediated immune response, and thus a more M1 polarisation of macrophages (Fukushima et al., 2006). The mouse strain also has a high complement activity which allows it to be used in research involving observation of the complement system (Gralinski et al., 2018).

1.7.1.2. BALB/c

While the C57BL/6J mouse strain is more Th1-meditate in immune response, the BALB/c strain has the opposite where the immune response is more Th2-mediated (Fukushima et al., 2006). This makes it a very suitable model for allergic and autoinflammatory diseases (De Vooght et al., 2010, Saunders et al., 2016). And while the C57BL/6J mouse has high complement activity, the BALB/c mouse still produces a higher humoral response in comparison to the C57BL/6J mouse (Fornefett et al., 2018). As a results of the more Th2-type response found in BALB/c mice, macrophage response also reflects this, with C57BL/6J mice having a more M1 polarisation of macrophages and BALB/c mice having a more M2 polarisation (Mills et al., 2000).

1.7.1.3. A/J

Unlike C57BL/6J mice, A/J mice require a bit more special care with regards to breeding as they have reduced productivity and the incidence of non-productive matings is also high, making them quite challenging to breed. When comparing to the C57BL/6J mouse strain, A/J have a more Th2-mediated immune response, as

opposed to the Th1-mediate immune response that is favoured in C57BL/6J mice (Sellers et al., 2012). However, what is interesting about this strain of mice is that the mice naturally develop muscular dystrophy after four to five months of age (Ho et al., 2004), which can lead to muscular atrophy which is a characteristic seen in HA (Wojdasiewicz et al., 2018). The A/J mice also display different responses to the C57BL/6J mice with regards to response to vascular injury and haemostasis, an important aspect when investigating haemophilia A (Hoover-Plow et al., 2006).

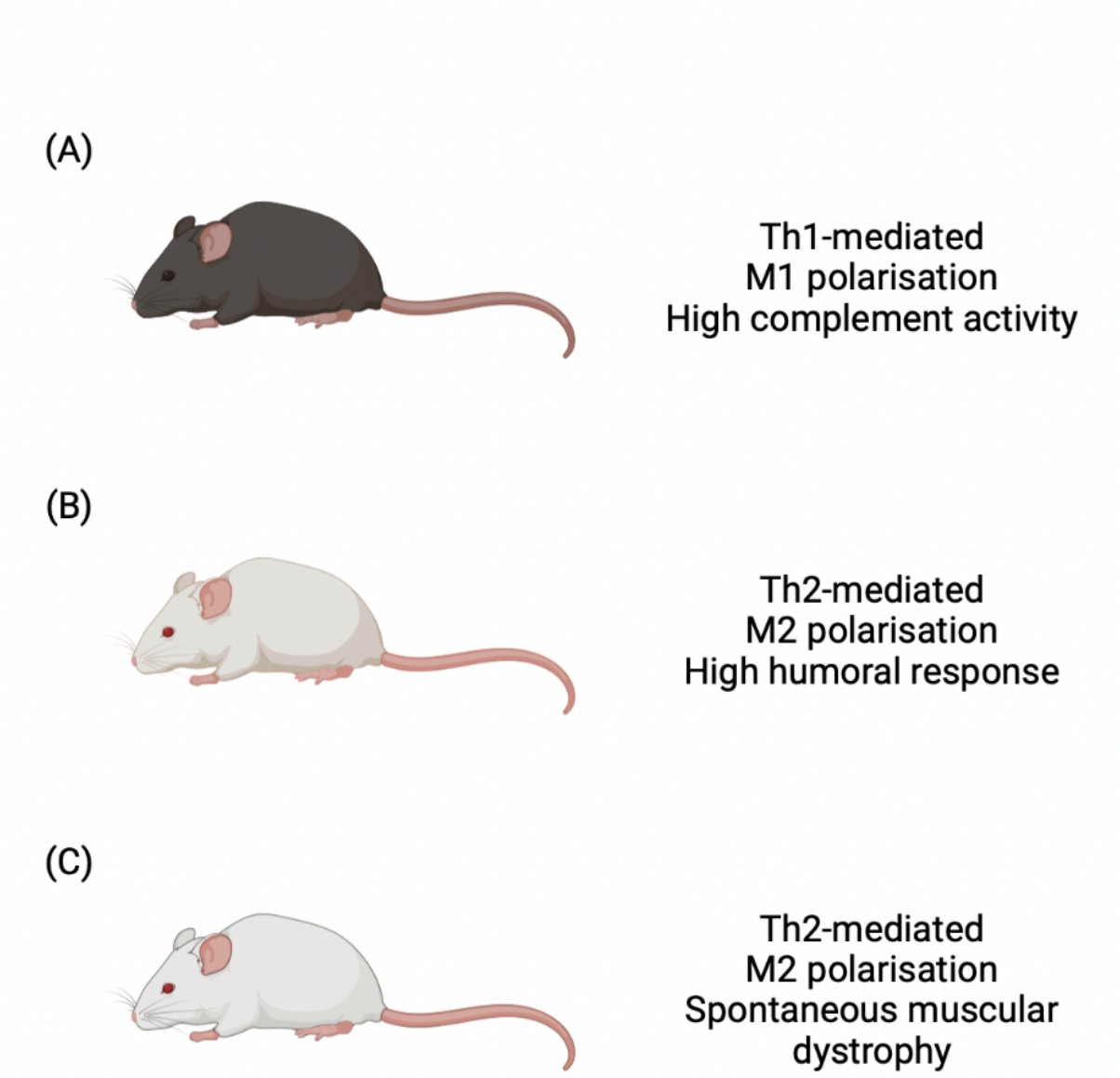

Figure 1.6. Each mouse strain has a different favoured immune response as well as predispositions unique to its specific background. (A) C57BL/6J mice are Th1-mediated, favour M1 polarisation of macrophages, and have high complement activity. **(B)** BALB/c mice are more Th2 immune response mediated, favour M2 polarisation of macrophages, and have a much higher humoral response than C57BL/6J mice. **(C)** A/J mice are more Th2-mediated compared to C57BL/6J mice, favour a more M2 polarisation of macrophages, and also develop spontaneous muscular dystrophy. Figure created in Biorender.

1.7.2. Dual-knockout mouse model strains

Dual-knockout mice are genetically modified mice that have been engineered specifically to lack two different genes. The use of dual-knockout strains is something that has been performed in many research experiments and is not something novel (Chavali et al., 2014, Lemoine et al., 2016). However, the novel mouse model created in this lab has yet to be generated with another knockout model, where another gene has not been generated alongside the *F8* mutation in the same mouse.

1.7.2.1. Cx3cr1

Cx3cr1$^{-/-}$ mice lack expression of Cx3cr1, a receptor for the chemokine Cx3cl1, and exhibit altered immune responses (Cardona et al., 2006). These mice show a wide range of altered immune responses, including impaired dendritic cell migration and T cell priming, thus affecting the viral response (Hertwig et al., 2016), as well as decreased monocyte recruitment to inflammatory sites, ultimately leading to impaired wound healing (Sindrilaru et al., 2011). Not only this but the *Cx3cr1*$^{-/-}$ mice also display altered bone homeostasis and are more susceptible to bone loss and osteoporosis (Xiong et al., 2018). Alteration of the Cx3cl1/Cx3cr1 interaction has been noted in a range of human diseases (Lee et al., 2018).

1.7.2.2. Il4ra

The *Il4ra*$^{-/-}$ mouse model lacks functional IL-4 receptors and has been widely used in the study of the role of IL-4 in immune responses. The mice exhibit impaired Th2 immune responses, which include reduced IgE production, eosinophil recruitment, altered macrophage polarisation, and airway hyperresponsiveness (Finkelman et al., 1993, Mohrs et al., 2001, Weng et al., 2018). In addition to its effects on immune cells, *Il4ra*$^{-/-}$ have been used in research showing reduced collagen deposition and fibrosis, implicating IL-4 in tissue repair and fibrosis (Nguyen et al., 2020, Allen, 2023). These mice have been key in the investigation of the role of IL-4 in the pathogenesis of autoimmune diseases. Dependent on the context, IL-4 can act as a promoter or a suppressor in the development of autoimmune diseases such as systemic lupus erythematosus, rheumatoid arthritis, and multiple sclerosis (Jacob et al., 2011, Luo et al., 2022, Xu et al., 2010b).

1.7.2.3. St2 (or Il1rl1)

T1/ST2 or IL1RL1 is a member of the IL-1 receptor family that has been implicated in a number of diseases (Matarazzo et al., 2022). The *Il1rl1*$^{-/-}$ mouse model has been used to show decreased levels of disease severity in asthma and experimental autoimmune encephalomyelitis (Gordon et al., 2016, Xu et al., 2017). Studies have also used this knockout mouse in research to find a potential role for IL1RL1 in the pathogenesis of RA (Hong et al., 2011, Akhabir and Sandford, 2010). Not only this, but *Il1rl1*$^{-/-}$ mice have been shown to have reduced bone density, suggesting a potential role for IL1RL1 in bone metabolism (Lima et al., 2015).

1.7.2.4. Il33

Il33$^{-/-}$ mice have been used to elucidate immune responses in a variety of diseases (De la Fuente et al., 2015, Demyanets et al., 2021, Monticelli et al., 2015). The knockout mice exhibit impaired Th2 immune responses as well as impaired wound healing (Liew et al., 2016, Millar et al., 2017). Of importance to note, elevated levels of IL-33 have been found in patients with diseases like RA, particularly exacerbating the pathogenesis of the disease (Xu et al., 2010a, Hong et al., 2011). Working together with ST2 along the IL-33/ST2 axis, many observations have been made in tandem with the *St2*$^{-/-}$ mouse model that prove that the IL-33/ST2 axis could have a vital role in a number of diseases (Lima et al., 2015, De la Fuente et al., 2015, Allegra et al., 2019, Schwartz et al., 2016).

1.8. The IL-33/ST2 Axis

The ST2 receptor was first identified in 1989 as an orphan receptor before the discovery of its ligand IL-33 in 2005 (Tominaga, 1989, Schmitz et al., 2005). The ST2 receptor can be found in a soluble form (sST2), where it acts as a decoy receptor to prevent IL-33/ST2 signalling, or as a membrane-bound form (ST2), where the receptor promotes secretion of inflammatory cytokines via NF-κB signalling. ST2 can be found expressed on a number of immune cells including Th2 cells, Treg cells, and ILC2s (Griesenauer and Paczesny, 2017). As seen in Figure 1.7, the IL-33 ligand binds to sST2, where free IL-33 is sequestered by the receptor and prevents signalling. However, when IL-33 binds to the ST2 receptor it forms a heterodimer with IL1-RAP,

initialising NF-κB signalling through the MyD88 pathway, ultimately leading to the expression of inflammatory cytokines (Schmitz et al., 2005, Liew et al., 2016). A host of diseases has been associated with the IL-33/ST2 axis including RA, asthma, and pulmonary fibrosis (Gordon et al., 2016, Shi et al., 2018, Xu et al., 2010a).

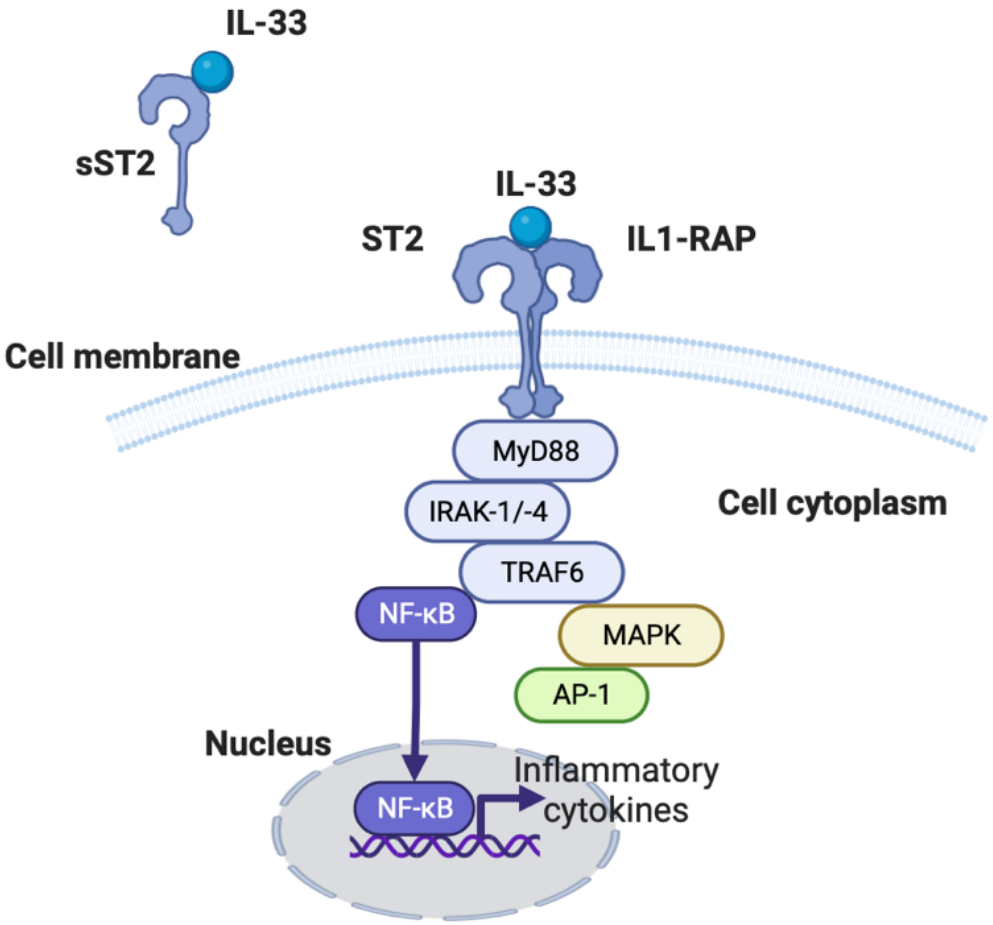

Figure 1.7. The IL-33/ST2 signalling pathway. The IL-33 cytokine binds to sST2, where the decoy receptor blocks signalling down the pathway, or to the ST2/IL1-RAP dimer, where further signalling in the cell activates the release of inflammatory cytokines. Figure created in Biorender and adapted from (Griesenauer and Paczesny, 2017).

1.9. Thesis objectives

In this chapter, I have outlined the comorbidity, HA, as well as the potential roles that certain immune cells and genes might play in the progression of HA. However, despite the extensive research already in place, our knowledge of exact causes of HA are still not well developed. It is also clear that certain genes do play a role in HA, as seen in the research done in the *F8*$^{tm1-/-}$ mouse model, but there still remains the question of whether or not the truncated FVIII proteins produce may have a potential effect on the microenvironment of the mouse. Thus, in this thesis, I will characterise the development and progression of HA in this novel mouse model, *F8*$^{em1-/-}$.

The first objective in this thesis is to establish the novel mouse model as a suitable model of HA. There exists already a suitable and well-characterised model of HA, the *F8*$^{tm1-/-}$ mouse model, but the establishment of the *F8*$^{em1-/-}$ mouse model allows us to analyse the resulting HA development regarding a microenvironment that has had completely no exposure to any form of FVIII protein, namely any truncated FVIII protein. Secondly, the ability to generate new dual-knockout models allows an innovative way to analyse the potential roles of certain genes in the HA model. And lastly, the third objective was to further establish HA models in the *F8*$^{em1-/-}$ mice using different mouse strain backgrounds. In this thesis, I chose to focus on the BALB/c and A/J mouse strain backgrounds to investigate the effects of different immune backgrounds on the progression of HA. Thus, establishing a model with varied backgrounds to reflect the heterogeneity found in man.

1.9.1. Aims

With the *F8*$^{em1-/-}$ mouse model established as a suitable model for severe haemophilia A, my aims are summarised as threefold:

1. To characterise the novel mouse model *F8*$^{em1-/-}$ in the progression of haemophilic arthropathy.
2. To utilise dual-knockout mice to analyse the potential roles of genes in haemophilic arthropathy in the *F8*$^{em1-/-}$ mouse model.
3. To exploit the heterogeneity of mouse strain backgrounds to create a more reflective research model for haemophilic arthropathy.

Chapter 2 – Methods

2.1. Ethics

All mice used in this thesis were bred in a Specific Pathogen Free (SPF) facility in individually ventilated cages (IVCs) under positive pressure. The temperature was maintained in the range of 20 – 24 °C, and the humidity was maintained in the range of 45 – 65%, as per EU legislation (2010/63/EU). The SPF facility operated under a continuous cycle of 12:12 light cycle. All mice used were on a C57BL/6J strain background unless otherwise stated (Chapter 5). Mice used in experiments were all male mice and were age-matched, specifically between the age of 10 to 14 weeks, unless otherwise stated. All animal experiments were performed in compliance with the Health Products and Regulatory Authority (HPRA) under individual authorisation number AE19136/I481 and approved by Trinity College Dublin's ethical review board (AREC) under Project Licence AE19136/P108.

Blood for plasma controls were obtained from healthy donors through the Irish Blood Transfusion Service and approved by local ethics committee (Number: 20180403). Blood from PwsH were from the Irish Personalised Approach to the Treatment of Haemophilia (iPATH) project, with informed consent from the patients (Approval number: 20180404). These samples were screened for FVIII activity at blood collection and plasma samples with <10% FVIII activity were used for further analysis. The cohort in this analysis comprises of 39 PwsH with an average age of 39.9 years (range: 19 to 76 years).

2.2. Mice

2.2.1. Mice strains

2.2.1.1. Generation of $F8^{em1Pfal}$ ($F8^{em1-/-}$) on a C57BL/6J background

The generation of the *$F8^{em1-/-}$* mouse model was done through a previous lab member's PhD thesis (Byrne, 2021). The mouse model was created using CRISPR/Cas9 technology to provide a novel microenvironment, allowing the lab to research into inhibitor development, bleeding phenotype, and arthropathy without any major genomic rearrangements. Using C57BL/6J zygotes was injected with crRNA,

assembled in a Cas9 ribonucleoparticle, through standard protocols (Aida et al., 2015). The zygotes were then transferred to pseudo-pregnant CD1 females and offspring screened for the desired mutation. The 2bp mutation in exon 1 of the *F8* gene ultimately results in the FVIII protein not being translated.

2.2.1.2. Generation of Crosses

2.2.1.2.1. Cx3cr1

In order to create the $F8^{em1-/-}/Cx3cr1^{-/-}$ strain of mice, homozygous female $F8^{em1-/-}$ mice were bred with homozygous male $Cx3cr1^{-/-}$ mice (Jax number: 00582). The system in Figure 2.1 was used in order to create $F8^{em1-/-}$ (homozygous or hemizygous)/$Cx3cr1^{-/-}$ (homozygous) mice.

2.2.1.2.2. Il4ra

In order to create the $F8^{em1-/-}/Il4ra^{-/-}$ strain of mice, homozygous female $F8^{em1-/-}$ mice were bred with homozygous male $Il4ra^{-/-}$ mice (mice generated by Prof Frank Brombacher) (Barner et al., 1998). A similar system in Figure 2.1 was used in order to create $F8^{em1-/-}$ (homozygous or hemizygous)/$Il4ra^{-/-}$ (homozygous).

2.2.1.2.3. St2 (or *Il1rl1*)

In order to create the $F8^{em1-/-}/St2^{-/-}$ strain of mice, homozygous female $F8^{em1-/-}$ mice were bred with homozygous male *Il33r* mice ($St2^{-/-}$ mice or $Il1rl1^{-/-}$ mice) (Cayrol and Girard, 2018). A similar system as in Figure 2.1 was used to create $F8^{em1-/-}$ (homozygous or hemizygous)/$St2^{-/-}$ (homozygous) mice.

2.2.1.2.4. Il33

The generation of $F8^{em1-/-}/Il33^{-/-}$ strain of mice was done through breeding of homozygous female $F8^{em1-/-}$ mice with homozygous male $Il33^{-/-}$ mice (Zhong et al., 2019). A similar system as in Figure 2.1 was used to create $F8^{em1-/-}$ (homozygous or hemizygous)/$Il33^{-/-}$ (homozygous) mice.

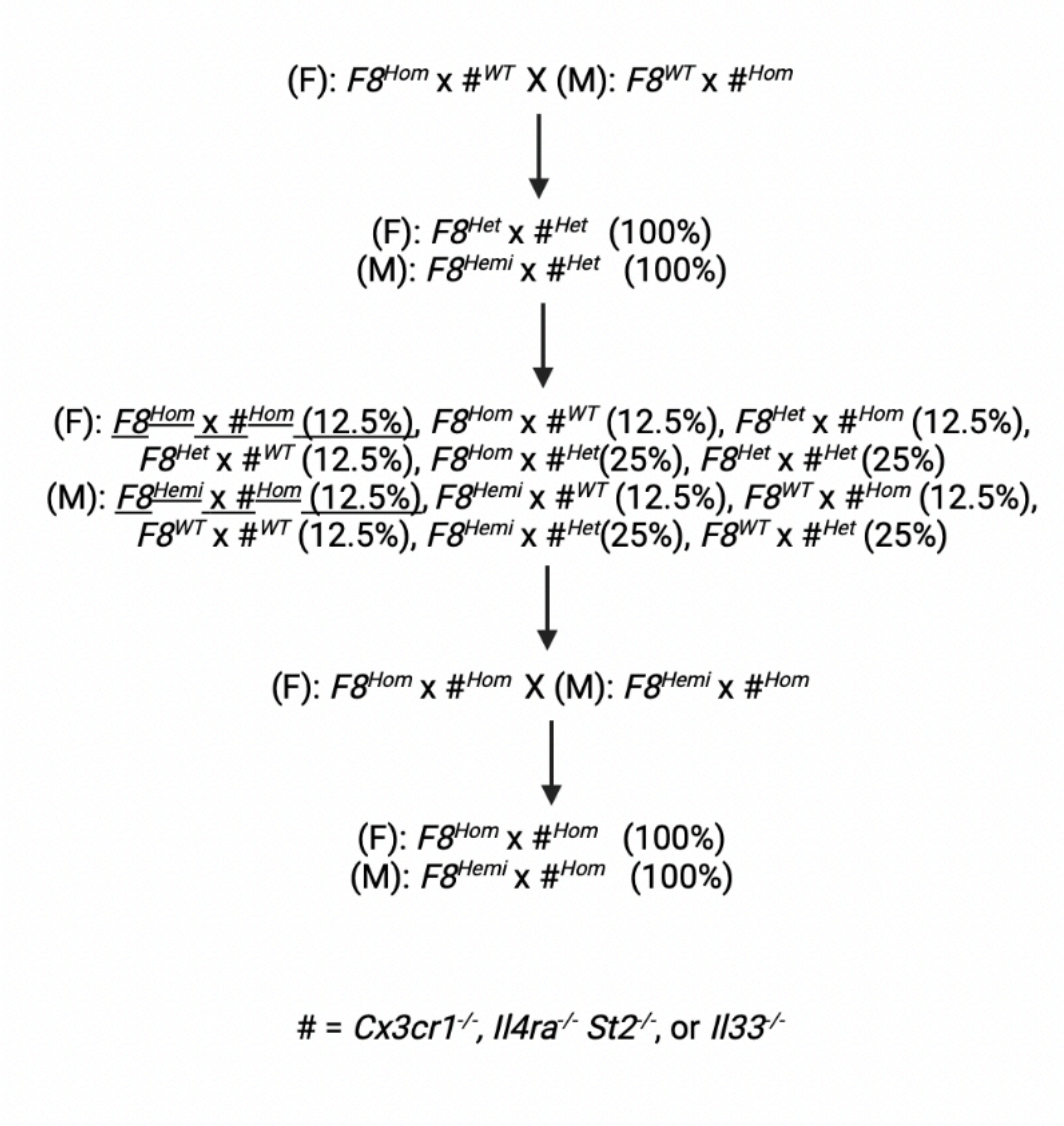

Figure 2.1. Generation of crossed strains. Method for achieving dual-knockout mouse strains. Figure created in Biorender.

2.2.1.3. Generation of four strains

The generation of the other strains (BALB/c, and A/J) was done through speed congenics as in a previous lab member's PhD thesis (Byrne, 2021). In summary, mice with the highest genetic material of the desired strain from each generation was chosen for further breeding and this method repeated for each generation of offspring, accelerating the breeding of the mice. Thus, the number of generations required before the recipient strain bore 99.9% sequence identity was greatly reduced to just after ten generations.

2.3. Genotyping

As disruption in a specific gene is used as a method in science to study the implications and roles the gene plays, this can be used to create a “homozygous knockout” in the diploid mouse model. To identify a mouse to be a knockout for a particular gene, we used genotyping to identify this. A mouse may also be a homozygous wildtype, meaning they have two functional copies of the gene. A heterozygous mouse possesses one functional and one non-functional copy of the gene. These general terms, knockout/homozygous, heterozygous, and wildtype, are used but do not identify all genotypes of mice as some may be X-linked, thus males that possess a non-functional copy of the gene are termed “hemizygous” (Hemi), as seen in the mouse model used in this project. Ear punches are used to identify mice and these samples are used to genotype each individual mouse.

2.3.1. Lysis/Wizard Lysis

For standard genotyping, to each tube containing sample (ear punches from mice), polymerase chain reaction (PCR) Direct Lysis Buffer (100 μl; Viagen, CA) and Proteinase K (1.5 μl; Sigma, UK) was added, lid closed, and vortexed. This removes proteins and contaminants from the samples. The tubes were then placed on a heat block at 55°C for approximately 3 hours, mixing the contents using a vortex at every hour interval. The temperature was then raised to 85°C for an additional 45 minutes to denature the enzyme and the samples were stored at -20°C until further use.

Master mixes were made up containing various amount of DreamTaq Buffer, dNTPs, primers (5’ and 3’), DreamTaq enzyme, and water. The master mix was pipetted into PCR tubes and DNA from previously lysed samples were added. Appropriate controls – Homozygous (Hom), Heterozygous (Het), WT (Wildtype), water – were also run in conjunction with the samples.

For genotyping of *F8*$^{em1-/-}$ mice, Wizard SV lysis procedure (MyBio, Ireland) was used for genotyping. This protocol was validated by a previous PhD student’s research (Byrne, 2021). Reagents were added as per Table 2.1 to a 1.5 ml Eppendorf tube containing the ear punch. This was left overnight for approximately 16 – 18 hours in a heat block at 55°C. Lysates were removed from the heat block and Wizard SV Lysis

Buffer (250 μl) was added to each sample and transferred to individual mini column assemblies. Columns were spun at 13,000 x g for 3 minutes at room temperature, and flow through was discarded. To each column, Column Wash Solution (550 μl; with 95% ethanol added as directed) was added and spun at 13,000 x g for 1 minute. Flow through was discarded. The wash steps using Column Wash Solution were repeated for a total of four times. Columns were then spun at 13,000 x g for 2 minutes to dry. Columns were transferred to sterile minifuge tubes and milli-Q water (65 μl) was added to each column directly and left to incubate for 4 minutes at room temperature. Columns in the minifuge tubes were then spun at 13,000 x g for 1 minute and eluted DNA was measured for concentration and purity using a Nanodrop spectrophotometer (Nanodrop 1000-Spectrophotometer). DNA was stored at -20°C until further use.

Table 2.1. Wizard SV Lysis master mix.

Reagent	Amount to be added per sample
Nuclei Lysis Solution	210 μl
0.5 M EDTA (pH 8.0)	50 μl
Proteinase K (20 mg/ml)	10 μl
RNase A Solution (4 mg/ml)	5 μl
Total	275 μl

2.3.2. Polymerase Chain Reaction (PCR)

PCR master mix was made up as per Table 2.2. Lysed DNA samples were added to PCR tubes, along with the master mix. Appropriate controls were also run in a thermal cycler (Bio-Rad) in tandem as per PCR protocol (Table 2.3). Once the PCR was complete, products were subjected to SpeI enzyme digest (Sigma, UK) (Table 2.4) and following electrophoresis, band(s) at different weights were images at 273bp, 200bp, and 73bp, depending on the genotype of the *F8*$^{em1-/-}$ mouse.

Table 2.2. *F8*$^{em1-/-}$ PCR master mix.

Reagent	Amount to be added per sample
10x Dreamtaq Green Buffer	4 μl
dNTPs	1.6 μl
Forward primer (see Appendix I)	1 μl
Reverse primer (see Appendix I)	1 μl
Dreamtaq polymerase	0.2 μl
Milli-Q water	10.2 μl
Template DNA	2 μl
Total	20 μl

Table 2.3. *F8*$^{em1-/-}$ PCR programme.

Step	Action	Temperature (°C)	Time
1	Denaturation	95	2 minutes
2	Denaturation	95	30 seconds
3	Annealing	61	30 seconds
4	Extension	72	45 seconds
Repeated Steps 2 – 4 for 35 cycles			
5	Extension	72	5 minutes
6	Store	4	Infinite
Total time			~ 1hr 10 minutes

Table 2.4. *F8*$^{em1-/-}$ enzyme digest master mix.

Reagent	Amount to be added per sample
Buffer H	2 μl
SpeI	1 μl
Milli-Q water	7 μl
PCR template reaction mix	10 μl
Total	20 μl

2.3.3. Gel electrophoresis

Once the PCR reaction was completed for standard genotyping, samples were run on a 1.5% agarose gel. The gel was made up by adding 1.5 g agarose (Sigma, UK) to 100 ml of tris-borate-EDTA buffer (TBE). The flask was heated in the microwave for approximately 1.5 minutes or until all agarose was fully dissolved. Ethidium bromide (1.5 μl; Sigma, UK) was added to the flask, swirled and then poured into the mould. Once the gel was set it was immersed in buffer and DNA ladder (Invitrogen, UK) loaded along with the samples. Gels were run at 100 V for 40 minutes and then imaged using a Fusion FX gel documentation system (GelDoc; Vilber Lourmat, Germany).

For the Wizard SV lysis, once the enzyme digest reaction was completed, samples were run on a 2.5% agarose gel. The gel was made up by adding 2.5 g agarose to 100 ml TBE. The flask was heated in the microwave for approximately 1.5 minutes or until all the agarose powder had fully dissolved. Ethidium bromide (2.5 μl) was added to the flask, swirled, and then poured into the mould. Once the gel was set it was immersed in buffer and DNA ladder loaded along with the samples. Gels were run at 110 V for 40 minutes and the imaged on the GelDoc (Figure 2.2).

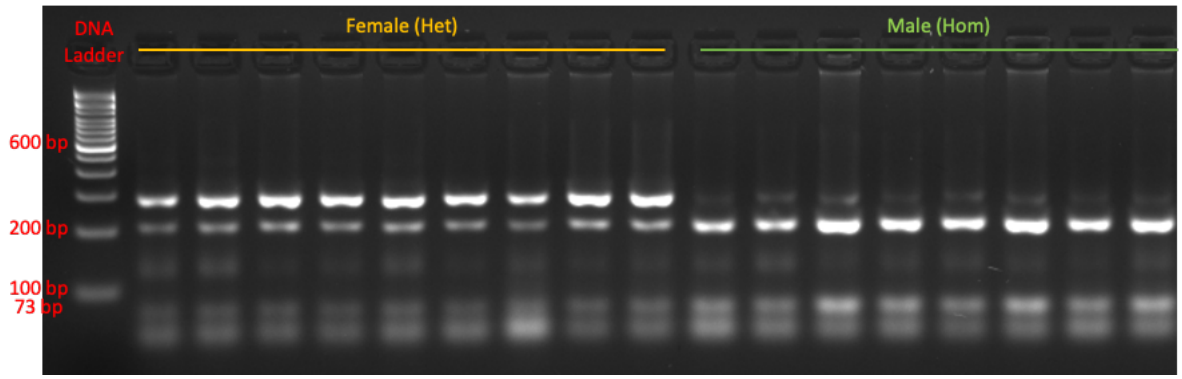

Figure 2.2. Genotypes for *F8*$^{em1-/-}$ mice. Female pups (yellow) were genotyped along with male pups (green), showing some of the various genotypes possible (Het and Hemi, respectively). Base pairs are in 100 bp increments in Lane 1 (left column), where the large bright band on the DNA ladder is 600 bp. If the *F8*$^{em1-/-}$ mutation is present, the digested PCR product will yield two bands, one at 200 bp and one at 73 bp. The undigested product will remain at 273 bp.

2.4. Experimental haemophilic arthropathy

This model was developed by Dr Narine Hakobyan, where a one-time sub-patellar injury using a 30-gauge needle was used to induce HA (Hakobyan et al., 2008, Hakobyan et al., 2016).

2.4.1. Protocol

Mice were first anaesthetised using gaseous isoflurane. Mice were then shaved on the right hind leg before using a 30-gauge needle to induce a one-time sub-patellar puncture. The right hind leg was bent at a 90° angle and the needle used to make a mark under the patella before inserting the needle approximately 2mm into the knee joint, as seen in Figure 2.3.

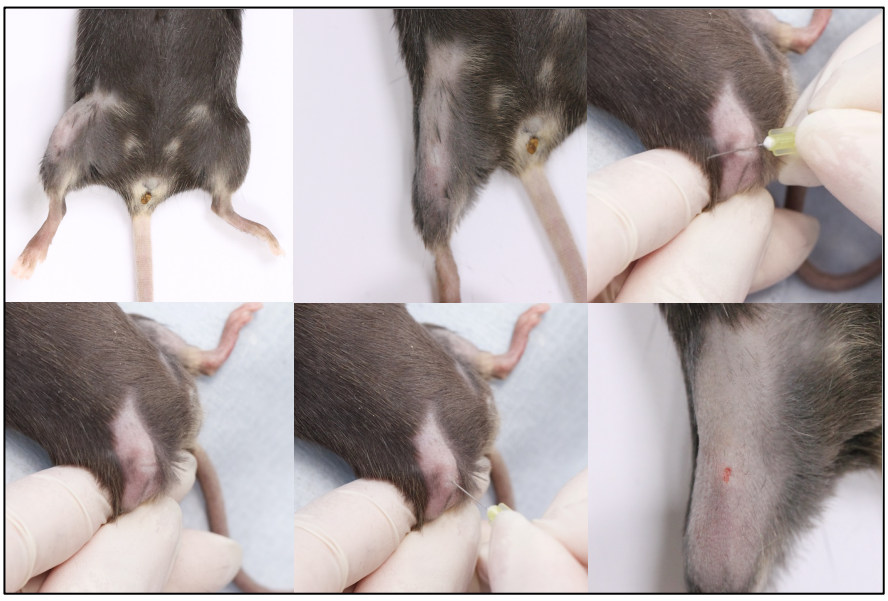

Figure 2.3. Experimental haemophilic arthropathy induced by needle puncture set up. The right hind leg was bent in a 90° angle. A 30-gauge needle was used to mark out the bottom of the patella. The needle was then inserted perpendicular to the fibula and removed, producing a blood spot.

2.4.2. Scoring and monitoring

Mice were scored and monitored (Appendix II) daily as per HPRA license (AE19136/P108). Mice were treated with buprenorphine (0.1 mg/kg of body weight) via subcutaneous injection every 12 hours for the first 72 hours. Mice were scored daily throughout the experiment based on gait, physical appearance, and unprovoked

behaviour. Any mouse reaching 3 in a single category or achieving a total score of 6 was removed from the experiment and humanely euthanised.

2.5. Blood collection

Mice were first anaesthetised using 2.5% tribromoethanol (240 mg/kg of body weight) intraperitoneally. Blood was collected via cardiac puncture into sodium citrate microcontainers (0.109M; 9:1 v/v). Blood samples collected from mice were centrifuged at 2,500 x g for 15 minutes at room temperature and plasma was collected into clean 1.5 ml Eppendorf tubes before storing at -20°C or -80°C.

2.6. Tissue dissection and processing

2.6.1. Synovium

Synovium was extracted from the knee joint and placed into clean Eppendorf tubes and immediately placed in liquid nitrogen for RNA extraction, and synovium taken for flow cytometry was placed in a 1.5 ml Eppendorf tube with 1% collagenase D (500 μl; Roche, Ireland) and RPMI medium (500 μl).

Once euthanised, the area of the leg was sprayed down with 70% ethanol and the skin removed to expose the joint as seen in Figure 2.4. Using a scalpel, an incision was made across the quadricep muscles, ensuring that the cut was deep enough that the femur was felt when cutting down. With a pair of forceps, the lower half of the dissected quadriceps was pulled down toward the direction of the ankle, removing the quadricep muscle, tendon, and patella. The synovium was then exposed and possible to remove using non-ridged forceps. The removed synovium was placed immediately into the appropriate tube depending on whether it was used for RNA extraction or for flow cytometry.

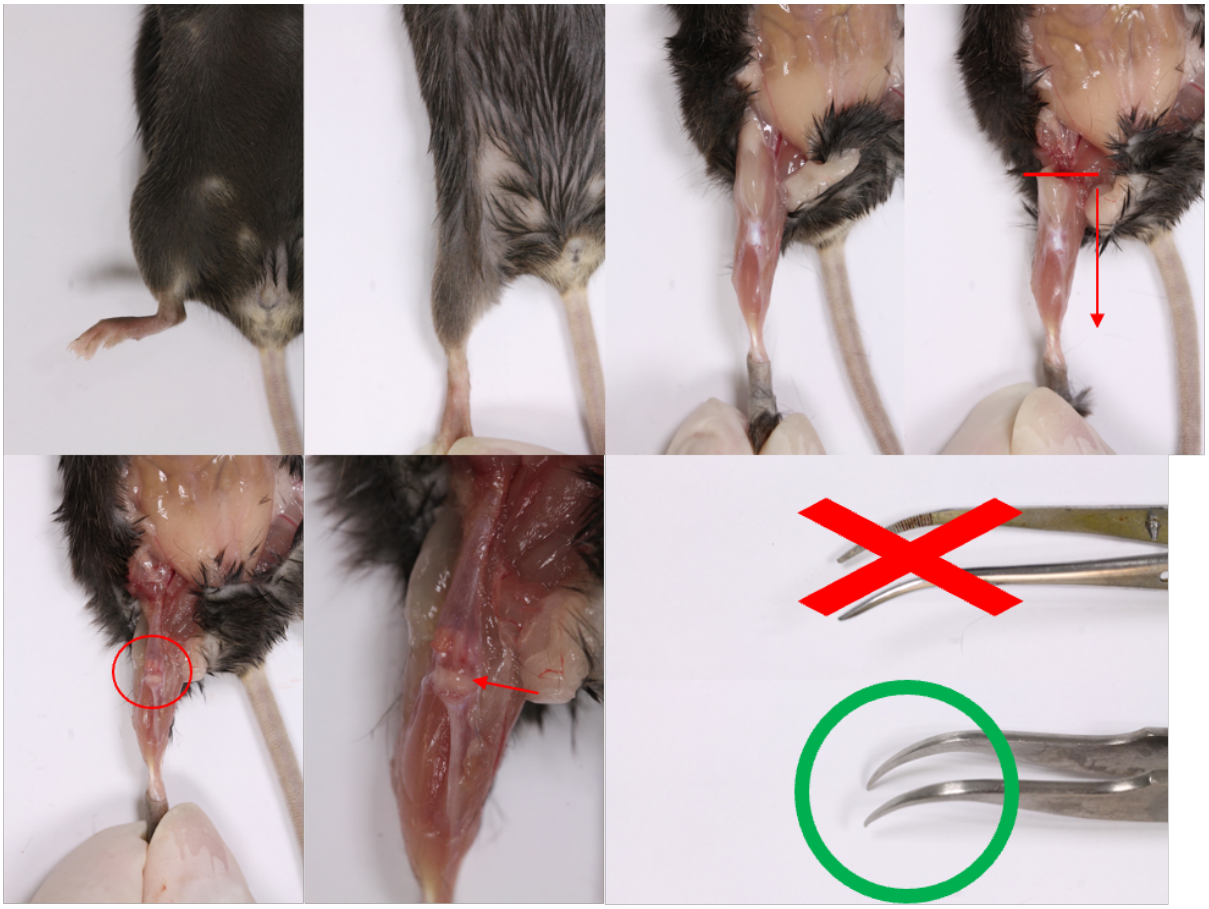

Figure 2.4. Synovium extraction. The leg was sprayed with 70% ethanol and the muscle, tendon, and patella were removed to expose the synovium for extraction. The extraction of the synovium was done only with non-ridged forceps.

2.6.2. Legs for micro-computed tomography (mCT) and histology

Mice were euthanised and the skin around the leg removed to expose the leg. Legs used for mCT and histology were taken from the hip joint to the ankle joint. Once extracted, the legs were placed in 10% formal saline (Table 2.5).

Table 2.5. Formal saline composition.

Reagents	Amount to be added
Sodium chloride (Sigma, UK)	9 g
Formaldehyde (Sigma, UK)	100 ml
Water	900 ml
Total	1000 ml

2.7. Histology and micro-computed tomography (mCT)

2.7.1. Bone fixation and mCT

Mice were killed and the hind legs dissected, and skin removed. Hind legs were placed in 10% formal saline and left for a minimum of 48 hours. These legs were the scanned using a ScanCo μCT40. The scan settings were as follows: 70kV, 114 mA, 8W. Each scan was 414 slices at medium resolution, with the patella used as an indication of the centre of the scan.

2.7.2. Bone decalcification and scout view

Fixed legs were decalcified in EDTA solution (Table 2.6) for ten days, changing the decalcifying solution every approximately 2.5 days. Fixed and fully decalcified hind legs were then sent to the Trinity Biomedical Sciences Institutes histology suite for processing.

Table 2.6. EDTA decalcifying solution composition.

Reagents	Amount to be added
EDTA (Sigma, UK)	200 g
Sodium hydroxide (Sigma, UK)	32 g
PBS	1000 ml
Mixed until all dissolved	
Adjusted solution to pH7.4 using hydrochloric acid	
Brought volume up to 1333 ml	

Tissues received back from processing were dehydrated via six increasing concentrations of ethanol baths (70%, 95% then 100% four times for 60 – 120 seconds each time), followed by two xylene baths and two paraffin (58°C) baths for 60 seconds each and left overnight in liquid paraffin.

2.7.3. Slide preparation

Processed samples were submerged in molten paraffin in the paraffin embedding station (Leica EG1150H) and samples were embedded by placing them in moulds with liquid paraffin in the desired orientation. A backing was placed on top, and the mould filled to the top with liquid paraffin. Moulds were left on a cooling plate (Leica EG1150C)

for approximately 30 minutes at 4°C to solidify the block. Once solidified the embedded samples were taken out of the moulds and sectioned. Embedded samples were cut using a microtome (Leica RM2235) at 5 μm and placed onto water at 50°C. Sections were placed on glass slides and left to dry overnight.

2.7.4. Haematoxylin and eosin (H&E) staining

Haematoxylin binds to basophilic substances, such as DNA and RNA, and stains the structures violet. Eosin binds to acidophilic substances, such as proteins in the cytoplasm, and stains the structures pink. Slide sections were deparaffinised in xylene for 10 minutes. They were then rehydrated in decreasing concentrations of industrial methylated spirit (IMS) (100% for 6 minutes, 95% for 6 minutes and 70% for 3 minutes) until rehydrated in water for 3 minutes. Slide sections were then placed in haematoxylin stain (VWR, USA) for 8 minutes then washed with water. They were then placed in eosin stain (VWR, USA) for 3 minutes then washed with water. Slide sections were dehydrated in increasing concentrations of IMS (70% for 1 minute, 95% for 2 minutes and 100% for 3 minutes) and then cleared in xylene for 20 minutes. Coverslips were fixed on each slide using DPX mountant (Sigma, UK) and left to dry overnight before imaging.

2.7.5. Perls' Prussian blue staining

Dilute mineral acid hydrolysis occurs due to the addition of hydrochloric acid in the reaction, which causes ferric ions to be released from protein bound tissue deposits. Potassium ferrocyanide binds to ferric ions and this reaction causes the formation of ferric ferrocyanide, Prussian blue.

$$K_4[Fe^{II}(CN_6)] + Fe^{III}Cl_3 = KFe^{III}[Fe^{II}(CN_6)] + 3KCl$$

Due to presence of haemosiderin deposition, which is a source of ferric iron, the above reaction may occur. Thus, any haemosiderin deposition that may be present in samples shows as a Prussian blue colour, in contrast to the light pink colour that the rest of the tissue is stained. Slide sections were deparaffinised in xylene for 10 minutes. They were then rehydrated in decreasing concentrations of IMS (100% for 6 minutes, 95% for 6 minutes and 70% for 3 minutes) until rehydrated in water for 3 minutes.

Equal amounts of potassium ferrocyanide (4%) solution (Sigma, UK) and hydrochloric acid (4%) (Sigma, UK) were mixed together to provide a working solution. Slide sections were then placed in the working solution twice for 10 minutes each time, rinsing with distilled water between each change. The slides were then counterstained with nuclear fast red (Sigma, UK) for 3 minutes and then rinsed in running tap water for 1 minute. The slides were quickly dehydrated in increasing concentrations of IMS (10 dips in 95% and 20 dips in 100%) and were then cleared in xylene for 6 minutes. Coverslips were fixed on each slide using DPX mountant and left to dry overnight before imaging.

2.7.6. Safranin O staining

Safranin O staining allows for clear visualisation of bone structure, particularly the cartilage and mucin. Cartilage, mucin, and mast cells are stained a red-orange colour and the amount present is proportional to the intensity of the colour stained on the slide. Nuclei appear black with safranin O staining and cytoplasm stains a blue-green colour. Slide sections were deparaffinised in xylene for 10 minutes. They were then rehydrated in decreasing concentrations of IMS (100% for 10 dips and 95% for 10 dips) until rehydrated in water with 3 changes of water. Slides were stained with Weigert's haematoxylin working solution (Sigma, UK) for 10 minutes followed by a wash in running tap water for 10 minutes. They were then stained with fast green solution (Sigma, UK) for 5 minutes and rinsed quickly in 1% acetic acid for no more than 10 – 15 seconds. The slides were then stained in 0.1% safranin O solution (Sigma, UK) for 5 minutes. The slides were quickly dehydrated in increasing concentrations of IMS (10 dips in 95% and 20 dips in 100%) and were then cleared in xylene for 6 minutes. Coverslips were fixed on each slide using DPX mountant and left to dry overnight before imaging.

2.7.7. Image and scoring

All slides were scanned using Aperio Scanscope software and equipment and imaged using Aperio Scanscope software and Leica DM3000 LED microscope. Sections of knee joints were scored using the histological HA score from Vøls *et al.,* 2019 (Table 2.7) (Vols et al., 2019).

Table 2.7. Histological HA score. Taken from Vøls *et al.* 2019 (Vols et al., 2019).

Score	0	1	2	3
Synovitis (Haematoxylin and eosin)	No changes	Increased numbers of lining cell layers and/or slight proliferation of subsynovial tissue	Increased number of lining cell layers. Moderate proliferation of subsynovial tissue and/or infiltration of few inflammatory cells	Increased number of lining cell layers. Massive proliferation of subsynovial tissue and/or infiltration of large numbers of inflammatory cells
Bone remodelling (Haematoxylin and eosin)	No bone remodelling	A single area of focal bone remodelling	Moderate bone remodelling covering <50% of the cortical bone surface, and/or formation of subchondral cysts	Severe bone remodelling covering >50% of the cortical bone surface, with or without subchondral cysts
Cartilage degradation (Safranin O)	No cartilage degradation	Loss of proteoglycan and/or chondrocytes in the superficial cartilage layer (above the tidemark) without structural changes	Loss of proteoglycan and chondrocytes extending through the calcified layer of cartilage, and/or fibrillations without loss of cartilage	Erosions extending through the calcified cartilage
Haemosiderin deposition (Perl's Prussian Blue)	No haemosiderin deposition	Minor haemosiderin deposition, with on average <5% of FOV in the three most intensely stained areas	Moderate haemosiderin deposition, with on average between 5-25% of FOV in the three most intensely stained areas	Severe haemosiderin deposition, with on average >25% of FOV in the three most intensely stained areas

2.8. Flow cytometry

2.8.1. Sample collection

Mice were killed and legs were extracted and placed in PBS, or 70% ethanol if needed to be kept sterile. In a cell culture hood, legs were removed from solution and placed extended in a sterile petri dish. Using a sterile disposable scalpel, an incision was made above and below the patella and removed with a pair of sterile forceps. The synovial capsule was exposed, and synovium removed using another pair of sterile forceps and placed in a tube containing 0.5 ml RPMI and 0.5 ml 1% collagenase D. The tubes were then left in a shaking incubator for 1 hour at 37°C at 200 rpm. The tubes containing the samples were then vortexed for 1.5 minutes before centrifuged at 300 x g for 5 minutes at 4°C. The resulting cell pellet was then resuspended in sterile RPMI (200 μl) and red blood cell lysis (BD Pharm lyse) performed for samples contaminated with blood. Cells were counted using a haemocytometer.

2.8.2. Staining

At all stages of staining and incubation periods, the cells were kept in the dark and at 4°C. Each washing stage of the staining process was performed at 1500 rpm at 4°C for 5 minutes. LIVE/DEAD™ Fixable Aqua Dead Cell Stain Kit (Molecular Probes, Invitrogen, Ireland) was used to assess cell viability at a 1 in 1000 dilution in PBS for 30 minutes. Cells were then washed in FACS buffer and incubated with Fc Block (BD Bioscience, UK) at 1 in 100 dilution with FACS buffer for 20 minutes. Fluorochrome-labelled cell surface antibodies were used at a 1 in 200 dilution with FACS buffer and incubated for 30 minutes before washing with FACS buffer. Cells were then resuspended in FACS buffer and events acquired on the flow cytometer.

2.8.3. Data collection and Analysis

Flow cytometry was performed in the flow cytometry facility in Trinity Biomedical Sciences Institute. A BD LSRFortessa was used alongside FACS Diva programme. All analysis was performed using FlowJo™ version 10.7.1.

The flow gating strategy utilised in this thesis is shown in Figure 2.5. Cells collected during flow cytometry were gated based on forward scatter (FSC) and side scatter (SSC), measuring the relative cellular height (size) and granularity, respectively.

Singlets were gated for further analysis, with double discrimination based on one excluding gate of FSC-A vs FSC-H. Live cells were gated for further analysis based on the negative staining for LIVE/DEAD™ Fixable Aqua Dead stain.

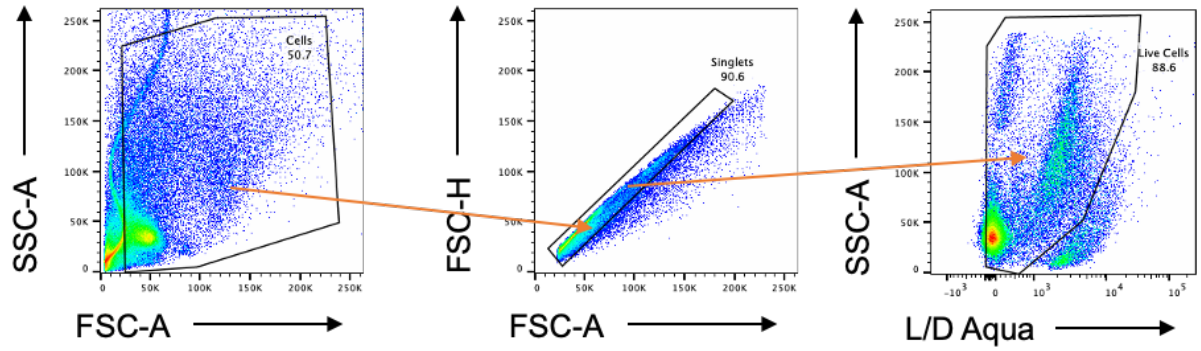

Figure 2.5. Representation of flow gating strategy. Cells were gated on the top flow plot, before gating on singlets, followed by gating for live cells. Orange arrows indicate cell population selected for further gating.

2.9. RNA

2.9.1. RNA Extraction

RNA was extracted from tissue using a Qiagen RNeasy Mini Kit (Qiagen, Germany). All equipment was cleaned before, after, and in between each sample using RNALater (Sigma, UK), 70% ethanol, and milli-Q water. Buffer RLT (350 µl) was added to each tube containing snap frozen tissue and homogenised using a tissue grinder (IKA T10 basic ULTRA-TURRAX). The tubes were then centrifuged for 3 minutes at 21,000 x g. The supernatant was taken, and equal parts of 70% ethanol was added and mixed by pipetting. 700 µl of the mixture was transferred to a RNeasy mini spin column. The columns were centrifuged for 15 seconds at 8,000 x g and the flowthrough discarded. 700 µl Buffer RW1 was added to the spin columns and centrifuged for 15 seconds at 8,000 x g and flowthrough discarded. 500 µl Buffer RPE was added to the spin columns and centrifuged for 15 seconds at 8,000 x g and flowthrough discarded. An additional 500 µl Buffer RPE was added to the spin columns and centrifuged for 2 minutes at 8,000 x g. The spin columns were then transferred to new 2 ml collection tubes and centrifuged for 1 minute at 21,000 x g to dry the membrane. The spin columns were then transferred to new 1.5 ml collection tubes. 30 µl RNase-free water was added directly to the membrane of each tube and incubated at room temperature

for 4 minutes. The spin columns were then centrifuged for 1 minute at 8,000 x g to elute the DNA. A Nanodrop was used to determine the concentration of each sample and stored at -80°C until further use or used immediately to convert to complimentary DNA (cDNA).

2.9.2. cDNA synthesis

For cDNA synthesis, QuantiTect Reverse Transcription Kit (Qiagen, Germany) was used to convert RNA to cDNA.

Template RNA was thawed on ice, and genomic DNA (gDNA) Wipeout Buffer, Quantiscript Reverse Transcriptase (RT), Quantiscript RT Buffer, RT Primer Mix, and RNase-free water were also thawed along with the RNA, and then kept on ice. The genomic DNA elimination was prepared on ice as according to Table 2.8 below.

Table 2.8. gDNA elimination reaction master mix.

Reagents	Amount to be added
gDNA Wipeout Buffer	2 μl
Template RNA	3 μl
RNase Free Water	9 μl
Total Volume	14 μl

Samples were incubated for 2 minutes at 42°C, then placed immediately on ice. The RT master mix was then prepared according to Table 2.9 below.

Table 2.9. RT reaction master mix.

Reagents	Amount to be added
Quantiscript Reverse Transcriptase	1 μl
Quantiscript RT Buffer, 5x	4 μl
RT Primer Mix	1 μl
Entire gDNA Elimination Reaction	14 μl
Total Volume	20 μl

RNA from the gDNA elimination reaction was added to each tube containing the RT reaction master mix. Samples were then incubated for 30 minutes at 42°C, followed by an incubation for 3 minutes at 95°C. The samples were then either placed on ice and proceeded directly with real-time PCR or stored at -20°C until further use.

2.9.3. Reverse transcription-quantitative PCR (RT-qPCR)

TaqMan assay primers were used for analysis as per Table 2.10 from ThermoFisher. The genes listed in Table 2.10 were chosen based on previous experiments in HA but also research in RA and OA. The genes are involved in the inflammation of the diseases, either in an anti- or pro-inflammatory way.

Table 2.10. TaqMan RT-qPCR assay primer list.

Target gene	TaqMan Probe
Tnf	Mm00443258_m1
Il6	Mm00446190_m1
Il1b	Mm01336189_m1
Il4ra	Mm01275139_m1
Il33	Mm00505403_m1
Il1rl1	Mm00516117_m1

2.9.4. NanoString nCounter Analysis

Synovial RNA was normalized to 30 ng/μl and processed for NanoString analysis using nCounter Mouse Immunology Panel (561 genes (547 immunology-related mouse genes and 14 internal reference controls; XT-CSO-MIM1-12)) and nCounter Mouse Myeloid Panel (754 genes (734 immunology-related mouse genes and 20 internal reference controls; PP-MMII2-12)). Samples were analysed on a NanoString nCounter MAX Analysis system (NanoString Technologies Inc, UCD, Ireland). Subsequent analysis was performed using nSolver software. NanoString nCounter analysis utilises the RNA directly to analyse gene expression. The RNA strands are directly targeted with specific capture and reporter probes for the gene of interest to form a target-probe complex. Once excess probes are removed, the complexes are immobilised on the surface before counting the reporter probes and analysed through

the software. The use of RNA samples directly reduces any variability that might be caused due to conversion to and amplification of cDNA.

2.10. Enzyme-linked Immunosorbent Assay (ELISA)

2.10.1. Cytokine ELISA

2.10.1.1. Tissue Factor (TF) ELISA

TF ELISA kit (R&D systems, Germany) was used to analyse plasma samples from mice. Washing steps were done three times by tipping contents of the plate out into the sink and then using PBST (see Table 2.11 for reagent constitution) before removing the liquid from the plate, by tapping on the bench until dry. Plates were coated with the capture antibody (50 μl), using the working concentration (42 μl in 5 ml PBS). Wet tissue paper was added to a lidded container, the ELISA plate placed into the container and sealed. This was left overnight in the fridge. The plate was washed followed by a blocking step, where 1% BSA/PBS (300 μl) was added to each well and incubated at room temperature for one hour. The plate was washed before the working concentration (75 μl in 500 μl 1% BSA/PBS) of standard was added (100 μl), with the top standard (A) being the working concentration followed by a 1 in 2 dilution from rows B – G, and the last two wells acting as blanks with no standard present. Plasma samples (50 μl) were then added as unknowns to the plate and incubated at room temperature for 2 hours. The plate was washed and detection antibody (50 ml; working concentration: 84 μl in 5 ml 1% BSA/PBS) added and incubated at room temperature for 2 hours. The plate was washed and diluted streptavidin-HRP (50 μl) was added to each well, then incubated at room temperature for 20 minutes in darkness. The plate was washed, and substrate solution (50 μl) was added to each well before incubating at room temperature for another 30 minutes in darkness. Once the colour was developed, stop solution (25 μl) was added to each well and plate was read at 490 nm using Soft Max Pro 5.4.

2.10.1.2. von Willebrand Factor (vWF) ELISA

For the vWF ELISA, mouse vWF ELISA kit (AssayGenie, Ireland) was used to analyse plasma samples from mice. All reagents were brought to room temperature before starting the assay. Wash buffer was made up according to manufacturer's instructions,

as seen in Table 2.11. The wash steps included adding wash buffer (350 μl) to each well, incubating for 1 – 2 minutes, before decanting the solution tapping the plate on the bench to dry. The wash step is repeated three times each time. Standard solutions were by centrifuging the standard at 10,000 x g for 1 minute before adding Reference Standard and Sample Diluent (1 ml) before inverting to mix. The dissolved solution was used as the top standard and the remaining seven were diluted from the top standard by a 1 in 2 dilution, with the last standard being blank for the control well. Both the biotinylated detection antibody and the concentrated HRP conjugate were diluted from a 100x solution to a working concentration of a 1x solution. The standards, control standard, and samples (50 μl each) were added to each well. The plate was sealed and incubated at 37°C for 90 minutes. Liquid was aspirated from the plate and working solution biotinylated detection antibody (50 μl) was immediately added to each well. The plate was resealed and incubated at 37°C for 1 hour. The plate was then washed before HRP Conjugate (50 μl) was added to each well. It was then resealed and incubated at 37°C for 30 minutes. The plate was decanted, and the wash step repeated before adding Substrate Reagent (90 μl) to each well. The plate was resealed and incubated at 37°C for 15 minutes in darkness. Stop solution (50 μl) was added to each well after 15 minutes and the plate read immediately at 450 nm using Soft Max Pro 5.4.

2.10.2. Multiplex analysis assay

Meso Scale Discovery (MSD) multiplex assay kits (MSD, USA) were used to analyse a wide range of murine analytes (Appendix III). For each wash step, PBST (150 μl) was added to each well and tapped out on the bench until all liquid removed. This was repeated three times for each wash step. For one plate, each biotinylated antibody (200 μl) was added to the assigned linker (300 μl) and mixed by vortexing and incubating at room temperature for 30 minutes. Stop solution (200 μl) was then added to each tube and mixed by vortexing then incubated at room temperature for 30 minutes again. Each U-PLEX linker-coupled antibody (600 μl) was combined and mixed by vortexing and the solution made up to 6 ml with stop solution. Multiplex coating solution (50 μl) was added to each well. The plate was sealed and incubated at room temperature while shaking for one hour before the plate was washed. During this incubation period, the calibrators for the standard were brought to room

temperature and reconstituted using Diluent 41 (250 μl). Each calibrator (50 μl) was added and made up to 250 μl with Diluent 41 to be used as the top standard. The remaining 7 standards were made up by using a 1 in 4 dilution, with the final dilution being blank and having no calibrator. Once the plate was washed, standards (25 μl) were added into columns 1 and 2 and samples (25 μl) were added as unknowns. Diluent 41 (25 μl) was then added to each well. The plate was incubated shaking at room temperature for one hour. During this incubation period, each 100x detection antibody (60 μl) was combined and volume brought up to Diluent 45. Once the plate was washed, the detection antibody solution (50 μl) was added to each well and incubated shaking at room temperature for one hour. The plate was then washed, and MSD GOLD Read Buffer B (150 μl) was added to each well before bringing the plates to read using the MSD Workbench 4.0 programme.

Table 2.11. Reagent constitution for TF ELISA, vWF ELISA, and MSD assay.

Reagent	Constitution
PBST (TF ELISA, MSD assay)	0.05% Tween in PBS
Phosphate citrate buffer (TF ELISA)	7.38 g $Na_2HPO_4.12H_2O$, 2.04 g Citric acid, 200 ml distilled H_2O, pH adjusted to pH 5
1% BSA/PBS (TF ELISA)	1 g BSA, 100 ml PBS
Wash buffer (vWF ELISA)	30 ml Concentrated Wash Buffer, 720 distilled H_2O

2.11. FIX Assay

FIX complex replacement has been indicated in some PwsH, where inhibitors to rFVIII have rendered haemophilia A treatments ineffective (Quade-Lyssy et al., 2014). The FIX complex, working independently of FVIII activity, could potentially be an effective treatment for PwsH who have developed inhibitors. Thus, I used an FIX assay to measure the levels in some of the mouse models in this thesis. Biophen™ FIX chromogenic assay (Hyphen Biomed, Germany) was used to analyse the level of FIX protein activity. Calibrators and controls were reconstituted as per manufacturer's instructions. Calibrators were diluted using R4 buffer and a high range (5 – 200%) dilution series was made using a 1 in 50 dilution for the top standard. Samples were diluted 1 in 100 using R4 buffer for the assay and then the following amounts were

added to the 96-well plate. Calibrators and samples (50 μl each) were added to the plate incubated at 37°C. Reconstituted R1 reagent (50 μl) was added to each well, mixed, and incubated at 37°C for 2 minutes. Then reconstituted R2 reagent (50 μl) was added to each well, mixed, and incubated at 37°C for 3 minutes. Then reconstituted R3 reagent (50 μl) was added to each well, mixed, and incubated at 37°C for 2 minutes. The reaction was then stopped by adding 20% acetic acid (50 μl) to each well. Once stopped, the plate was read immediately at 405 nm using Soft Max Pro 5.4.

2.12. Statistical Analysis

Statistical analysis was conducted by unpaired Student or paired *t* test, Welch's *t* test, Mann-Whitney test, or one-way ANOVA on GraphPad Prism (Version 8.0), with the relative test(s) indicated in the figure legends. Unpaired Student *t* test was used in the context of two independent groups of equal sizes. Paired *t* test was used in the context of dependent samples. Welch's *t* test was used in the context of two independent groups of unequal sizes. Mann-Whitney test was used in the context of two independent groups, but the assumption of normality was not met. One-way ANOVA was used to compare three or more groups. Data were represented as mean ± standard deviation (SD) or mean ± standard error of mean (SEM), used as appropriate and indicated in figure legends. Lowest and highest sample sizes (n) were given as a range when groups were not of equal sample size. Differences were expressed as two-tailed *p* values, where $p < 0.05$ is assessed as statistically significant. Each *p* value range was determined as ns = $p \geq 0.05$, * = $p < 0.05$, ** = $p < 0.01$, *** = $p < 0.001$, and **** = $p < 0.0001$.

The analysis for human assays was performed by a lab member using log-transformation and standardised to generate normal distributions. The resulting values were expressed as unit measures in SDs above or below the population mean (mean = 0). Values within ± 3 SD units from the mean were considered reliable after log transformation and standardisation.

Chapter 3 – The *F8$^{em1-/-}$* Model at Basal Phenotype and during Experimental Haemophilic Arthropathy

3.1. Results

The creation of a new mouse model guided our lab to analyse whether it was suitable for use as a model of severe haemophilia A. With prolonged aPTT and bleeding time, and undetectable FVIII activity, previous lab members have shown that this model was indeed suitable to be used as a mouse model of severe haemophilia A. The *F8$^{em1-/-}$* mouse model was comparable with the *F8$^{tm1-/-}$* mouse model. However, previous lab members noted spontaneous bleeding in the *F8$^{em1-/-}$* mice (Byrne, 2021).

With the differences seen in previous lab members' data, I wanted to investigate the development of haemophilic arthropathy in *F8$^{em1-/-}$* mice. I sought to further identify any basal differences in the *F8$^{em1-/-}$* mouse model at different ages before moving on to the mouse model in the context of development in an experimental HA model. Thus, investigating whether there were any differences depending on age in the mouse model. To understand and to be able to identify any differences found during the experimental HA time course, I first applied the same techniques to determine the basal phenotype before investigating the experimental HA time course.

Thus, my aims for this chapter were to identify any basal phenotypes of the *F8$^{em1-/-}$* mice, to characterise the progression of HA in *F8$^{em1-/-}$* mice, and to identify any variations in specific genes during HA progression in *F8$^{em1-/-}$* mice.

3.1.1. There is no significant difference in the basal phenotype of 11-week-old male *F8$^{em1-/-}$* mice when compared to matched WT controls

Before inducing HA in *F8$^{em1-/-}$* mice, the basal level at 11-weeks old was first investigated. mCT and histological analyses were used. mCT was used to identify any differences that may be present in bone volume and density between WT and *F8$^{em1-/-}$* mice. H&E staining was used to identify synovitis and bone remodelling. Safranin O staining was used to identify any differences in cartilage degradation. Perls' Prussian Blue staining was used to identify any deposits of haemosiderin.

There were no significant differences between the knee joints of WT and *F8$^{em1-/-}$* mice when analysed using mCT. In Figure 3.1 (A) we see representative images of the graphs in Figure 3.1 (B) where volume and density had no significant difference between the two groups. The histological results also reflected this. H&E staining, as in Figure 3.1 (C) and (D), showed no difference in bone remodelling. However, it is of interest to note that while there were no signs of synovitis in either the WT control group nor the *F8$^{em1-/-}$* group, the *F8$^{em1-/-}$* group had a slightly thinner synovial membrane when compared with matched WT control mice. Analysing the knee joint using Safranin O staining, as in Figure 3.1 (E) and (F), we see no difference in cartilage degradation between the two groups. There was also no significant difference seen between the two groups when looking for haemosiderin deposition, with no deposits found in either group as seen in Figure 3.1 (G) and (H).

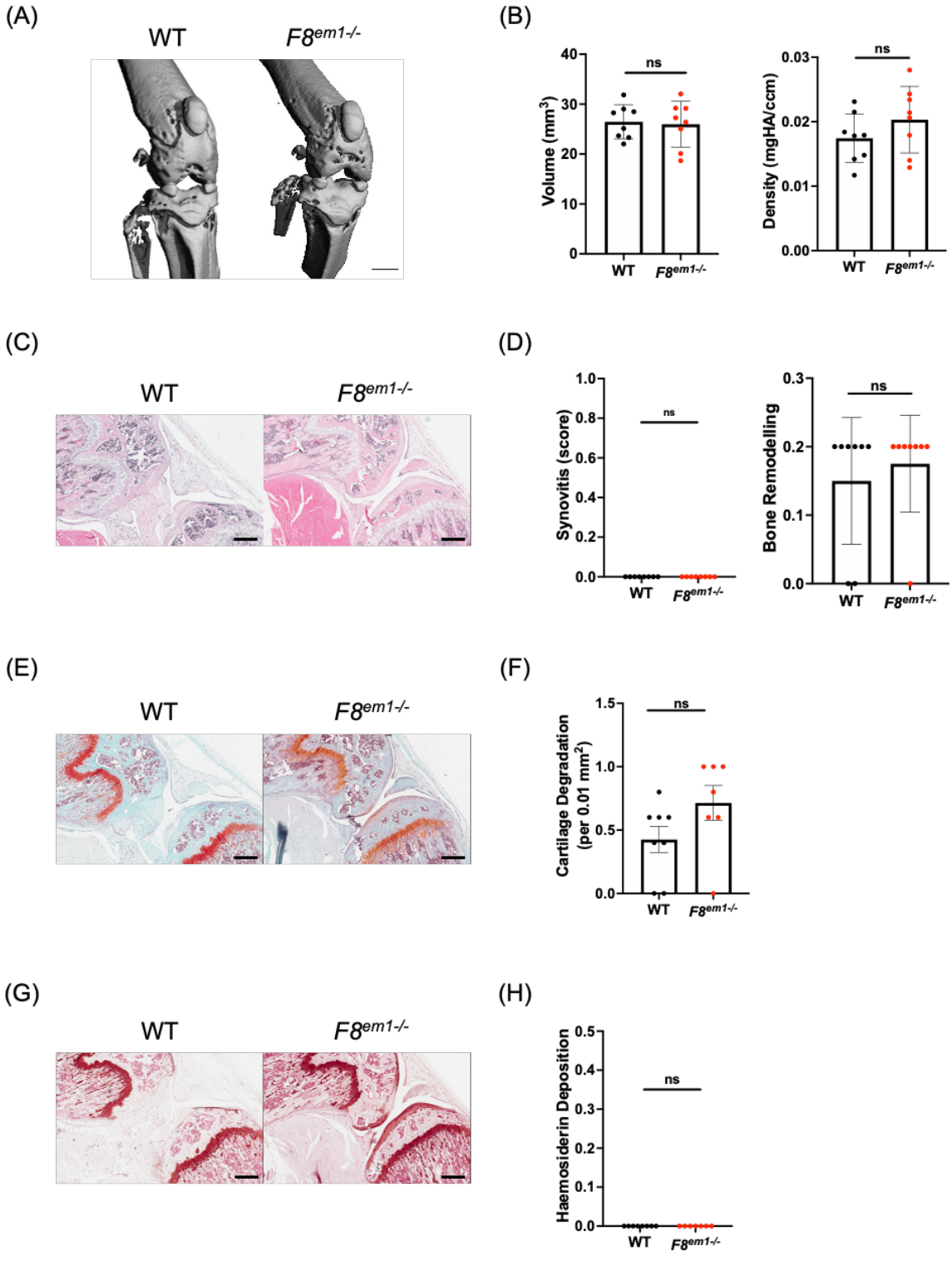
(A)
WT
F8em1-/-
(B)
Volume (mm3)
Density (mgHA/ccm)
ns
WT
F8em1-/-
(C)
WT
F8em1-/-
(D)
Synovitis (score)
Bone Remodelling
ns
WT
F8em1-/-
(E)
WT
F8em1-/-
(F)
Cartilage Degradation (per 0.01 mm2)
ns
WT
F8em1-/-
(G)
WT
F8em1-/-
(H)
Haemosiderin Deposition
ns
WT
F8em1-/-

Figure 3.1. mCT and histology analysis of *F8*$^{em1-/-}$ mice compared to matched WT control mice showed no significant difference in basal phenotype at age 11-weeks old. (A) 3D scans of representative images of WT and *F8*$^{em1-/-}$ mice legs using a ScanCo μCT40. Bar = 1 mm. **(B)** Bone volume and density analysis of WT and *F8*$^{em1-/-}$ mice (n = 8). Graphs presented as mean ± SD. **(C)** H&E staining of representative images of graphs of synovitis and bone remodelling in (D). Bar = 400 μm. **(D)** Synovitis and bone remodelling in WT and *F8*$^{em1-/-}$ mice (n = 8). Graphs presented as mean ± SD. **(E)** Safranin O staining of representative images of graph in (F) of cartilage degradation. Bar = 400 μm. **(F)** Cartilage degradation in WT and *F8*$^{em1-/-}$ mice (n = 7 – 8). Graph presented as mean ± SEM. **(G)** Perls' Prussian Blue staining of representative images of graph in (H) of haemosiderin deposition. Bar = 400 μm. **(H)** Haemosiderin deposition analysis in WT and *F8*$^{em1-/-}$ mice (n = 7 – 8). Graph presented as mean ± SEM. Statistical analysis using Welch's *t* test.

3.1.2. There is no significant difference in the basal phenotype of 6-month-old male *F8$^{em1-/-}$* mice when compared to matched WT controls

To further investigate whether any differences would arise in the *F8$^{em1-/-}$* mouse model compared to WT mice due to aging, the same techniques used at 11-weeks old were employed to further analyse any differences that may arise at age 6-months old in the groups.

Overall, there were no major differences in the *F8$^{em1-/-}$* mouse model when compared to matched WT control mice. In Figure 3.2 (A) and (B) we see that during mCT analysis we see no visual difference and there are also no significant differences between the two groups in the volume or density. Similar to what we see at 11-weeks old, there is no significant difference between the two groups histologically. There was no signs of synovitis or bone remodelling, as seen in Figure 3.2 (C) and (D), when using H&E staining to identify the structures. There was no significant difference between the two groups in cartilage degradation nor haemosiderin deposition as seen from the safranin O and Perls' Prussian blue staining in Figure 3.2 (E) and (F), and in Figure 3.2 (G) and (H), respectively.

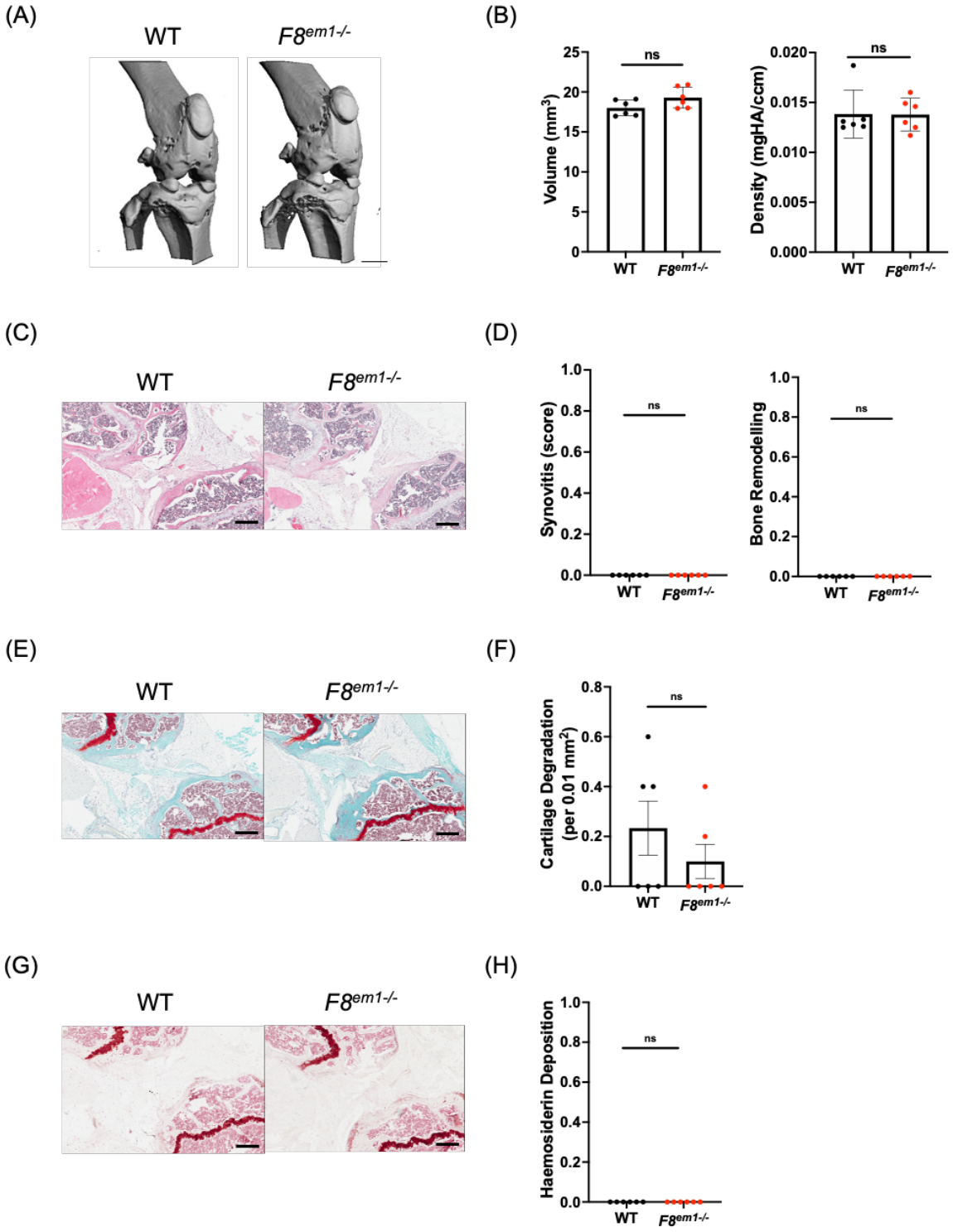
(A)
WT
F8em1-/-
(B)
Volume (mm3)
Density (mgHA/ccm)
ns
WT
F8em1-/-
(C)
WT
F8em1-/-
(D)
Synovitis (score)
Bone Remodelling
ns
WT
F8em1-/-
(E)
WT
F8em1-/-
(F)
Cartilage Degradation (per 0.01 mm2)
ns
WT
F8em1-/-
(G)
WT
F8em1-/-
(H)
Haemosiderin Deposition
ns
WT
F8em1-/-

Figure 3.2. mCT and histology analysis of *F8*$^{em1-/-}$ mice compared to matched WT control mice showed no significant difference in basal phenotype at age 6 months old. (A) 3D scans of representative images of WT and *F8*$^{em1-/-}$ mice legs using ScanCo μCT40. Bar = 1 mm. **(B)** Bone volume and bone density analysis of WT and *F8*$^{em1-/-}$ mice (n = 6). Graphs presented as mean ± SD. **(C)** H&E staining of representative images of graphs of synovitis and bone remodelling in (D). Bar = 400 μm. **(D)** Synovitis and bone remodelling analysis of WT and *F8*$^{em1-/-}$ mice (n = 6). Graphs presented as mean ± SD. **(E)** Safranin O staining of representative images of graph of cartilage degradation in (F). Bar = 400 μm. **(F)** Cartilage degradation analysis of WT and *F8*$^{em1-/-}$ mice (n = 6). Graph presented as mean ± SD. **(G)** Perls' Prussian Blue staining of representative images of graph of haemosiderin deposition in (H). Bar = 400 μm. **(H)** Haemosiderin deposition analysis of WT and *F8*$^{em1-/-}$ mice (n = 6). Graph presented as mean ± SD. Statistical analysis using Welch's *t* test.

3.1.3. Both the basal phenotype and experimental haemophilic arthropathy in male *F8*$^{em1-/-}$ mice are comparable to *F8*$^{tm1-/-}$ mice

While the *F8*$^{em1-/-}$ mice were comparable to matched WT mice at basal levels, I wanted to ensure that the *F8*$^{em1-/-}$ mice were also comparable to *F8*$^{tm1-/-}$ mice both during experimental HA and at basal levels. Previous data from the lab has already shown that the *F8*$^{em1-/-}$ mouse model displays the same characteristics as the *F8*$^{tm1-/-}$ mice when looking at aPTT, bleeding time etc (Byrne, 2021). However, there had been no previous data on the comparability during experimental HA. Thus, I sought to investigate any differences or similarities between the two groups.

During experimental HA, both the *F8*$^{em1-/-}$ mice and *F8*$^{tm1-/-}$ mice displayed the typical traits seen in experimental HA. Both had increased joint size (Figure 3.3 (A)) and lowered haematocrit levels (Figure 3.3 (B)) throughout the experiment before returning to normal levels. While there were significant differences between the two groups during experimental HA, the basal levels, as seen in Figure 3.3 (C – F), of the knee joint showed no differences when analysed using mCT and histology staining. These results showed that while both mouse models work as a model for HA, the *F8*$^{em1-/-}$ mouse model showed significantly more severe outcomes, when comparing joint size change and haematocrit, in the time course of experimental HA.

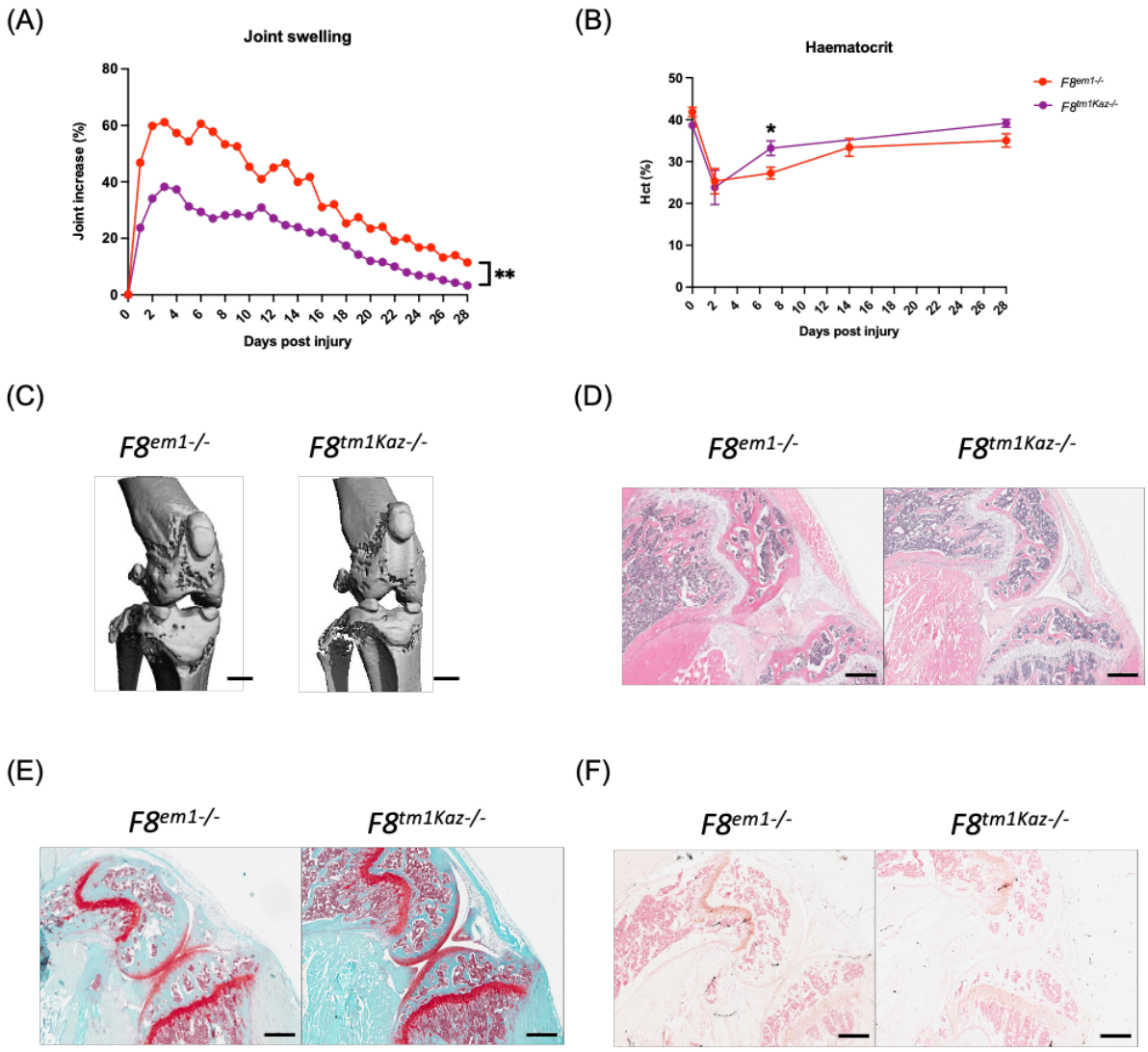

Figure 3.3. Experimental HA is suitable in *F8*$^{em1-/-}$ mice, comparable with the *F8*$^{tm1-/-}$ mice. (A) Percentage increase of joint measurements in *F8*$^{em1-/-}$ and *F8*$^{tm1-/-}$ mice (n = 7 – 18) during experimental HA. **(B)** Haematocrit levels of *F8*$^{em1-/-}$ and *F8*$^{tm1-/-}$ mice (n = 6 – 19) during experimental HA time points. **(C)** Representative mCT images of knee joints at basal level of *F8*$^{em1-/-}$ and *F8*$^{tm1-/-}$ mice. Bar = 1 mm. **(D)** Representative H&E histology images of knee joints at basal level of *F8*$^{em1-/-}$ and *F8*$^{tm1-/-}$ mice. **(E)** Representative Safranin O histology images of knee joints at basal level of *F8*$^{em1-/-}$ and *F8*$^{tm1-/-}$ mice. **(F)** Representative Perls' Prussian Blue histology images of knee joints at basal level of *F8*$^{em1-/-}$ and *F8*$^{tm1-/-}$ mice. Bar = 400 μm for (D – F). Statistical analysis using area under the curve followed by Student's *t* test.

3.1.4. *F8*$^{em1-/-}$ mice have a significant difference in bleeding and bone structure when compared to matched WT controls during experimental haemophilic arthropathy

Once established as a suitable model for experimental HA, I proceeded to investigate the progression in the new mouse model. Timepoints of Day 0, 2, 7, 14, and 28 were chosen throughout the experiment to analyse using mCT and histology staining that were used in previous experiments.

As the experiment progressed, the external bleeding increased greatly before resolving back to normal. As seen in Figure 3.4 (A), bleeding occurs around the knee joint where the injury was induced. The largest bleed seen on Day 2 compared to the other time points of the experiment, with haematocrit also being the lowest at this time point as well (Figure 3.3 (C and D)). However, while the bleeding was greatest seen at Day 2, this was not the case of the bone structure of the knee (Figure 3.3. (B)). As HA progressed, the bone structure was degraded and bone volume was decreased, with the lowest point of volume being on Day 7 compared to the other time points, as seen in Figure 3.3 (E). Along with the volume of bone, density also returned to within normal levels as the experiment progresses. Overall, the blood loss was reflected in the increase in joint size throughout the experiment, with lower haematocrit levels indicating bleeding into the joint, most significantly on Day 2. However, the onset of bone degradation was after Day 2 of the experiment.

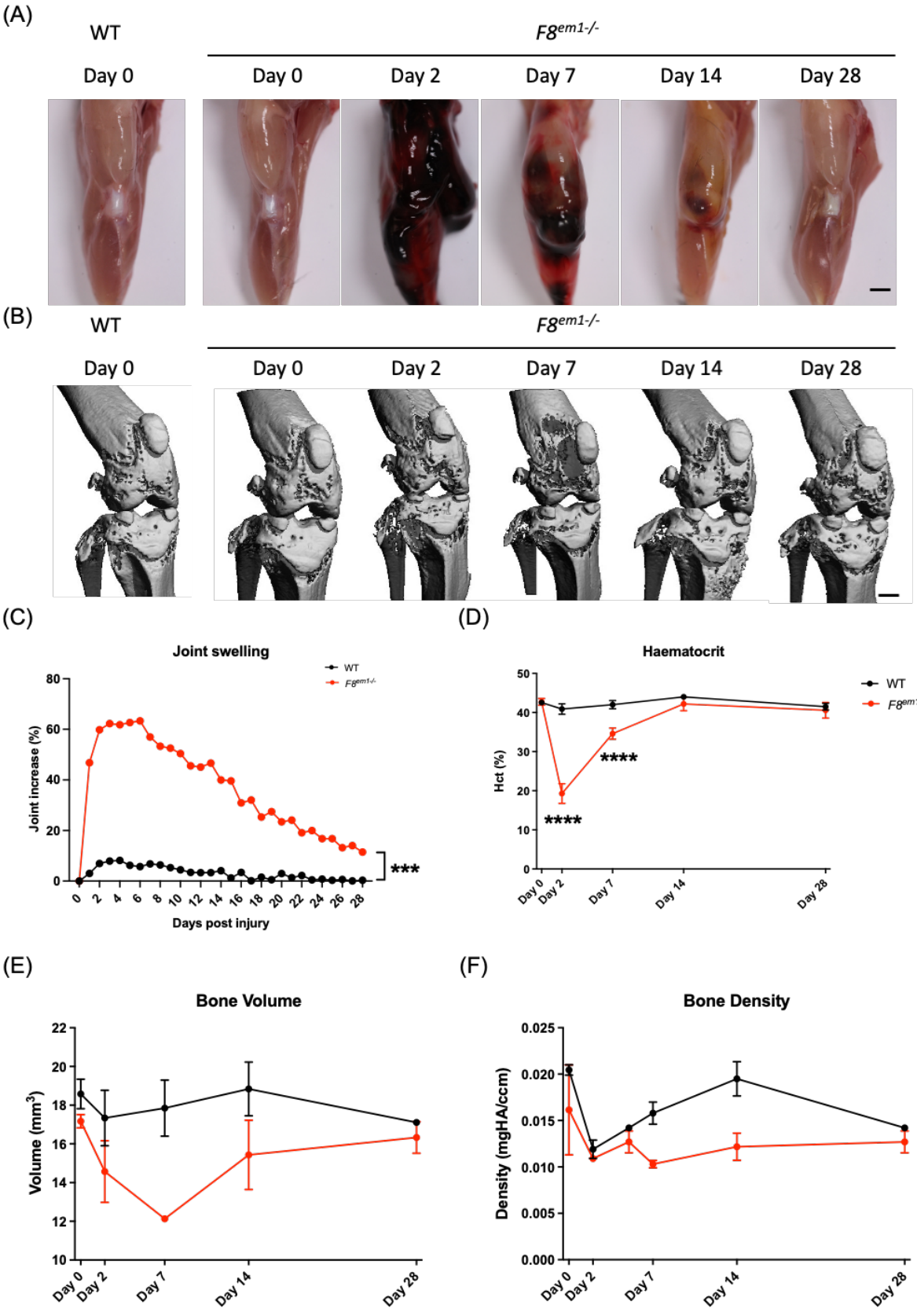
(A)
WT
F8em1-/-
Day 0
Day 0
Day 2
Day 7
Day 14
Day 28
(B)
WT
F8em1-/-
Day 0
Day 0
Day 2
Day 7
Day 14
Day 28
(C)
Joint swelling
WT
F8em1-/-
Joint increase (%)
Days post injury
***
(D)
Haematocrit
WT
F8em1-/-
Hct (%)
****
****
Day 0
Day 2
Day 7
Day 14
Day 28
(E)
Bone Volume
Volume (mm3)
Day 0
Day 2
Day 7
Day 14
Day 28
(F)
Bone Density
Density (mgHA/ccm)
Day 0
Day 2
Day 7
Day 14
Day 28

Figure 3.4. *F8*$^{em1-/-}$ mice showed significant differences during experimental HA compared to matched WT mice. (A) Images of external bleeding in knee joints of *F8*$^{em1-/-}$ mice during time points of experimental HA. Bar = 1 mm. **(B)** mCT images of knee joints of *F8*$^{em1-/-}$ mice during time points of experimental HA. Bar = 1 mm. **(C)** Percentage increase of joint measurements in *F8*$^{em1-/-}$ mice compared to matched WT mice (n = 12 – 18) during experimental HA. **(D)** Haematocrit levels of *F8*$^{em1-/-}$ mice compared to WT mice (n = 12 – 18) during experimental HA time points. **(E)** and **(F)** Bone volume and density of *F8*$^{em1-/-}$ mice compared to matched WT mice (n = 1 – 4) during experimental HA. Statistical analysis using area under the curve followed by Student's *t* test.

3.1.5. *F8*$^{em1-/-}$ mice show significant differences histologically when compared to matched WT controls during experimental haemophilic arthropathy

Previous data showed clear differences in the external bleeding and mCT analysis and further analysis using histological stains showed notable differences in the various time points throughout HA.

As seen in Figure 3.5 (A), H&E, Safranin O and Perl's Prussian Blue staining were applied to the sections of the knee joint from *F8*$^{em1-/-}$ mice from various time points throughout the time course of experimental HA. From induction of the injury, there was an increase in bleeding, as seen in Day 2 and Day 7, which slowly resolved thereafter. However, there was clear synovitis in the knee joint from Day 7 onwards and while this became attenuated as time progressed, even at the last time point (Day 28) we still saw signs of synovitis, as seen in Figure 3.5 (B). Bone remodelling also increased at Day 2, as seen in Figure 3.5 (C), and peaked at Day 7 before slowly returning within normal range by the end of the experiment. There was no significant difference in cartilage degradation throughout the experiment, with the only difference observed at the end of the experiment (Figure 3.5 (D)). While synovitis slowly decreased as the experiment progressed, haemosiderin deposition increased at Day 2 but remained elevated to the end of the experiment (Figure 3.5 (E)).

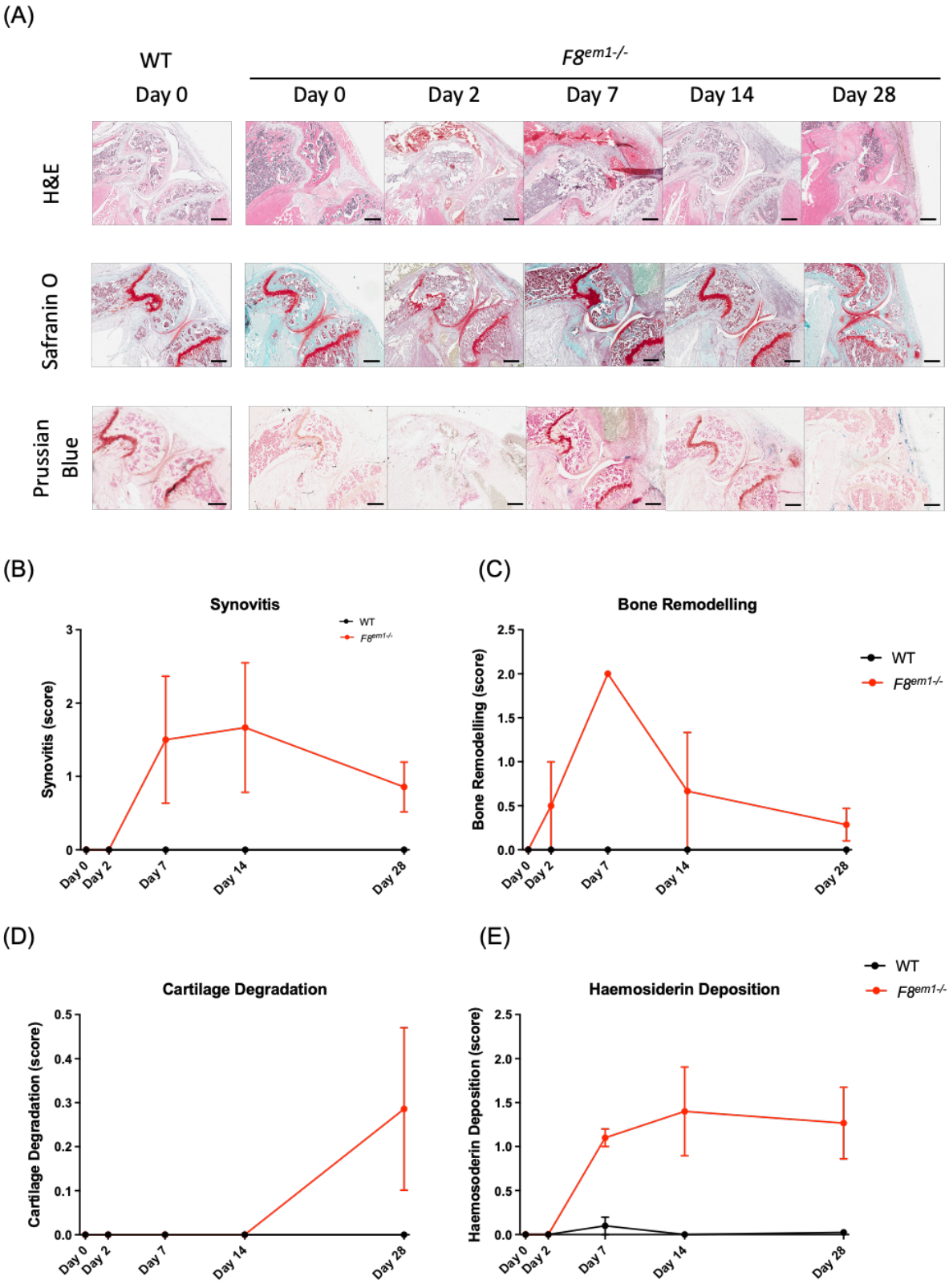
(A)
WT
Day 0
F8em1-/-
Day 0
Day 2
Day 7
Day 14
Day 28
H&E
Safranin O
Prussian Blue
(B)
Synovitis
WT
F8em1-/-
Synovitis (score)
Day 0
Day 2
Day 7
Day 14
Day 28
(C)
Bone Remodelling
Bone Remodelling (score)
(D)
Cartilage Degradation
Cartilage Degradation (score)
(E)
Haemosiderin Deposition
Haemosoderin Deposition (score)

Figure 3.5. *F8*$^{em1-/-}$ mice showed significant differences in the knee joint during experimental HA compared to matched WT mice. (A) Histology staining (H&E, Safranin O, Perls' Prussian Blue) showed notable differences in *F8*$^{em1-/-}$ mice compared to matched WT control mice during experimental HA. Bar = 500 μm. **(B)** Synovitis score of *F8*$^{em1-/-}$ mice compared to matched WT control mice (n = 2 – 7) during experimental HA. **(C)** Bone remodelling score of *F8*$^{em1-/-}$ mice compared to matched WT control mice (n = 2 – 7) during experimental HA. **(D)** Cartilage degradation score of *F8*$^{em1-/-}$ mice compared to matched WT control mice (n = 3 – 8) during experimental HA. **(E)** Haemosiderin deposition score of *F8*$^{em1-/-}$ mice compared to matched WT control mice (n = 2 – 9) during experimental HA. Statistical analysis using area under the curve followed by Student's *t* test.

3.1.6. RNA analyses of *F8*$^{em1-/-}$ mice showed significant differences when compared to matched WT control mice during experimental haemophilic arthropathy

The synovial capsule is largely affected by the progression of HA and thus I extracted the synovium from knee joints for analysis. RNA was extracted from the synovial membranes of mice at timepoints of the experiment (Day 0, Day 2, Day 7, Day 14, and Day 28). RNA samples were pooled at each time point to acquire high enough sample concentration for analysis, however limits the experiment to one biological replicate. The differential expression of genes was analysed using Multiplex qPCR NanoString analysis, with use of nSolver software for analysis. Pro-inflammatory- associated genes (Figure 3.6 (A)) were increased in the synovium post-injury, including *Tnf* and *Il1b* as well. The increase in expression was also confirmed using RT-qPCR (Figure 3.6 (B)).

nSolver analysis of the NanoString Innate Immunology cassette showed notable elevation in *Tnf*, *Il6*, *Il1b*, *Il4ra*, *Il1rl1*, and *Il33*. There was clear increase in expression on Day 2 for each gene as seen in the heat map in Figure 3.6 (A). The *F8*$^{em1-/-}$ mice were comparable to the WT mice at Day 0, with no elevation of gene expression. However, this increased drastically in the *F8*$^{em1-/-}$ mice Day 2 post-injury. Some genes remained elevated on Day 7 post-injury in the *F8*$^{em1-/-}$ mice, but expression for all genes returned to basal levels by Day 28.

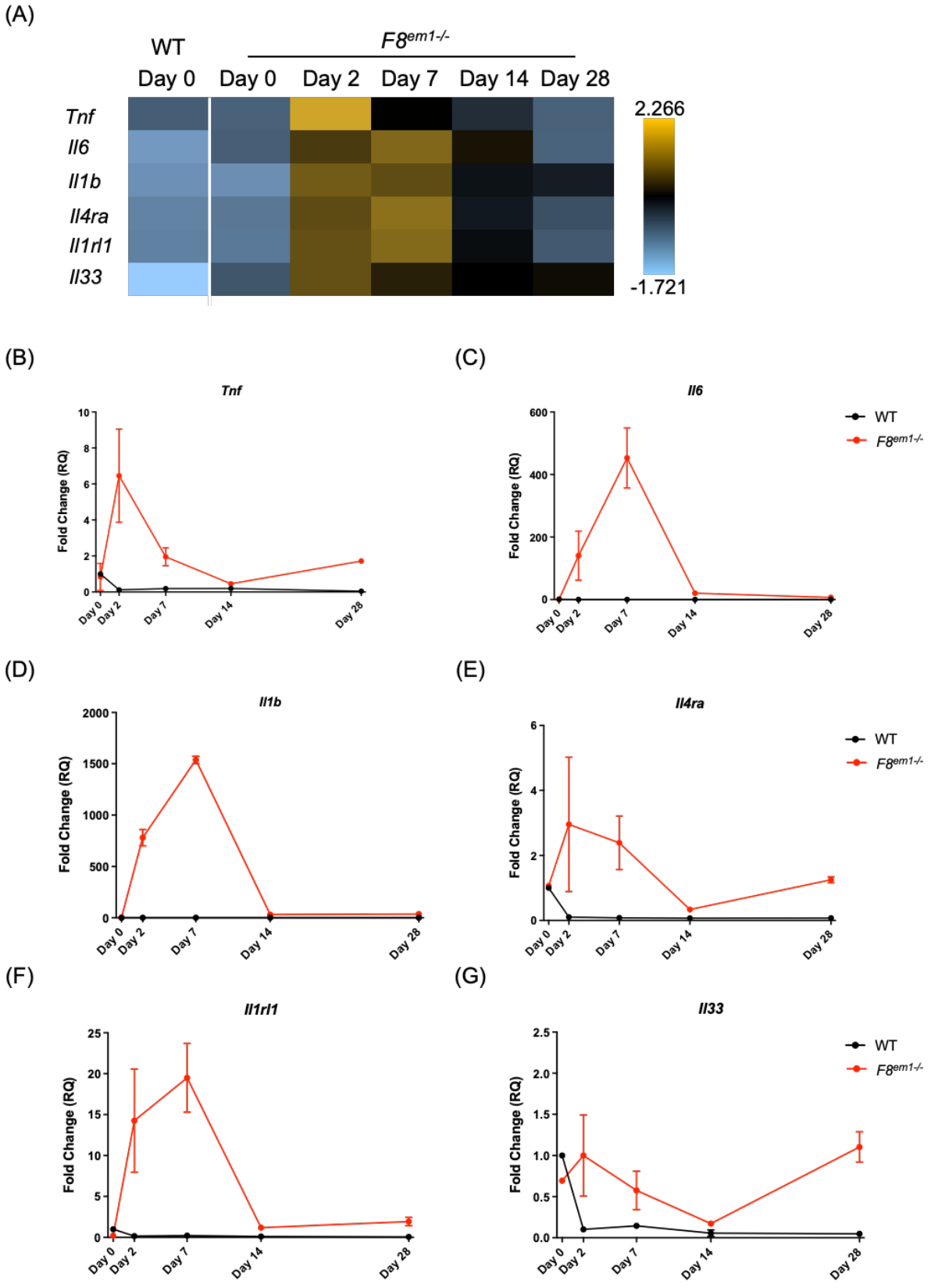
(A)
WT
F8em1-/-
Day 0
Day 0
Day 2
Day 7
Day 14
Day 28
Tnf
Il6
Il1b
Il4ra
Il1rl1
Il33
2.266
-1.721
(B)
Tnf
(C)
Il6
(D)
Il1b
(E)
Il4ra
(F)
Il1rl1
(G)
Il33
Fold Change (RQ)
WT
F8em1-/-
Day 0
Day 2
Day 7
Day 14
Day 28

Figure 3.6. RNA analyses of synovial samples of *F8*$^{em1-/-}$ mice during experimental HA showed significant differences compared to matched WT control mice. (A) Heat map of various genes upregulated during experimental HA. Synovium from individual mice (n = 3) were pooled for analysis. **(B – G)** RT-qPCR of *F8*$^{em1-/-}$ mice plasma samples during experimental HA compared to WT mice for *Tnf*, *Il6*, *Il1b*, *Il4ra*, *Il1rl1*, and *Il33*, respectively. Synovium from individual mice (n = 3) were pooled for analysis and run in duplicate. Statistical analysis using paired *t* tests.

3.1.7. Flow analysis of *F8*$^{em1-/-}$ mice on Day 2 when compared to *F8*$^{em1-/-}$ mice on Day 0 showed large increases in cell populations

With clear effects on the progression of HA when an induced injury occurs, I sought to find any immunological differences present within the knee joint. Using the methods stated in Chapter 2.8, the synovium was extracted and processed as per protocol. All samples collected for flow analysis was immediately placed in the RPMI/Collagenase D solution after extraction and processed in a timely manner.

The results, as seen in Figure 3.7 (A), showed a large increase in cells after the induction of HA on Day 2 in both the WT mice and *F8*$^{em1-/-}$ mice. The total number of live CD45^{+}CD11b^{+}F4/80^{+} macrophages was greatly increased in WT mice. However, the percentage of the total number of live macrophages was significantly less in the *F8*$^{em1-/-}$ mice compared to matched WT mice on both Day 0 and Day 2. Figure 3.7 (B) shows the pooled samples from each strain on Day 0 and Day 2, showing a great increase in CD11b^{+}F4/80^{+} macrophages in WT mice, but no significant difference in the *F8*$^{em1-/-}$ mice when comparing cell numbers as the percentage of live cells. In Figure 3.7 (C), the absolute numbers for both WT mice and *F8*$^{em1-/-}$ mice, comparing the absolute numbers of CD11b^{+}F4/80^{+} macrophages, are shown. While the *F8*$^{em1-/-}$ mice still showed a lower number of cells compared to the matched WT mice, both groups showed an increased in cells on Day 2 compared to Day 0.

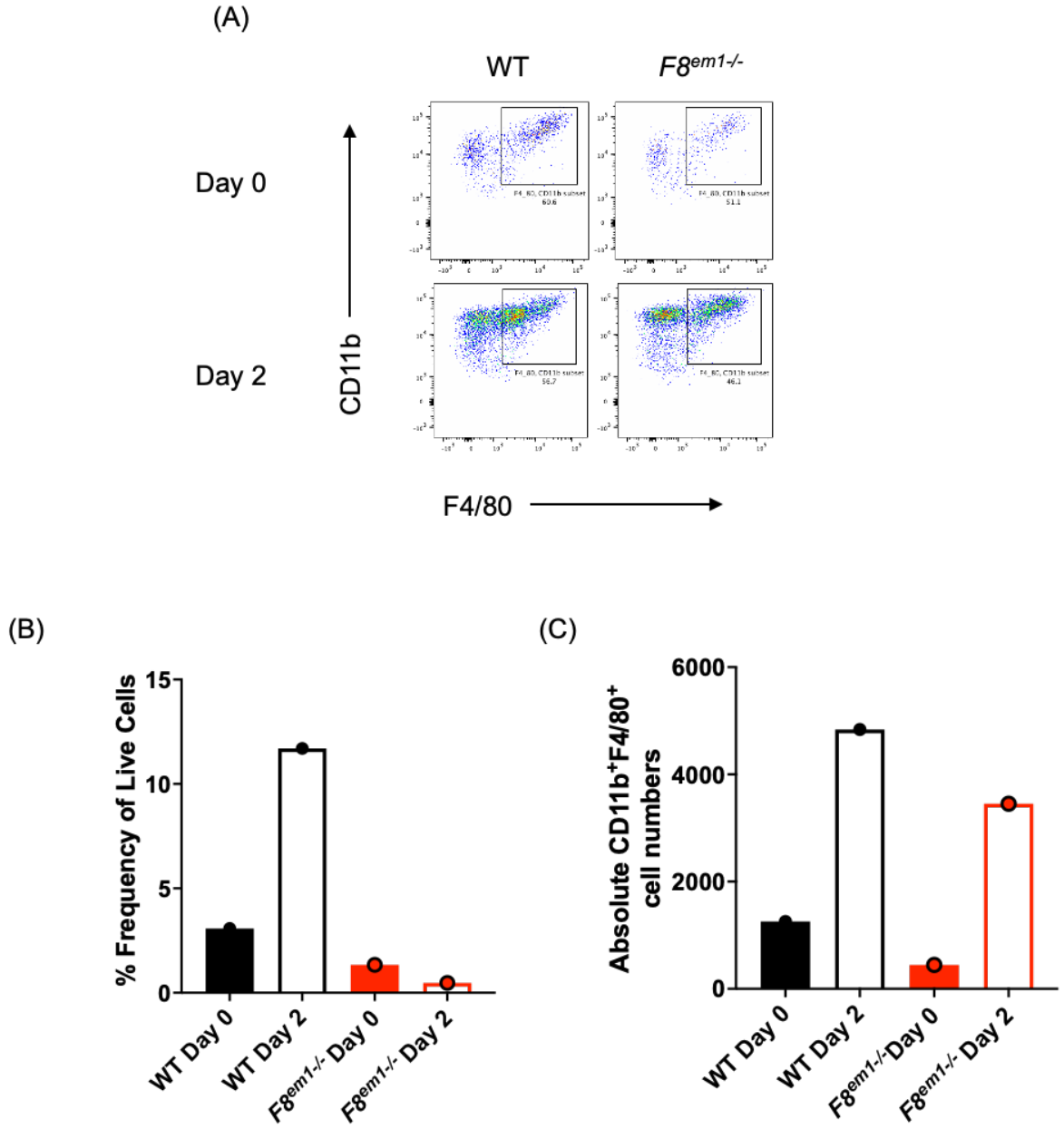

Figure 3.7. There is a large increase in absolute number of macrophages on Day 2 after induced HA in WT mice and the *F8*$^{em1-/-}$ mice. (A) Macrophages were identified as singlets, live cells, CD45^{+}, CD11b^{+}, F4/80^{+} cells. The number on the flow plot represents the CD11b^{+}F4/80^{+}. **(B)** Percentage frequency of CD11b^{+}F4/80^{+} cells in live cells in WT and *F8*$^{em1-/-}$ mice on Day 0 (pre-injury) and Day 2 (post-injury). **(C)** Absolute total CD11b^{+}F4/80^{+} cell numbers in WT and *F8*$^{em1-/-}$ mice on Day 0 (pre-injury) and Day 2 (post-injury). Synovium from individual mice (n = 3) were pooled for analysis. Statistical analysis using one-way ANOVA.

3.2. Discussion

The results from this chapter show that not only is the *F8*$^{em1-/-}$ mouse model suitable for use in an experimental haemophilic arthropathy model, but that it can be used to investigate the progression of HA as well in a 4-week time course.

Initially, with the new mouse model it was unsure if any specific characteristics would develop with age. In general, with skeletal development being an important stage during adolescence, we wanted to simulate this same age range in the mouse model. The ideal time to use the mice were at approximately 10 – 12 weeks of age. However, while this is useful to reflect such a critical time in skeletal development, I needed to be certain that any developments would not occur simply due to age and not just as a result of induced HA. Thus, by analysing the same basal levels in the 6-month-old *F8*$^{em1-/-}$ mice, I showed no significant differences in the age-matched WT mice. Thus, the analysis of the *F8*$^{em1-/-}$ mouse model compared to matched WT mice showed for certain that the following results were not a matter of artifacts due to aging.

The widely used *F8*$^{tm1-/-}$ mouse model proves to be a useful model for severe haemophilia A. However, as shown by previous lab members, this novel mouse model for severe haemophilia A, *F8*$^{em1-/-}$ mice, proved to be a more useful model with no risk of passenger mutations, as described in Chapter 1.6.2. Not only this, but the use of this model showed clear advantages as previously described in this chapter. The *F8*$^{em1-/-}$ mice showed spontaneous bleeding, including into and around the knee joint, which is more reflective of the human population and what occurs in PwH who develop HA.

While we see that bone structure, in terms of volume and density, returned back to within basal levels at the end of the 28-day experiment, during this time, the bone structure was weakened significantly. Similar to OA and RA, the risk of osteoporosis or any condition that may cause weakening of the bones can lead to an increase in fractures in bones. The pathogenesis of HA progresses to a normal level at the end of the experiment but during this period where bone integrity is compromised, the likelihood of injury is greatly increased. Inflammation is also increased in the joint, as seen with the elevation of pro-inflammatory genes during HA progression. This

actually occurs slightly prior to the degradation of bone and cartilage degradation; the order being inflammation occurring, followed by reduced bone integrity, and then increased cartilage degradation and haemosiderin deposition. What would be of interest to further research would be to see if attenuation of certain inflammatory genes impact the way HA progresses and whether or not it would increase or decrease the severity of the progression of the disease.

As mentioned, a number of both pro-inflammatory and anti-inflammatory associated genes were upregulated during the progression of HA, namely towards the beginning of the time-course. With the induction of the injury, increased expression of these genes was a predicted response with pro-inflammatory cytokines recruiting immune cells to the site of injury, and the production of anti-inflammatory cytokines to ensure that the inflammatory signalling did not go unchecked. With the increased expression of *Il4ra* in the synovium of *F8*$^{em1-/-}$ mice, this would indicate a potential role for Th2 response. As time progresses after the injury occurs, blood begins to pool within and around the knee joint so an immune response, both innate and adaptive, would be expected. However, in the experiment the *Il33* and *Il1rl1* (or *St2*) gene expressions were also elevated which may indicate a potential role for the IL33-ST2 axis. The stimulation of the IL-33/ST2 axis can directly affect the Th1 and Th2 response of the immune system which may potentially affect the progression of HA as well. With the peak of these genes being on Day 2 and Day 7, this indicates that a critical time point for the progression of HA is the first week occurring after the injury.

While my initial readings of literature led me to believe that perhaps macrophages would be the largest culprit in the progression of HA (Culemann et al., 2019, Cooke et al., 2018, Hooiveld et al., 2003c, Nieuwenhuizen et al., 2014), it seemed that there was another cell population at play here. As seen in the flow plots in Figure 3.7 (A), there was indeed an increase in macrophages as a response to the needle-induced injury. However, there was a clear population that were $CD45^{+}CD11b^{+}$ but $F4/80^{-}$. With that in mind, the likelihood of this population being neutrophils is extremely high, potentially indicating a role for neutrophils in the development and progression of HA. Of course, without further investigation, it would not be clear whether or not the increase of neutrophils had a major impact on the progression of HA. Particularly with the number of mice necessary to perform flow analysis on one experimental sample,

the use of flow to analyse this data was not sensible. The number of events collected was only possible up to one million and no further, even after using the full amount of synovium cells collected and further experimentation, with experimental replicates, would require more mice than using a different route to analyse immunity within the synovial capsule.

The data I have gathered here shows that the *F8*$^{em1-/-}$ mouse model is suitable for use as a model of severe haemophilia A, particularly in the investigations into the progression of HA. Not only that but there are clear significant differences present in the *F8*$^{em1-/-}$ mouse model that are not found in matched WT or *F8*$^{tm1-/-}$ mice. The severity of HA in this new mouse model indicates clearly in the progression of HA the potential critical time points in the development of the disease that could be used to focus on interventions to attenuate the severity of the disease. Not only this, but the clear elevation of gene expression at these critical timepoints is something that can be utilised to further analyse the specific genes and/or immune cells that are culprit to the progression of HA. This can and has been done in a number of manners but the use of novel mouse models, including dual-knockout mice and the *F8*$^{em1-/-}$ mouse model on various backgrounds as opposed to only C57BL/6J, is something to exploit as we will see in the following chapters.

Chapter 4 – Role of Innate Immunity in Haemophilic Arthropathy

4.1. Results

The increase in expression of multiple genes, as well as the increase in certain cell types, during the HA timeline indicates a role for immunity in the progression of the disease. Using novel mouse models, it may be possible to identify the specific cell type, or types, that may be specifically involved in the development and/or progression of HA.

The use of double knockout mice in research is not something novel. As mentioned in Chapter 1.7.2, there are a number of genes that have roles in the pathogenesis of arthropathies (Xiong et al., 2018, Luo et al., 2022, Hong et al., 2011, Lima et al., 2015, De la Fuente et al., 2015, Burgess et al., 2019). Thus, an interruption in the expression of these genes could affect the homeostasis in the knee joint and predispose the model to either a more exacerbated or attenuated severity of HA (Buckley, 2019, Culemann et al., 2019). By specifying the genotype of a mouse that concurrently has the characteristics of severe haemophilia A, it allows experiments performed previously before to be used without the need for overhandling by using a depleting antibody for cell types. By preventing overhandling, we not only prevent stressing the mice but also prevent any chances of spontaneous bleeding from occurring in the mice, particularly in this novel mouse model of severe haemophilia A.

Previous data in Chapter 3 has shown that specific genes may have potential roles in the development and/or progression of HA, either attenuating or exacerbating the severity as the disease progresses. Thus, my aims for this chapter were to use novel mouse model knockouts to determine the role of a number of genes associated with innate and adaptive immunity in HA.

4.1.1. The *F8*$^{em1-/-}$/*Cx3cr1*$^{-/-}$ dual-knockout mice showed no significant difference to the *F8*$^{em1-/-}$ mouse model during experimental haemophilic arthropathy in terms of attenuation of the joint

In my investigation into the effects of certain genes that potentially have an effect on the progression of HA, I created a dual-knockout mouse as described previously in Chapter 2. By creating the *F8*$^{em1-/-}$/*Cx3cr1*$^{-/-}$ mouse model, I, along with another lab member, was able to investigate the effect the *Cx3cr1* gene had in the experimental HA model.

The *F8*$^{em1-/-}$/*Cx3cr1*$^{-/-}$ mice had needle injury induced HA along with control *F8*$^{em1-/-}$ mice to investigate the differences that may occur during HA. Repeated joint measures were taken daily but as seen in Figure 4.1 (A), no significant difference was observed. The *F8*$^{em1-/-}$/*Cx3cr1*$^{-/-}$ mice behaved in the same manner as the *F8*$^{em1-/-}$ mice, with the injury causing no more or less in the dual-knockout mice. The area under the curve (AUC) was calculated resulting in no significant difference between the two groups (Figure 4.1 (B)).

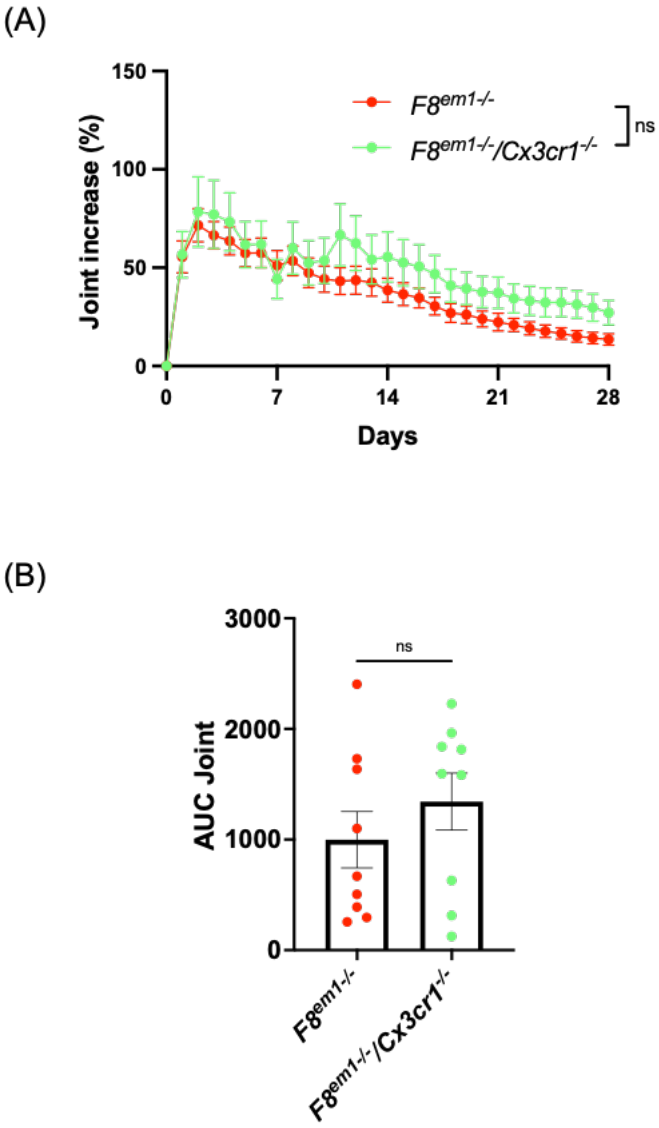

Figure 4.1. *F8*$^{em1-/-}$*/Cx3cr1*$^{-/-}$ mice showed no significant difference to matched *F8*$^{em1-/-}$ mice in induced HA injury. (A) Daily measurements of *F8*$^{em1-/-}$ mice (red) and *F8*$^{em1-/-}$*/Cx3cr1*$^{-/-}$ mice (green) showing the increase in joint measurement from basal levels as a percentage. **(B)** AUC of joint increase (%) from Figure 4.1 (A). Graph represented as mean ± SEM. n = 9. Statistical analysis using area under the curve followed by Student's *t* test.

4.1.2. The *F8*$^{em1-/-}$/*Il4ra*$^{-/-}$ dual knockout mouse model showed no significant difference to the *F8*$^{em1-/-}$ mouse model during experimental haemophilic arthropathy in terms of attenuation of the joint

While there was no significant difference in *F8*$^{em1-/-}$/*Cx3cr1*$^{-/-}$ mice, I continued to pursue the effects of genes that were affected during HA progression which led to the development of the *F8*$^{em1-/-}$/*Il4ra*$^{-/-}$ mouse model. With the upregulation of *Il4ra* during the progression of HA in *F8*$^{em1-/-}$ mice, I, along with another lab member, decided to explore the effect of using the dual-knockout *F8*$^{em1-/-}$/*Il4ra*$^{-/-}$ mouse model in induced HA.

The *F8*$^{em1-/-}$/*Il4ra*$^{-/-}$ mice showed no deviation from the previously used *F8*$^{em1-/-}$ mice with regards to the repeated daily joint measurement. The curve of the graph measuring the joint size change continued in the same trajectory as the *F8*$^{em1-/-}$ mice, with the peaks appearing at approximately the same days as well (Day 2), as seen in Figure 4.2 (A). Analysis of the AUC for the joint increase percentage of the graph in Figure 4.2 (A) showed that no significant difference was seen between the *F8*$^{em1-/-}$/*Il4ra*$^{-/-}$ mouse group and the *F8*$^{em1-/-}$ mouse group, as illustrated in Figure 4.2 (B).

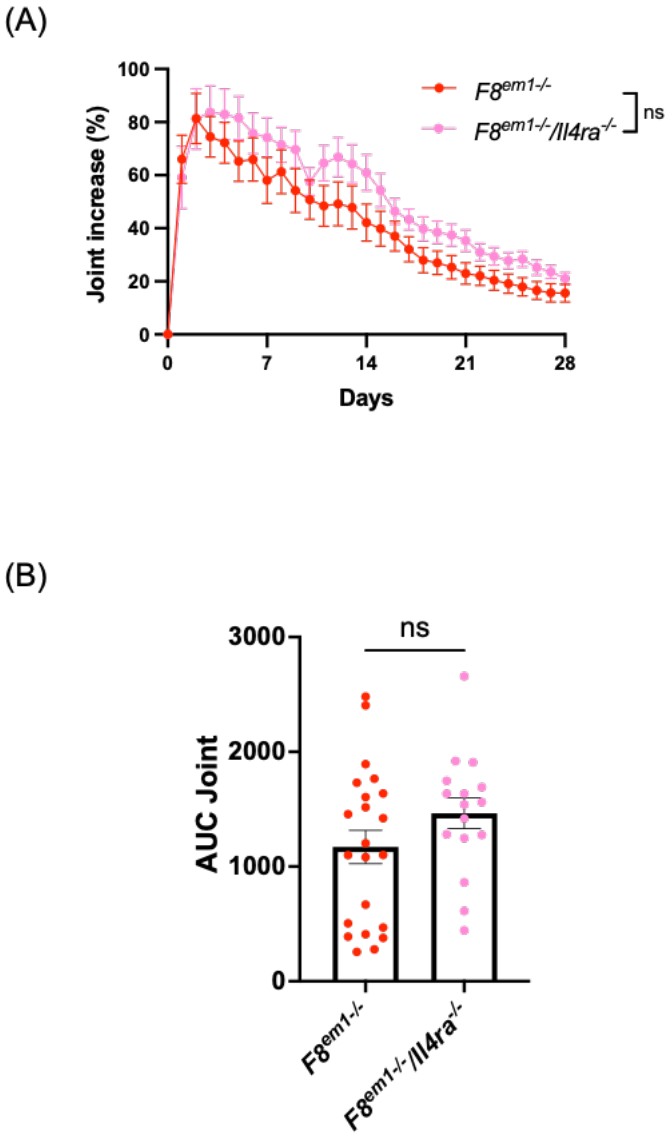

Figure 4.2. *F8*$^{em1-/-}$*/Il4ra*$^{-/-}$ mice showed no significant difference to matched *F8*$^{em1-/-}$ mice in induced HA injury. (A) Daily measurements of *F8*$^{em1-/-}$ mice (red) and *F8*$^{em1-/-}$*/Il4ra*$^{-/-}$ mice (pink) showing the increase in joint measurement from basal levels as a percentage. **(B)** AUC of joint increase (%) of Figure 4.2 (A). Graph represented as mean ± SD. n = 16 – 22. Statistical analysis using area under the curve followed by Student's *t* test.

4.1.3. A potential role of the IL-33/ST2 axis in the progression of haemophilic arthropathy

4.1.3.1. The F8$^{em1-/-}$/Il33$^{-/-}$ dual-knockout mouse model showed no significant difference to the F8$^{em1-/-}$ mouse model during experimental haemophilic arthropathy in terms of attenuation of the joint

As seen from the previous chapter, expression of *Il33* was elevated during HA progression. Thus, I, along with another lab member, sought to investigate the effects of *Il33* during induced HA using a dual-knockout mouse model. The variability in the increase of joint size from basal levels in the *F8$^{em1-/-}$/Il33$^{-/-}$* mice was greater than expected and while there was a notable increase in the percentage change of joint size, the difference was not significant compared to the *F8$^{em1-/-}$* mouse model, as seen in Figure 4.3 (A) and (B). However, as there was potential for the involvement of the IL-33/ST2 axis in the progression of HA, I performed a FIX assay, a vWF ELISA, and a TF ELISA (Figure 4.3 (C), (D), and (E), respectively) with another lab member. The results of these assays showed no significant difference between the *F8$^{em1-/-}$/Il33$^{-/-}$* mice group and the *F8$^{em1-/-}$* mice group. While previous data (Figure 4.3. (F) and (H)) showed elevation in the expression of *Il33* gene in the *F8$^{em1-/-}$* mouse model, knocking out the gene in the mouse model seemed to have no significant difference to the HA progression overall compared to the *F8$^{em1-/-}$* mouse model.

4.1.3.2. The F8$^{em1-/-}$/Il1rl1$^{-/-}$ dual-knockout mouse model showed significant differences to the F8$^{em1-/-}$ mouse model

I, along with another lab member, found the opposite with the *F8$^{em1-/-}$/Il1rl1$^{-/-}$* dual-knockout mouse model, where there was a significant difference between the *F8$^{em1-/-}$/Il1rl1$^{-/-}$* mice and the *F8$^{em1-/-}$* mice, as seen in Figure 4.3 (A) and (B). With the knockout of the *Il1rl1* (or *St2*) gene, the progression of HA was significantly less severe than in the *F8$^{em1-/-}$* model with a clear attenuation in the increase of the joint size in the progression of experimental HA. While there is a significant difference in FIX activity levels between the *F8$^{em1-/-}$/Il1rl1$^{-/-}$* mice and *F8$^{em1-/-}$* mice, the range is still within normal range of age-matched *Il1rl1$^{-/-}$* mice. The vWF ELISA and TF ELISA performed showed no significance, similar to that in the *F8$^{em1-/-}$/Il33$^{-/-}$* group. Previous data (Figure 4.3 (G)) showed significant elevation when RT-qPCR was performed on synovium samples throughout the timeline of experimental HA. This was also reflected in the

RNA samples used to analyse using NanoString technology, as seen in Figure 4.3 (H). The expression of *Il1rl1*$^{-/-}$ gene was elevated in both Figure 4.3 (G) and (H) on Day 2 and Day 7 before returning back to normal levels by Day 28 of the experiment.

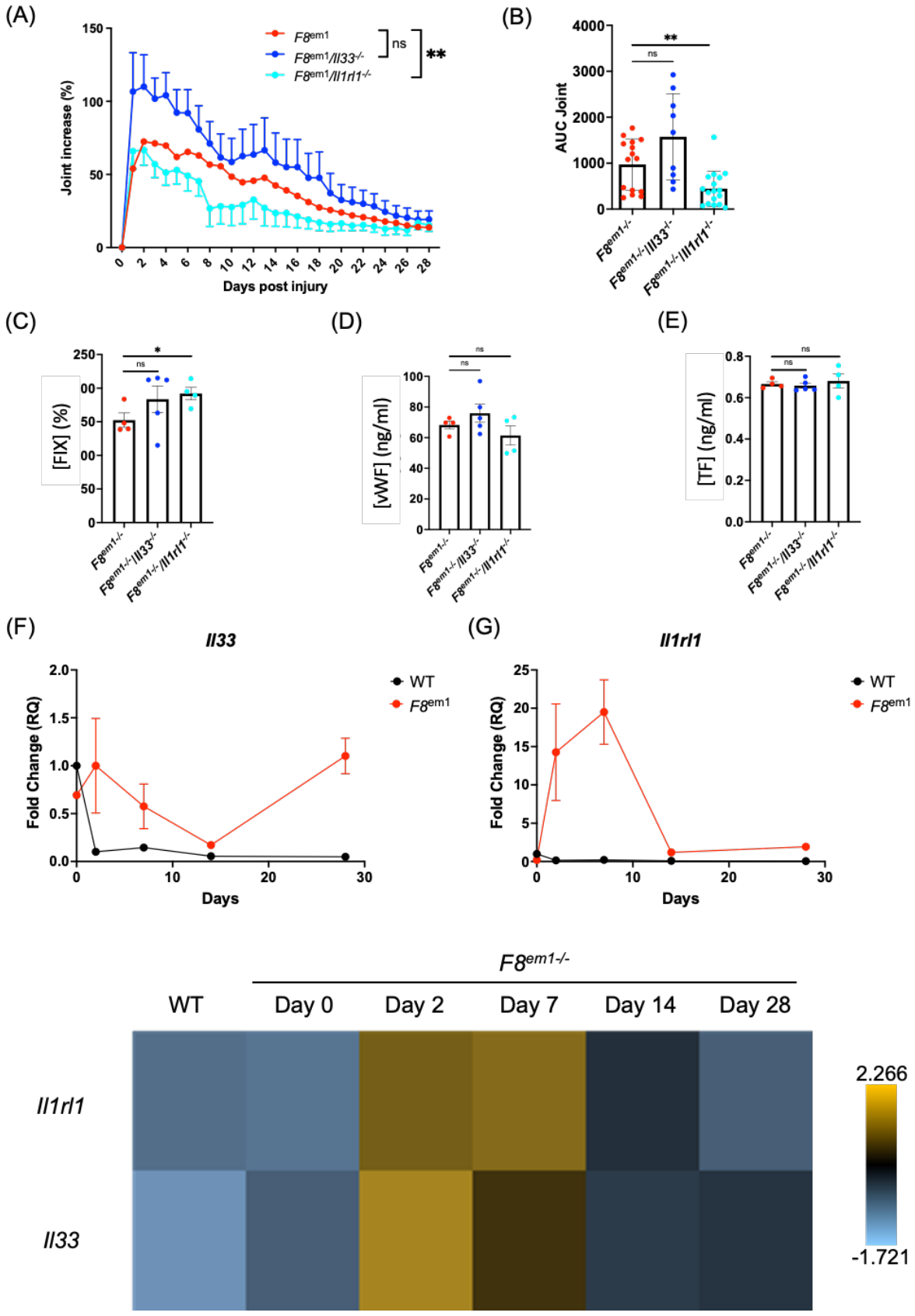
(A)
Joint increase (%)
Days post injury
F8em1
F8em1/Il33-/-
F8em1/Il1rl1-/-
ns
**
(B)
AUC Joint
**
ns
F8em1-/-
F8em1-/-/Il33-/-
F8em1-/-/Il1rl1-/-
(C)
[FIX] (%)
*
ns
(D)
[vWF] (ng/ml)
ns
(E)
[TF] (ng/ml)
ns
(F)
Il33
Fold Change (RQ)
Days
WT
F8em1
(G)
Il1rl1
Fold Change (RQ)
Days
WT
F8em1
F8em1-/-
WT
Day 0
Day 2
Day 7
Day 14
Day 28
Il1rl1
Il33
2.266
-1.721

Figure 4.3. Upregulation in the *Il1rl1* (or *St2*) gene shows significant difference in the *F8*$^{em1-/-}$ mice, indicating a potential role for the *Il33-St2* axis in the progression of HA. (A) Daily measurements of *F8*$^{em1-/-}$ mice (red), *F8*$^{em1-/-}$/*Il33*$^{-/-}$ mice (blue), and *F8*$^{em1-/-}$/*Il1rl1*$^{-/-}$ mice (turquoise) (n = 12 – 17) showing increase in joint measurement from basal levels as a percentage. **(B)** AUC of joint increase (%) of Figure 4.3 (A). **(C)** FIX activity levels in *F8*$^{em1-/-}$ mice, *F8*$^{em1-/-}$/*I33*$^{-/-}$ mice, and *F8*$^{em1-/-}$/*Il1rl1*$^{-/-}$ mice (n = 4 – 5). **(D)** vWF levels in *F8*$^{em1-/-}$ mice, *F8*$^{em1-/-}$/*I33*$^{-/-}$ mice, and *F8*$^{em1-/-}$/*Il1rl1*$^{-/-}$ mice (n = 4 – 5). **(E)** Tissue factors levels in *F8*$^{em1-/-}$ mice, *F8*$^{em1-/-}$/*I33*$^{-/-}$ mice, and *F8*$^{em1-/-}$/*Il1rl1*$^{-/-}$ mice (n = 4 – 5). **(F)** RT-qPCR of *F8*$^{em1-/-}$ mice plasma samples during experimental HA compared to WT mice for *Il33*. Synovium from individual mice (n = 3) were pooled for analysis and run in duplicate. **(G)** RT-qPCR of *F8*$^{em1-/-}$ mice plasma samples during experimental HA compared to WT mice for *Il1rl1*. Synovium from individual mice (n = 3) were pooled for analysis and run in duplicate. **(H)** Heatmap showing upregulation of *Il1rl1* and *Il33* genes in the progression of experimental HA in WT and *F8*$^{em1-/-}$ mice. Synovium from individual mice (n = 3) were pooled for analysis. Statistical analysis using area under the curve followed by Student's *t* test, or one-way ANOVA.

4.2. Discussion

The results from this chapter were to not only find genes that potentially may have a role in the progression of HA, but to also gain a better understanding of the genes that have a less to no significant role in the progression of HA. Thus, the results in this chapter have shown the role of the genes may play in the progression of HA.

Previous literature alluded to a pivotal role of the *Cx3cr1* gene in the integral structure to the knee joint. The lining surrounding the synovial capsule and fluid has been shown to have *Cx3cr1*-expressing macrophages. With the understanding that there would likely be an influx of macrophages from previous data (Chapter 3), the likelihood of the progression of macrophages being impacted was high. Thus, I used the dual-knockout $F8^{em1-/-}/Cx3cr1^{-/-}$ mouse model to analyse the effect that knocking out the *Cx3cr1* gene would have on the development and/or progression of HA. Synovial macrophages highly express *Cx3cr1*, and while these cells are highly specific, the role of *Cx3cr1* in these cell types is to maintain homeostasis within the knee joints and respond to inflammation by creating a tight barrier junction when necessary. However, the data gathered here as seen in Figure 4.1 (A) showed no significant difference between the $F8^{em1-/-}$ mice and the $F8^{em1-/-}/Cx3cr1^{-/-}$ mice. While the results showed no significant difference, the difference in joint size from basal level remained slightly more elevated in the $F8^{em1-/-}/Cx3cr1^{-/-}$ mouse group compared to the $F8^{em1-/-}$ mouse group. Further investigations would be needed but perhaps the effect of knocking the *Cx3cr1* gene had an effect on the progression of HA, with the clearance of the blood in the knee joint being stunted, thus not returning back to normal levels as quickly as the $F8^{em1-/-}$ mouse model.

While I investigated the innate side of the immune system, there was uncertainty as to whether the adaptive immune system also played a role in the development and/or progression of HA. With the $F8^{em1-/-}$ mouse model, I crossed an $Il4ra^{-/-}$ mouse to the model in order to utilise the novel mouse model and created a dual-knockout mouse model to investigate the effect of the *Il4ra* gene. While the results showed no clear significance in the effect of the *Il4ra* gene, there were similarities in the $F8^{em1-/-}/Il4ra^{-/-}$ mouse model to the $F8^{em1-/-}/Cx3cr1^{-/-}$ mouse model. The general trend reflects that seen in the $F8^{em1-/-}$ mouse model but the joint increase in the dual-knockout mouse

did not subside as quick as in the *F8*$^{em1-/-}$ mouse model. IL-4 has been implicated to have a potential positive effect on inflammatory diseases in the joint, such as RA. Concurrently, my previous data has shown an increase in *Il4ra* expression post-needle-induced HA in *F8*$^{em1-/-}$ mice. By knocking out the *Il4ra* gene in the *F8*$^{em1-/-}$ mouse model, to create the dual-knockout mouse, I expected exacerbation of the disease as seen in previous literature that showed just a single-nucleotide polymorphism for *IL-4R* had associated development of negative progression in RA. Thus, while finding no significant difference in the *F8*$^{em1-/-}$/*Il4ra*$^{-/-}$ mouse model, more work may be warranted to definitively conclude that there is no significant role played by the *Il4ra* gene in the novel *F8*$^{em1-/-}$ mouse model during the development and progression of HA.

The third dual-knockout model I utilised was the *F8*$^{em1-/-}$/*Il33*$^{-/-}$ mouse model. The results proved similar to the previous two models where no significant difference was found to the *F8*$^{em1-/-}$ mouse model. However, I also created a related dual-knockout, the *F8*$^{em1-/-}$/*Il1rl1*$^{-/-}$ mouse model which showed significant difference in the joint increase during the HA experiment. Lab members have previously shown that the *F8*$^{em1-/-}$/*Il1rl1*$^{-/-}$ mouse model showed a shorter aPTT compared to the *F8*$^{em1-/-}$ mouse model. Thus, the greater reduction in joint size reflects this with the percentage of joint increase from basal level returning to within normal range quicker.

In this project, the iPATH collaboration also involved analysis of plasma samples from PwsH. The processing and data analysis was performed by another lab member with ethics approval and permission to use data was granted. The plasma was processed in an ELISA to compare IL-33 and soluble ST2 concentrations in plasma from PwsH when compared with healthy control plasmas. The data showed that IL-33 protein in plasma samples from PwsH was not significantly different to that in healthy control plasma samples (Figure 4.4 (A)). However, when analysing the amount of soluble ST2 protein, there was a significant difference between the plasma samples from PwsH when compared with health control plasma (Figure 4.4 (B)). While we see elevated soluble ST2 in plasma from PwsH, as seen in Figure 4.4, but not IL-33, further work must be done in order to determine the exact role of the IL-33/ST2 axis in HA. The increase in soluble ST2 protein in plasma has been indicated to play a role in a number of diseases (Gordon et al., 2016, Hong et al., 2011, Shi et al., 2018). Soluble ST2 as

a biomarker for indication of prognosis of disease development and/or progression would allow for a non-invasive assessment and could subsequently lead to better outcomes for patients who may develop HA.

(A)

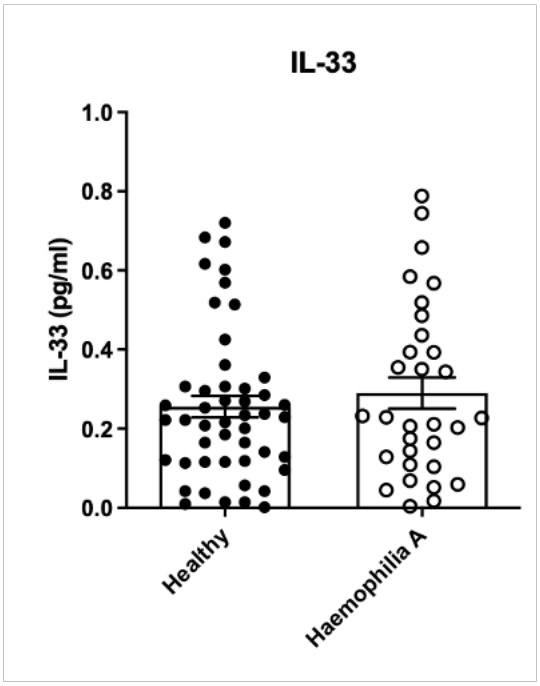

(B)

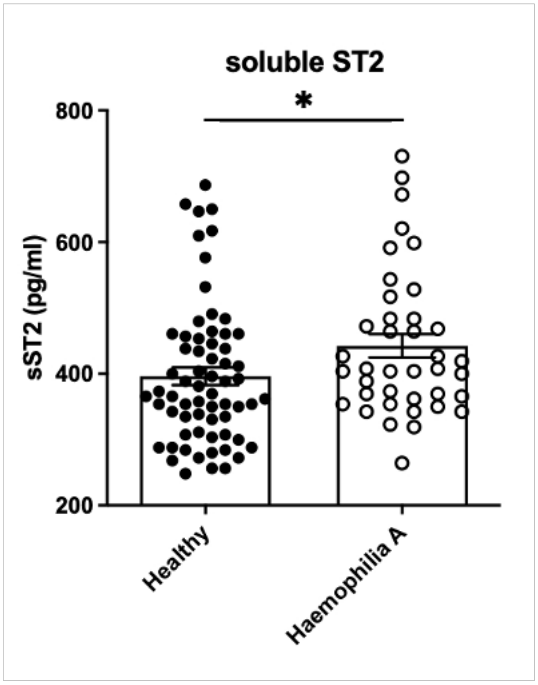

Figure 4.4. PwsH showed significant differences in soluble ST2 protein in plasma compared to healthy control plasma. (A) ELISA was used to detect IL-33 protein levels in healthy control plasma and in plasma from PwsH (n = 31 – 48). **(B)** ELISA was used to detect soluble ST2 protein levels in healthy control plasma and in plasma from PwsH (n = 39 – 65). Statistical analysis using Mann-Whitney test. This data analysis was performed by Dr Heike Hawerkamp and permission to use data was granted.

By utilising the dual-knockout models I have made, it is possible to continue the experimental work started here in this chapter, but also to further investigate the potential roles specific genes may play in the development and/or progression of HA. However, my data in this chapter has shown clear association of the IL-33/ST2 axis in HA in the *F8*$^{em1-/-}$ mouse model, which is further supported by the data found using plasma from PwsH.

Chapter 5 – The Effect of Mouse Heterogeneity on the Progression of Haemophilic Arthropathy

5.1. Results

The use of more than one mouse strain allows for the heterogeneity of haemophilia to be reflective of what is seen in the human cohort. While clear progress in our knowledge and understanding of the progression of experimental HA in a model of severe haemophilia A has been made, this focuses specifically on and only accounts for the one strain (C57BL/6J) being used. As previously discussed in Chapter 1.7.1, the choice of mouse strain can influence the outcome of a disease (De Vooght et al., 2010, Fukushima et al., 2006). Thus, the introduction of the same gene modification, in this case a CRISPR/Cas9 model, to different strains, other factors may also be considered that may or may not be affected by genetic background.

BALB/c mice tend to have a more Th2-mediated response in comparison to the more Th1-mediated response from the C57BL/6J strain. The difference in responses could potentially affect the outcome of HA, whether it be that it exacerbates or attenuates the disease or affects the progression of the disease. While there are more immunological differences when comparing the C57BL/6J and BALB/c mice, A/J mice develop muscular dystrophy as they age. With the importance of muscle on the development of HA (Hakobyan et al., 2005, Mulder and Llinas, 2004), the use of A/J mice allows comparison between the C57BL/6J mice to the A/J mice and, similar to the BALB/c strain, determine any exacerbation or attenuation of the disease in both the development and the progression of it.

Thus, my aims for this chapter were to determine any similarities or differences in experimental HA in the *F8*$^{em1-/-}$ mouse model but on other mouse strains, namely BALB/c and A/J.

5.1.1. Haemophilic arthropathy progression in the *F8$^{em1-/-}$* mouse model on a BALB/c background showed clear significant differences from the *F8$^{em1-/-}$* mouse model on a C57BL/6J background

5.1.1.1. Overall basal levels of BALB/c F8$^{em1-/-}$ mice were not significantly different when compared to BALB/c WT mice, except for when comparing bone density of knee joints and IL-33 in plasma

The first mouse strain I, along with another lab member, analysed after the C57BL/6J *F8$^{em1-/-}$* mouse model was the BALB/c *F8$^{em1-/-}$* mouse model. As the BALB/c *F8$^{em1-/-}$* mouse model was based on a different strain, some basal levels were analysed to investigate any differences between the BALB/c *F8$^{em1-/-}$* mice and matched BALB/c WT mice. As seen in Figure 5.1 (A), bone volume of the knee joints showed no significant difference. However, the bone density of BALB/c *F8$^{em1-/-}$* mice was higher (denser) than matched BALB/c WT mice, as seen in Figure 5.1 (B), at basal levels. This was significantly different with almost 0.005 mgHA/ccm difference between the BALB/c WT and *F8$^{em1-/-}$* mouse groups.

While physically there was significant difference between the two groups, namely bone density in the knee joints, there were no significant differences in the expression of various pro-/anti-inflammatory proteins in plasma samples. In Figure 5.1 (C – F), we see there is no significant differences in protein expression in plasma samples from BALB/c WT mice and BALB/c *F8$^{em1-/-}$* mice for TNFα, IL-6, IFNγ, and IL-1β respectively. However, in Figure 5.1 (G) we do see that the IL-33 is significantly lower in BALB/c *F8$^{em1-/-}$* mice compared to BALB/c WT mice.

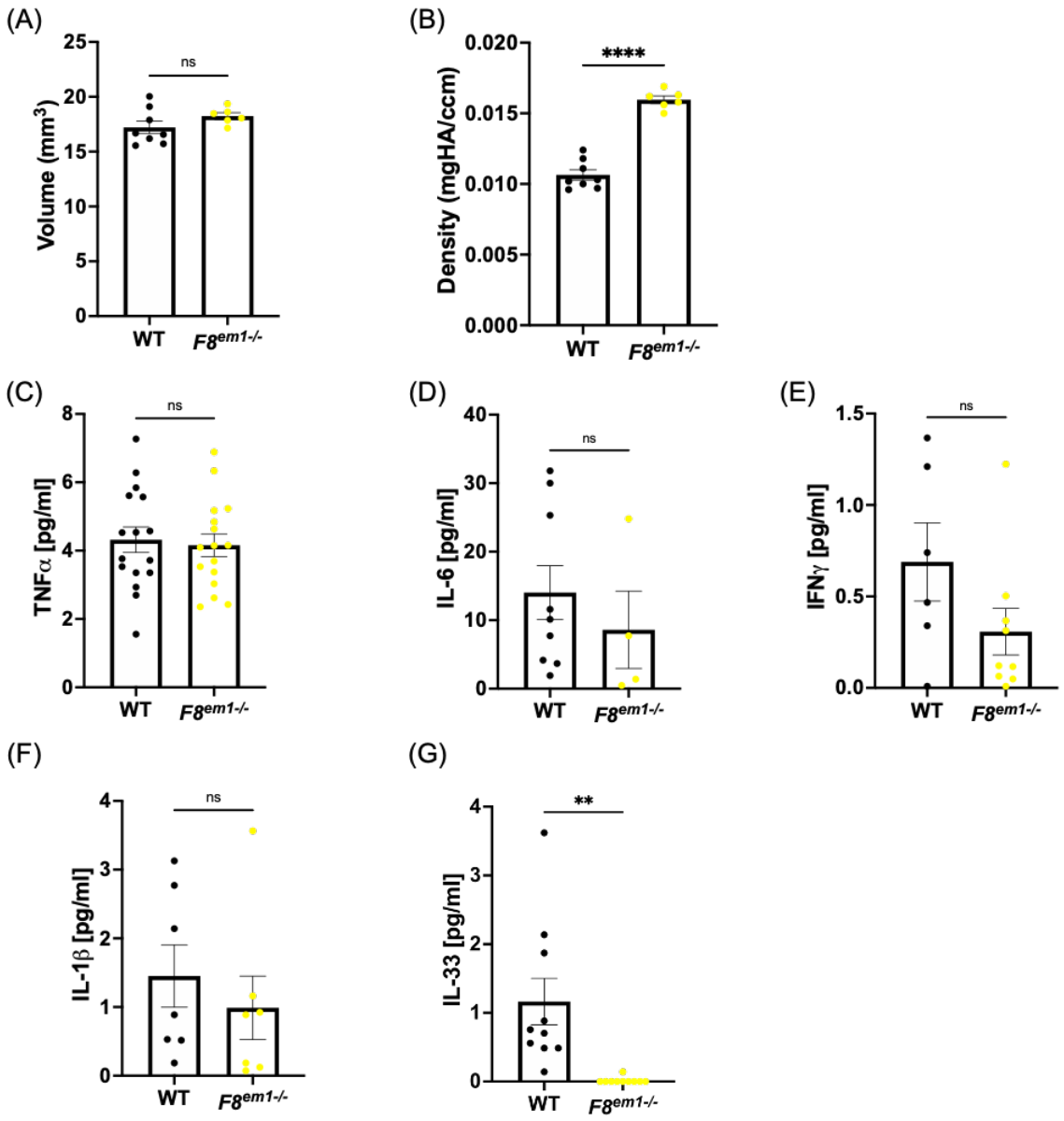

Figure 5.1. Basal levels in BALB/c *F8*$^{em1-/-}$ mice showed no significant difference to matched BALB/c WT controls, except in bone density of the knee joint. (A) Bone volume analysis of WT and *F8*$^{em1-/-}$ mice (n = 6 – 8) on a BALB/c background showed no significant difference. **(B)** Bone density analysis of WT and *F8*$^{em1-/-}$ mice (n = 6 – 8) on a BALB/c background showed significant difference between the two groups. **(C – G)** Multiplex analysis of plasma from WT and *F8*$^{em1-/-}$ mice (n = 6 – 16) on a BALB/c background showed no significant differences between the two groups when analysing TNFα, IL-6, IFNγ, and IL-1β respectively. IL-33 did show significant differences between the WT and *F8*$^{em1-/-}$ mice. All graphs represented as mean ± SEM. Statistical analysis using Welch's or Student's *t* test.

5.1.1.2. Experimental HA showed significant differences in the physical progression in BALB/c F8$^{em1-/-}$ mice compared to the C57BL/6J F8$^{em1-/-}$ mouse model

While we saw almost no basal differences between the BALB/c WT mice compared to the BALB/c *F8*$^{em1-/-}$ mice, the higher bone density could potentially have had an effect on the progression of induced HA in the BALB/c *F8*$^{em1-/-}$ mouse group. When compared to the C57BL/6J *F8*$^{em1-/-}$ mouse group, the severity of joint increase when measuring externally was significantly lower in the BALB/c *F8*$^{em1-/-}$ mice, as seen in Figure 5.2 (A) and (B). The C57BL/6J *F8*$^{em1-/-}$ mice had a peak at Day 2 as previously seen in Chapter 3. This is also seen in the BALB/c *F8*$^{em1-/-}$ mice with a peak appearing at Day 2 as well and continuingly reducing until the end of the 28-day experiment, as seen in Figure 5.2 (A). This was significantly lower in BALB/c *F8*$^{em1-/-}$ mice (approximately 45%) compared to C57BL/6J *F8*$^{em1-/-}$ mice (approximately 75%). However, while the trend for BALB/c *F8*$^{em1-/-}$ mice continues in the same fashion as the C57BL/6J *F8*$^{em1-/-}$ mice, the curve is significantly reduced as seen by comparison of the area under the curve (Figure 5.2 (B)).

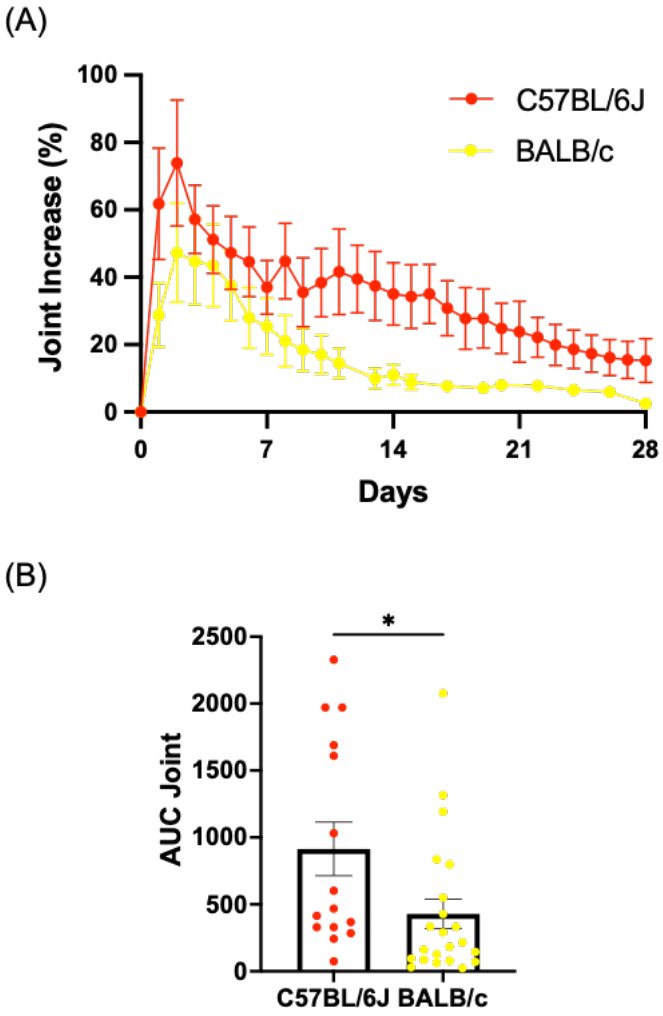

Figure 5.2. Experimental HA showed significant differences between the BALB/c *F8*$^{em1-/-}$ mouse model and the C57BL/6J *F8*$^{em1-/-}$ mouse model. (A) Percentage increase of joint measurements in the BALB/c *F8*$^{em1-/-}$ mouse model compared to the C57BL/6J *F8*$^{em1-/-}$ mouse model (n = 15 – 22). **(B)** AUC of joint increase (%) from Figure 5.2 (A). Graph represented as mean ± SD. Statistical analysis using area under the curve followed by Student's *t* test.

5.1.1.3. Immune cell-associated genes in BALB/c F8$^{em1-/-}$ mice showed no significant elevation compared with matched BALB/c WT mice

With previous flow cytometry data showing a higher number of infiltrating macrophages and potentially neutrophils as well, the use of NanoString nCounter analyses proved useful in analysing the possible differences between BALB/c WT and *F8$^{em1-/-}$* mice. Thus, I sought to analyse the RNA extracted from synovium of BALB/c WT and *F8$^{em1-/-}$* mice. As the resulting RNA from the extracted synovium was very low, the use of NanoString was still able to yield significant data as opposed to traditional RNA sequencing that requires more RNA concentration but also a higher quality. As seen in Figure 5.3 (A), macrophage associated genes from the NanoString Mouse Myeloid cassette (see Appendix IV for list) were elevated compared to matched WT mice. However, there were no significant expressions found between the two groups due to the low number of samples. The first two BALB/c *F8$^{em1-/-}$* mice showed elevation of a small number of genes but were not elevated in the third mouse. Similarly in the neutrophil associated genes (see Appendix IV for list) from the Mouse Myeloid cassette in Figure 5.3 (B), while some neutrophil associated genes were elevated, no significant expressions were found. As flow cytometry was previously performed, the same genes being analysed were analysed in the NanoString Mouse Myeloid cassette in Figure 5.3 (C). However, while there was elevation of some genes, overall, there was no significant difference.

(A)

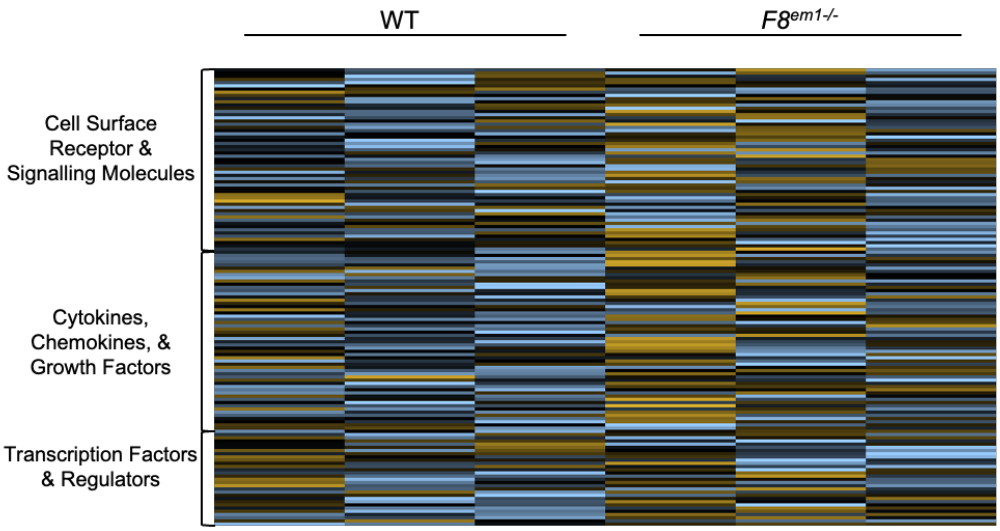
WT
F8em1-/-
Cell Surface Receptor & Signalling Molecules
Cytokines, Chemokines, & Growth Factors
Transcription Factors & Regulators

(B)

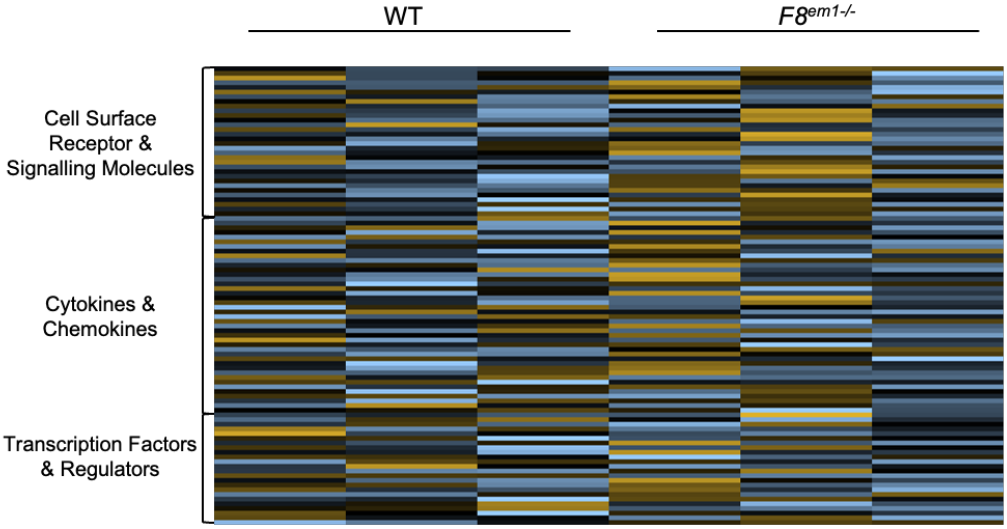
WT
F8em1-/-
Cell Surface Receptor & Signalling Molecules
Cytokines & Chemokines
Transcription Factors & Regulators

(C)

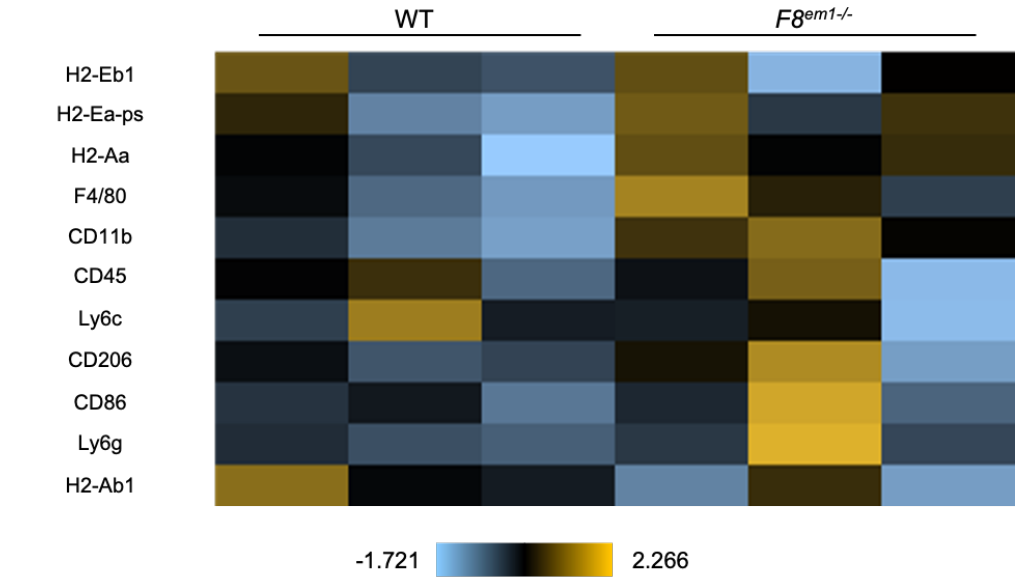
WT
F8em1-/-
H2-Eb1
H2-Ea-ps
H2-Aa
F4/80
CD11b
CD45
Ly6c
CD206
CD86
Ly6g
H2-Ab1
-1.721
2.266

Figure 5.3. Various genes associated with macrophages and neutrophils show elevation at basal level in BALB/c *F8*$^{em1-/-}$ mice compared to BALB/c WT mice. **(A)** Heat map constructed from NanoString Mouse Myeloid cassette Monocyte/Macrophage genes using the nSolver programme. Each column represents an individual mouse. **(B)** Heat map constructed from NanoString Mouse Myeloid cassette Neutrophil genes using the nSolver programme. Each column represents an individual mouse. **(C)** Heat map constructed from NanoString Myeloid cassette genes using the nSolver programme. Each column represents an individual mouse (n = 3).

5.1.2. Haemophilic arthropathy progression in the *F8*$^{em1-/-}$ mouse model on an A/J background showed no clear significant differences from the *F8*$^{em1-/-}$ mouse model on a C57BL/6J background

5.1.2.1. Overall basal levels of A/J F8$^{em1-/-}$ *mice were not significantly different when compared to A/J WT mice*

While the use of BALB/c *F8*$^{em1-/-}$ mice when compared to the C57BL/6J *F8*$^{em1-/-}$ mouse model proved to show significant difference in the severity of HA, the same might not necessarily be the same for other strains and so I, along with another lab member, looked into the A/J *F8*$^{em1-/-}$ mouse model. Thus, I analysed similar basal levels to that analysed before for the BALB/c *F8*$^{em1-/-}$ mouse model.

There was no significant difference in the physical analysis of the knee joint in terms of bone volume or bone density, as seen in Figure 5.4 (A) and (B), respectively, when comparing the A/J *F8*$^{em1-/-}$ mice to matched A/J WT mice. However, while no significant difference was seen in the A/J *F8*$^{em1-/-}$ mice, I still analysed the same protein levels in the plasma samples from A/J *F8*$^{em1-/-}$ mice (Figure 5.4 (C – G)). While overall there was no significant differences in pro-/anti-inflammatory proteins, one specifically did have a significant difference in the A/J *F8*$^{em1-/-}$ mice when compared to matched A/J WT mice. In Figure 5.4 (E), we see that the levels of IFNγ in plasma from A/J *F8*$^{em1-/-}$ mice was slightly higher than that see in A/J WT mice. While this pro-inflammatory protein was being expressed at a higher level, none of the other proteins analysed showed any significant difference.

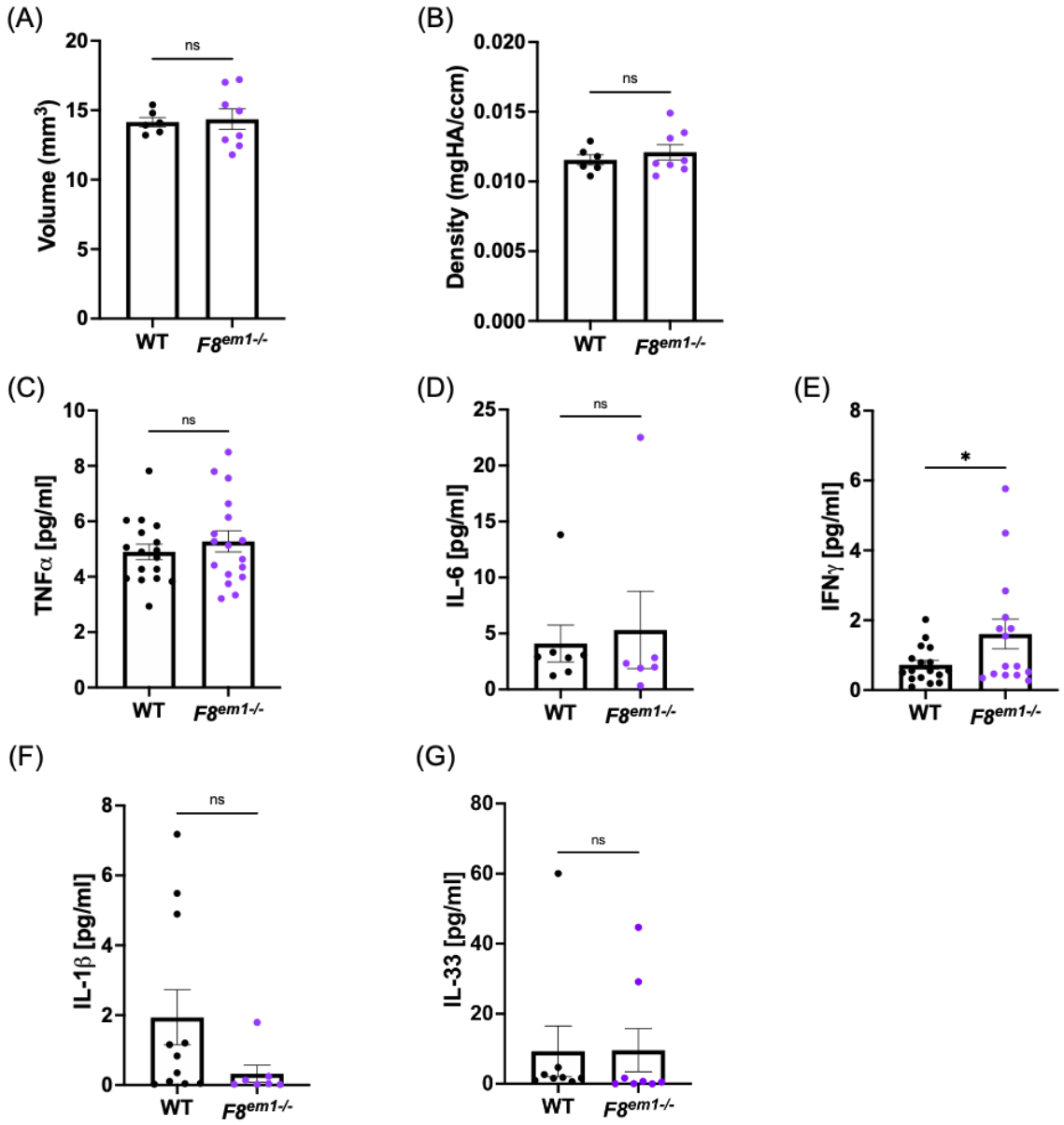

Figure 5.4. Basal levels in A/J *F8*$^{em1-/-}$ mice showed no significant difference to matched A/J WT controls, except in bone density of the knee joint. (A) Bone volume analysis of WT and *F8*$^{em1-/-}$ mice on a A/J background (n = 6 – 8) showed no significant difference. **(B)** Bone density analysis of WT and *F8*$^{em1-/-}$ mice on a A/J background (n = 6 – 8) showed no significant difference between the two groups. **(C – G)** Multiplex analysis of plasma from WT and *F8*$^{em1-/-}$ mice on a A/J background (n = 6 – 17) showed no significant differences between the two groups when analysing TNFα, IL-6, IFNγ, IL-1β, and IL-33, respectively. Statistical analysis using Welch's or Student's *t* test.

5.1.2.2. Experimental HA showed no significant differences in the physical progression in A/J F8$^{em1-/-}$ mice compared to the C57BL/6J F8$^{em1-/-}$ mouse model

While we saw no significant differences in the physical bone structure of the knee joint, there were differences in the expression of IFNγ in plasma which potentially could have impacted progression of HA. In the comparison of A/J *F8$^{em1-/-}$* mice to C57BL/6J *F8$^{em1-/-}$* mice in experimental HA as seen in Figure 5.5 (A) and (B), there was no significant differences in terms of area under the curve. However, unlike the BALB/c *F8$^{em1-/-}$* mouse model where the graph line mirrored that in the C57BL/6J but in a less severe way, the A/J *F8$^{em1-/-}$* mouse model, while still peaking within the first few days of the experiment, persisted for a longer period of time and did not return back to within normal baseline range. This can be seen clearly in the purple "A/J" line in Figure 5.5 (A) where the line increased sharply in the first few days, began to decrease but then continued to stay elevated for the remainder of the experiment. So, while there was no significant difference in the area under the curve, as seen in Figure 5.5 (B), the lines in Figure 5.5 (A) ended up overlapping as the experiment progressed as the C57BL/6J *F8$^{em1-/-}$* mouse model slowly returned back to within normal baseline range, but the A/J *F8$^{em1-/-}$* mouse model persisted.

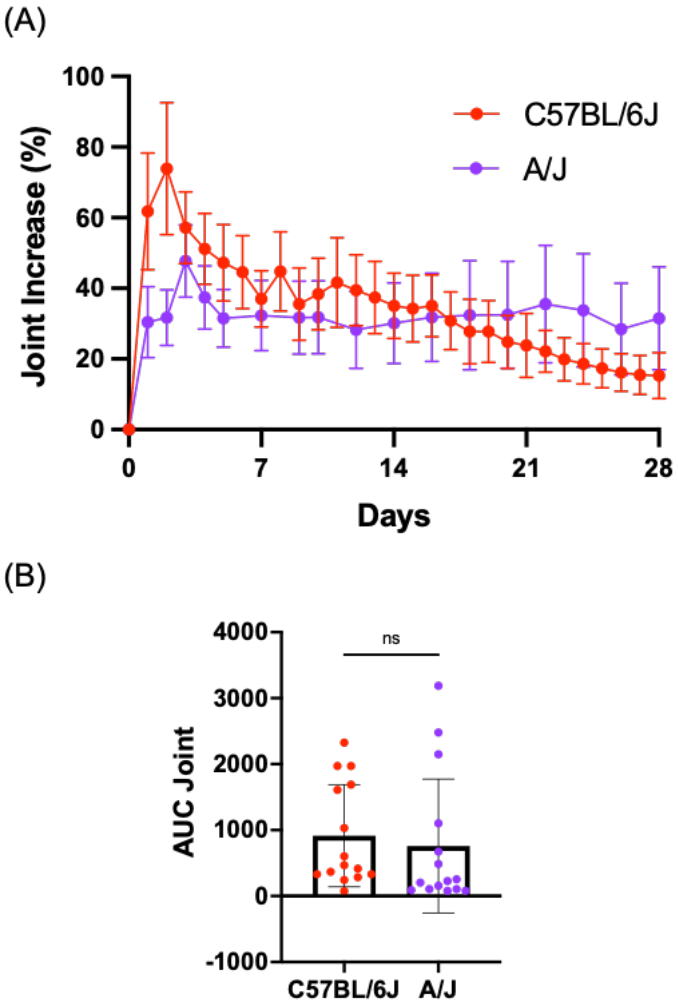

Figure 5.5. Experimental HA showed no significant difference between the A/J *F8*$^{em1-/-}$ mouse model and the C57BL/6J *F8*$^{em1-/-}$ mouse model. (A) Percentage increase of joint measurements in the A/J *F8*$^{em1-/-}$ mouse model compared to the C57BL/6J *F8*$^{em1-/-}$ mouse model (n = 15). **(B)** AUC of joint increase (%) from Figure 5.2 (A). Graph represented as mean ± SEM. Statistical analysis using area under the curve followed by Student's *t* test.

5.1.2.3. Immune cell-associated genes in A/J F8$^{em1-/-}$ mice showed no significant elevation compared with matched A/J WT mice

Similar to the BALB/c mice, I wanted to analyse the basal levels of gene expression in more depth when comparing A/J *F8*$^{em1-/-}$ mice to matched A/J WT mice. The RNA was extracted from the synovium in the same way as before, thus yielding in a very low amount of RNA but still suitable for NanoString nCounter analysis. While some genes were elevated in some samples for macrophage associated genes as seen in Figure 5.6 (A), there was no significant difference found. Again, similar to both the BALB/c *F8*$^{em1-/-}$ mouse model and the macrophage associated genes (see Appendix IV for list) in Figure 5.6 (A), there is elevation of certain genes in some samples but no significant difference in the neutrophil associated genes (see Appendix IV for list) (Figure 5.6 (B)). When analysing the differential gene expression of genes associated with macrophages from previous flow cytometry (Figure 5.6 (C)), there was elevation of gene expression particularly in one mouse (*F8*$^{em1-/-}$ mouse on the third column). However, in the first three genes analysed (H2-Eb1, H2-Ea-ps, and H2-Aa), there was significant elevation compared to the WT mice, potentially indicating a role for the MHC Class II in the progression of the A/J *F8*$^{em1-/-}$ mice and why the severity of HA remains elevated throughout the experiment.

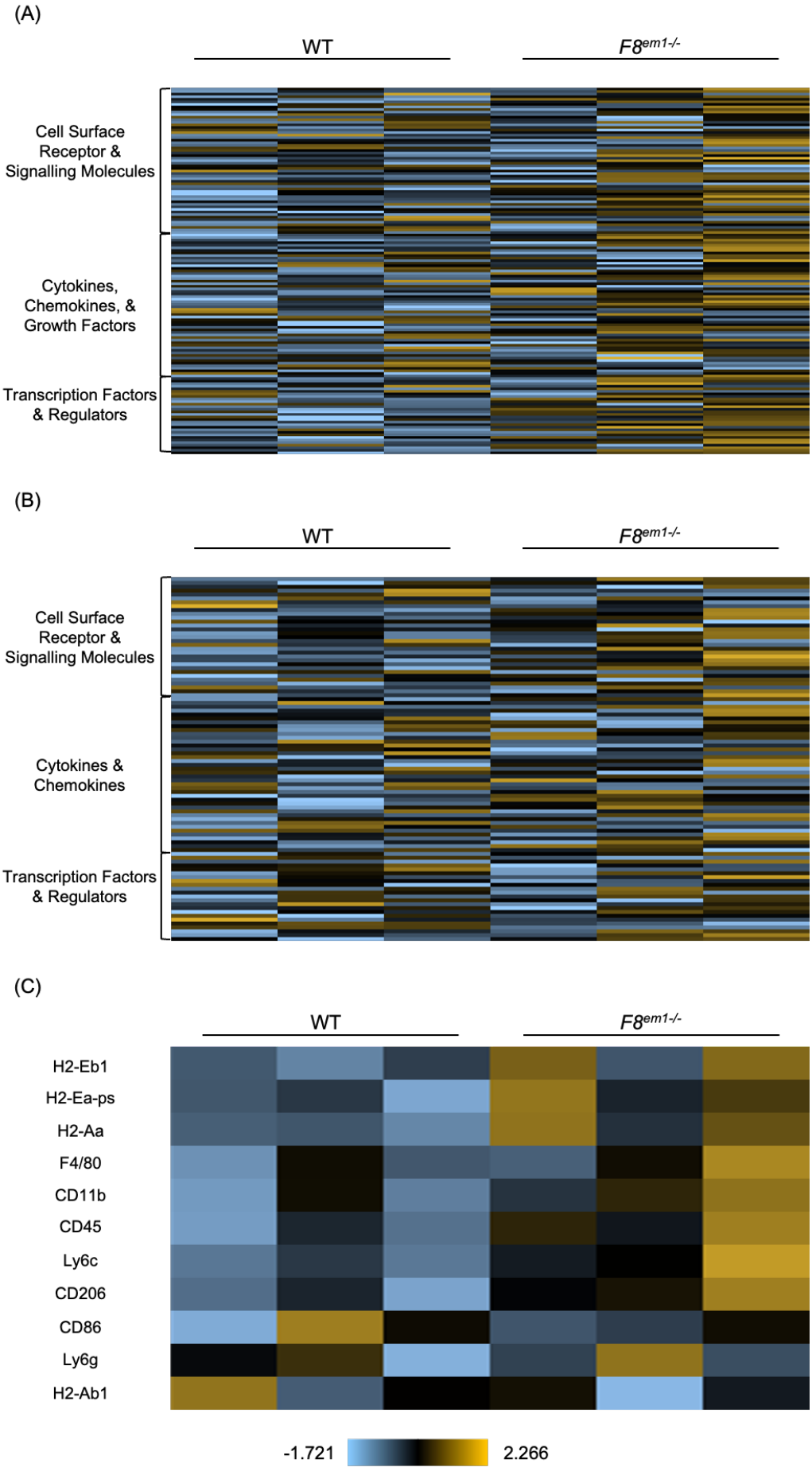
(A)
WT
F8em1-/-
Cell Surface Receptor & Signalling Molecules
Cytokines, Chemokines, & Growth Factors
Transcription Factors & Regulators
(B)
WT
F8em1-/-
Cell Surface Receptor & Signalling Molecules
Cytokines & Chemokines
Transcription Factors & Regulators
(C)
WT
F8em1-/-
H2-Eb1
H2-Ea-ps
H2-Aa
F4/80
CD11b
CD45
Ly6c
CD206
CD86
Ly6g
H2-Ab1
-1.721
2.266

Figure 5.6. Various genes associated with macrophages and neutrophils show elevation at basal level in A/J *F8*$^{em1-/-}$ mice compared to A/J WT mice. **(A)** Heat map constructed from NanoString Myeloid cassette Monocyte/Macrophage genes using the nSolver programme. Each column represents an individual mouse. **(B)** Heat map constructed from NanoString Myeloid cassette Neutrophil genes using the nSolver programme. Each column represents an individual mouse. **(C)** Heat map constructed from NanoString Myeloid cassette genes using the nSolver programme. Each column represents an individual mouse (n = 3).

5.2. Discussion

While previous chapters utilised novel mouse models, including dual-knockout mice, all remained on a C57BL/6J background. The heterogeneity found in the human population, and for PwsH, cannot be reflected in just one mouse strain when experiments are carried out. Thus, while some results showed no significance, the use of different mouse backgrounds allowed for a more comprehensive understanding of HA when comparing data from all three different mouse backgrounds: C57BL/6J, BALB/c, and A/J.

Before analysing the effects of experimental HA in the two other mouse strains, I first analysed any potential basal differences that may give an indication that the outcome would be different from the C57BL/6J strain. First, in the BALB/c mouse strain, there was no difference when comparing the BALB/c *F8*$^{em1-/-}$ mice to matched BALB/c WT mice with regards to the basal levels of various cytokine expression circulating in plasma from these mice. There was no significant difference which was what would be expected pre-injury. However, in the A/J mice, there was a significant difference found between the WT and *F8*$^{em1-/-}$ mice, specifically in IFNγ expression. However, this could be the result of a number of reasons as to why this was elevated. Spontaneous bleeding has been recorded for the *F8*$^{em1-/-}$ mouse model, with some not being as prominent and remaining as subclinical bleeds. These minor bleeds may potentially have triggered an immune response, and thus the raised levels of IFNγ occurred. Majority of *F8*$^{em1-/-}$ mice remained within the same range as the WT mice, bar two potential outliers. No bleeds were noted at the time of plasma collection from these mice; however, a full autopsy was not performed and thus cannot be confirmed whether the cause of the elevated levels of circulating IFNγ was due to a bleed or not.

The bone volume and density were also analysed in both the BALB/c and A/J *F8*$^{em1-/-}$ mice, comparing them with their matched WT mice. Whilst there was no significant difference found between the A/J WT and *F8*$^{em1-/-}$ mice, the BALB/c *F8*$^{em1-/-}$ mice did show significant difference to their matched WT mice. It has been reported that increased bone density leads to better outcomes in other inflammatory joint diseases, with the increase in density leading to reduced co-morbidities like osteoporosis and reduced bone fractures (Kareem et al., 2021). With the significant difference in bone

density in the BALB/c *F8*$^{em1-/-}$ mice compared to the matched WT mice, it was no surprise that this could affect the progression of HA. Thus, the attenuated severity could potentially be associated with the higher bone density in the BALB/c *F8*$^{em1-/-}$ mice, with the joint increase returning to within normal levels a lot sooner than C57BL/6J mice.

With significant difference found between the BALB/c *F8*$^{em1-/-}$ mice and the C57BL/6J *F8*$^{em1-/-}$ mice during the time course for experimental HA, I turned to look at potential immunological differences that could have affected the outcome of the experiment. The use of NanoString nCounter technology was to my advantage due to the need of low amounts of RNA. Thus, I analysed the RNA from synovium from WT and *F8*$^{em1-/-}$ mice on BALB/c and A/J strains. For both the BALB/c and A/J WT and *F8*$^{em1-/-}$ mice, no significant differences were found at basal levels for macrophages and neutrophils. While the specificity and ability for NanoString nCounter technology to use low amounts of RNA yields good results, the number of samples is still low and would require larger sample sizes to show any significant differences as the current data shows no differences. Thus, the conclusion found from these results is that the basal level from the BALB/c mice in their bone structure likely had more of an effect on the progression of HA when comparing to the C57BL/6J *F8*$^{em1-/-}$ mice, while A/J *F8*$^{em1-/-}$ mice showed no significant differences in basal levels structurally nor immunologically to the C57BL/6J *F8*$^{em1-/-}$ mice.

While my previous data from Chapter 3 and Chapter 4 indicated a vital role of the innate immunity in HA, there is still the question of whether certain cells in the adaptive immunity may also play a role in the development and/or progression of HA. I specifically chose the BALB/c mouse background to juxtapose the C57BL/6J background. Literature shows that C57BL/6J mice have a tendency for a Th1-mediated immune response, while the BALB/c mouse has a tendency for a Th2-mediated immune response. The varied natural responses of mice on different backgrounds could potentially lead to the discovery of a certain favoured response to an injury that causes HA. But more than that, it could help explain why the occurrence of HA in PwsH can have different severities, not excluding why some PwsH do not develop HA despite reporting injuries and bleeds into the capsule of the knee joint and why some develop HA despite not reporting injuries and bleeds into the capsule of the

knee joint. The BALB/c and A/J *F8*$^{em1-/-}$ mice both have a tendency to be more Th2-mediated in immunity compared to the C57BL/6J *F8*$^{em1-/-}$ mice that are more Th1-mediated. Previous experiments have shown significant increases in Th2-associated cytokines in both BALB/c and A/J, but not C57BL/6J (De Vooght et al., 2010). As seen in Figure 5.2 and Figure 5.5, both the BALB/c *F8*$^{em1-/-}$ mice and A/J *F8*$^{em1-/-}$ mice presented with lower joint increases compared to C57BL/6J *F8*$^{em1-/-}$ mice. The more Th2-biased immunity could be a major contributor to the lowered severity of HA in the BALB/c *F8*$^{em1-/-}$ mice and A/J *F8*$^{em1-/-}$ mice. The study conducted by De Vooght also showed that the Th2-mediated response was more prominent in BALB/c mice, and we see this reflected in the data in this chapter (De Vooght et al., 2010). When we compare the differences in levels of IL-33 in plasma in Figure 5.1 and Figure 5.4, there was no significant difference in Figure 5.4 in the A/J strain but when looking at the BALB/c strains, there is a significant difference between the BALB/c WT and *F8*$^{em1-/-}$ mice suggesting that a strong Th2-mediated response may be more beneficial to the outcoming severity of HA.

Of course, the data here is limited and more research is required to definitively pinpoint the exact differences that cause different strains of the same model to have different results. However, the preliminary data here allows for a significant leap into the analysis of heterogeneity in mouse strains in a mouse model of severe haemophilia A and indicates that research in haemophilia, as well as the co-morbidities associated with haemophilia, require more than just one type of model in order to capture the heterogeneity found in the human population.

Chapter 6 – Discussion and Future Directions

6.1. Discussion and Future Directions

The aim of this project was not only to establish this novel mouse model of severe haemophilia A in experimental haemophilic arthropathy, but to also elucidate potential markers that can be further exploited to attenuate the severity of progression of the disease.

The *F8*$^{em1-/-}$ mouse model differs from the *F8*$^{tm1-/-}$ mouse model in terms of FVIII protein production as well as characteristics. The *F8*$^{tm1-/-}$ mouse model produces a non-functional (truncated) FVIII protein which could potentially tolerise the immune system, whereas in the *F8*$^{em1-/-}$ mouse model there is no FVIII protein transcribed and thus this creates a naïve microenvironment in the model, as established by a previous lab member's PhD thesis (Byrne, 2021). This model was already established in the lab as a suitable model for severe haemophilia A and thus, with a model already breeding in the lab I chose to use it for my experiments. However, there were some advantages of using this model as it posed a microenvironment that had not previously been exposed to FVIII protein, which potentially could cause immune intolerance should rFVIII be introduced had it already been exposed. Thus, this provided a mouse model that could possibly be used to further experiment using rFVIII treatment. As mentioned previously, inhibitor development can lead to breakthrough or spontaneous bleeds, particularly in joint areas. This could have also created complications had I gone ahead with experiments looking at the effect of rFVIII in the attenuation of HA in this mouse model. Thus, by choosing this mouse model, there is already data for which further experimentation would be comparable. This mouse model also provided a new insight to the effects of spontaneous bleeds with the presence of a spontaneous bleeding phenotype, as described further on. The numbers required for each point were extrapolated using G-power as per the HPRA licence. However, this *F8*$^{em1-/-}$ model had an increase in the severity of HA when I was establishing it in the lab, something that was much higher than expected when comparing it to literature from the *F8*$^{tm1-/-}$ model. Thus, numbers for each time point did vary due to the need to remove some mice from the experiment based on the HPRA scoring. The large increase when measuring the joint, as well as the large variability found during the experimental

model, could potentially be attributed to the same cause as the spontaneous phenotype found in this model as it has been shown in previous research that subclinical bleeds are associated with an increase in severity of arthropathy (Bhat et al., 2015). Bleeds naturally occurred more frequently in this model and so the induced injury was heavily monitored (daily) throughout the experiment. Of course, the unexpected result of a much higher increased joint size then had a knock-on effect to my research as an amendment was needed to proceed. While seemingly small, this meant our approach to the experiment would also need more consideration, namely how extraction of the synovium from the leg would need to be considered more carefully, particularly now implementing the need to use red blood cell lysis on extracted samples. The presence of spontaneous bleeding is something that has been reported in our novel mouse model, and perhaps this could be related to previous research done by Wyseure showing impaired thrombin-activatable fibrinolysis inhibitor in haemophilia A mouse models (Wyseure et al., 2018, Wyseure et al., 2019). It is possible that the vascular structure could be one of the contributing factors to the spontaneous bleeds, and thus normalisation of this could lead to better control of spontaneous bleeding in the novel mouse model of haemophilia A. Subsequently, the development of bone pathology in HA after bleeding, both spontaneous and induced, could then be elucidated further (Vols et al., 2020). However, as is seen in PwH, bleeding is not always the direct cause of HA development (Valentino, 2010, Valentino et al., 2012). Thus, further research into the mechanisms of development or predispositions to the development of HA is needed.

While this thesis focused on mice from ages 10 to 12 weeks old, there is scope to identify the effects in older mice as bone development changes with age (Jackson et al., 2017, Jilka, 2013). Mouse models used at this age are able to reflect that seen in late adolescence in humans (Ackert-Bicknell et al., 2015, Dutta and Sengupta, 2016). However, while identification of signs of pathogenesis of HA is vital at this age due to the stage of bone growth (Aronstam et al., 1979, Weaver, 2002), haemarthroses does not stop at this age and continues on throughout life in PwsH. Chronic HA occurs after multiple injuries within a small timeframe, hence the need to identify target joints. Various factors may also affect the risk of developing HA (El-Mikkawy et al., 2019), and thus early diagnosis of any predisposition is advantageous to prevent the development and progression of HA. While the development of arthropathy may only

affect a small part of the quality of life of a patient, it is still significant and important for later on in life as joint damage remains as one of the main causes of disability in PwsH (Fischer et al., 2005, Rodriguez-Merchan, 1997). Thus, further research would be needed in addition to this work to identify any changes in biomarkers after a second induced injury to mimic the repeated haemarthroses found in target joints, and whether or not this changes from already identified biomarkers (Manon-Jensen et al., 2016). Certain genes, such as *Tnfa*, *Il1b,* and *Il6*, have been shown here to be involved in HA progression. However, the extent of their roles after a second injury is unknown and potentially could be more or less important after a second bleed into the same joint.

As seen from the flow analysis in Chapter 3, the total number of cells produced from pooled synovium from mice yielded a very low amount compared with typical flow cytometry procedures. Thus, RNA analysis was utilised to circumvent this issue. NanoString nCounter systems allows for very low amounts of RNA to be used for their cassette analyses and thus it was a more viable option that still allowed for in depth analysis of the synovium. The innate immunology cassette allowed analyses for multiple innate immune cells which included monocytes (macrophages), neutrophils, eosinophils, basophils, mast cells, and dendritic cells. With a role for the IL-33/ST2 axis in the mouse model, as well as the local proliferation of macrophages, the analysis of macrophages was particularly important to see if any particular genes were elevated in the $F8^{em1-/-}$ mice compared to matched WT mice (Jenkins et al., 2011). With n = 3 for each group, the presence of a mouse that potentially could have a bleed elsewhere from the knee joint is something that could have skewed one of the results in the NanoString nCounter analysis. It might be necessary to increase the sample size for the analysis to account for potential outliers as well. Overall, there were no significant differences in gene expression between the WT and $F8^{em1-/-}$ mice, with the outlier in the $F8^{em1-/-}$ mouse group as the exception.

The characterisation of the experimental HA model in the $F8^{em1-/-}$ mouse model was very successful, with clear paths of potential mechanisms that could be implicated in the pathogenesis of the disease. Within these potential mechanisms found during the experiment was the IL-33/ST2 axis. Thus, the establishment of the $F8^{em1-/-}/Il33^{-/-}$ dual-knockout mouse model and the $F8^{em1-/-}/Il1rl1^{-/-}$ dual-knockout mouse model allowed further analysis of the importance of the IL-33/ST2 axis in the pathogenesis of HA.

The progression of HA was significantly attenuated in the *F8*$^{em1-/-}$/*Il1rl1*$^{-/-}$ mouse model, indicating that the depletion of ST2 protein could potentially be a therapeutic target for patients diagnosed with HA. Not only that but it was found that the amount of circulating sST2 protein in plasma samples from PwsH was significantly elevated. Elevated ST2 protein has also been found in patients with RA as well, another arthropathy with similarities to HA (Shi et al., 2018). Thus, the same mechanisms found in RA could potentially be the same in HA. With various therapeutics available, such as astegolimab, an anti-ST2 monoclonal antibody, that could potentially be used in conjunction with FVIII replacement this could improve patient outcomes after haemarthroses (Yousuf et al., 2022, Kelsen et al., 2021). Further research using biological interventions in the HA model using the *F8*$^{em1-/-}$ mouse model could elucidate further the dose that would be required to help reduce severity of the bleed.

IL-33 is an alarmin in the IL-1 family and plays a major role in inhibiting osteoclastogenesis (Lima et al., 2015, Matarazzo et al., 2022). Thus, an imbalance in bone homeostasis could also cause the bone structure to be further affected in HA, as seen already in mouse models of haemophilia A (Weitzmann et al., 2019). This imbalance has already been seen in RA, thus similar mechanisms may be at play in the pathogenesis of HA (Shim et al., 2018). While IL-33 works as anti-osteoclastogenic, it also promotes Th2-associated cytokines (Schmitz et al., 2005). As previously stated, a more Th2-mediated response could be important for the progression of HA. With impaired Th2 immune responses, *F8*$^{em1-/-}$/*Il33*$^{-/-}$ mice had an increase in joint size change throughout the experiment. Thus, the hypothesis of whether a more Th2-mediated response could be beneficial to the outcome after inducing haemarthrosis needed further investigation. BALB/c mice are known to be good models for allergy and auto-immune diseases, with their more Th2-mediated immune response. Thus, comparison of the same single nucleotide polymorphism but on a C57BL/6J background versus a BALB/c background could identify the importance of the different immune systems. Indeed, we saw the attenuation of the disease in BALB/c *F8*$^{em1-/-}$ mice. This poses promising targets for patients with HA. Certain DMARDs/anti-rheumatic drugs have already been shown to suppress both Th1 immune responses, but to a lesser extent Th2 immune responses in mice (Yamaki et al., 2005). Seeing how these approved drugs affect our model of HA could improve our understanding of

the exact mechanism leading to chronic HA, while also exploring the use of these drugs in the treatment of HA.

The IL-33/ST2 axis in HA would require more experimentation to fully elucidate the exact point in the pathway that could play a role in HA pathogenesis. The results from Chapter 4 show this pathway could be targeted for co-therapeutics. Within the IL-33/ST2 pathway, as seen in Figure 1.7, MyD88 could be targeted using a small molecule inhibitor in the *F8*$^{em1-/-}$ mouse model and progression of disease tracked using the same methods in Chapter 3. The small molecule inhibitor to MyD88, M20, works by targeting the MyD88-TIR domain and subsequently production of pro-inflammatory markers such as TNFa and IL-6 can be reduced (Song et al., 2021). Should this not be effective in attenuating the disease at this point in the pathway, other drugs could be used. Astegolimab is an ST2 inhibitor that is studied for use in diseases such as severe asthma (Kelsen et al., 2021). Administering the inhibitor to *F8*$^{em1-/-}$ mouse model would block the IL-33/ST2 pathway by directly binding to the ST2 receptor (Kotani et al., 2022). However, with the drug in the process of gaining FDA approved, and side effects studied, the use of the inhibitor as a co-therapeutic could potentially have great benefits for patients with HA including attenuation or even prevention of the disease. While this thesis has focused in more on the IL-33/ST2 axis and the effects of Th2-mediated response, there is scope to analyse further mechanisms that may also play a role in the development and progression of experimental HA. A potential role for the *Lcn2* gene has been seen in the *F8*$^{em1-/-}$ mouse model as well. Preliminary data (not shown) analysing the expression of the *Lcn2* gene in *F8*$^{em1-/-}$ mice compared to matched WT mice showed an increase in expression in the *F8*$^{em1-/-}$ mice in the first week of the time course. Serum lipocalin 2 (LCN-2) levels have been tested in clinical settings in RA with a significantly higher level in RA patients than in serum of controls (Gulkesen et al., 2017). Thus, by using a *Lcn2*$^{-/-}$ mouse model with the *F8*$^{em1-/-}$ mouse model (to create a dual-knockout mouse), further research on this specific mechanism can be conducted to identify another potential pathway in the pathogenesis of HA.

I have focused on two other strain backgrounds along with the C57BL/6J model. However, the DBA/1 mouse model has been used in many experiments involving arthropathy research. The use of this mouse model could be of potential value as

already it is a well-established model in arthropathy research for collagen-induced arthritis (CIA) and collagen antibody-induced arthritis (CAIA) (Myers et al., 1997, Khachigian, 2006). While CIA and CAIA provide models for RA, it cannot be doubted that the choice of DBA/1 mouse strain does not play a factor. The DBA/1 mouse model is particularly suitable for research in arthropathies as the mouse strain is susceptible to the spontaneous development of arthritis, already predisposing them to the development of arthropathy (Braem et al., 2012). Thus, with the DBA/1 *F8*$^{em1-/-}$ mouse model, the mouse would be predisposed to spontaneous bleeds as well as the development of arthritis, reflecting the heterogeneity found in the human population and diversifying the predisposition of the *F8*$^{em1-/-}$ model. Further experimentation with the DBA/1 line, using the same experimental techniques as in Chapter 3, could elucidate the benefit of certain drugs to prevent the pathogenesis of HA. Methotrexate could be administered pre- and/or post-injury to reduce joint damage and should this be successful in the context of HA, the use of the drug could be taken alongside factor replacement. The drug is available as a tablet form and thus injections would not be necessary and would create less complications for the patient should they be using antibodies like emicizumab, where injection sites are limited and rotated with each injection (Morrow, 2018).

6.2. Conclusions

In conclusion, this PhD thesis has established a working experimental HA model using a novel mouse model of severe haemophilia A. The spontaneous bleeding phenotype found in the *F8*$^{em1-/-}$ mouse model is something that requires more attention when conducting experiments but adds a more comprehensive likeness to what we see in PwsH. Similarly, our lab was able to develop the same model on various strain backgrounds and thus I was able to investigate the effects of genetic backgrounds on the pathogenesis of HA, something more reflective of the patient population. The use of dual-knockout strains also aids in the research for experimental HA, as the handling of mice is greatly reduced, and specific gene targets can be investigated. The exact mechanism(s) of the pathogenesis of HA is something that requires more research, but this thesis has identified several potential pathways that could play a major role, namely the IL-33/ST2 axis and Th2-mediated responses. These results provide a

potential therapeutic target to improve patient outcome for those who are at risk of developing HA.

Appendices

Appendix I

Primers for *F8*$^{em1-/-}$ genotyping were as below.

Genotyping primers:

Primer name	Primer Sequence
Forward primer (US*F8*_F2)	5'-CATGCAAATAGCACTCTTCGCTTG-3'
Reverse primer (US*F8*_R3)	5'-CTTTTCTCCATGTCAGTAGAAACAACC-3'

Appendix II

HPRA scoring parameters and sheets for experimental HA induced by needle puncture.

Procedure 05 – Experimental haemophilic arthropathy induced by needle puncture

Scoring parameters:

Gait	
0	Normal
1	Reduced ambulation
2	Significantly reduced ambulation, decreased response to stimuli
3	Complete lack of ambulation, no response to stimuli
Physical appearance	
0	Normal
1	Lack of grooming
2	Piloerection, nasal/ocular discharge
3	Piloerection, hunched posture
Unprovoked behaviour	
0	Normal
1	Reduced interest in surroundings
2	Reduced mobility, decreased alertness
3	Vocalization, inactive

ACTIONS:

- **Mice will be humanely euthanised if they reach an overall score of 6.**
- **Mice will be humanely euthanised if they reach a score of 3 in any individual category.**

Procedure 05 – Experimental haemophilic arthropathy induced by needle puncture

User:

Experimental number:

Date started:

Cage:

Date	Gait	Physical appearance	Unprovoked behaviour	Overall score

ACTIONS:

- **Mice will be humanely euthanised if they show sustained leg impairment.**

Appendix III

MSD murine analytes

Plate 1	IFNg	**Plate 2**	IL33
	TNFa		IL31
	IL12p70		IL17F
	IL10		IL17C
	IL6		IL17A
	IL5		IL16
	IL4		
	IL2		
	IL1b		
	KC		

Appendix IV

List of macrophage associated genes and list of neutrophil associated genes analysed in the NanoString Mouse Myeloid cassette.

Macrophage associated genes					**Neutrophil associated genes**	
2900026A02Rik	Cd40	Flt1	Irf7	Ripk2	2810417H13Rik	Il10
Acad10	Cd47	Flt3	Irf8	Runx2	Alox5ap	Il10ra
Acly	Cd68	Fn1	Itgam	S100a10	Amica1	Il15ra
Acod1	Cd69	Furin	Kalrn	S100a11	Anxa1	Il18
Acot11	Cd70	Fzd4	Kcnq1ot1	S100a4	Arg1	Il18r1
Acot3	Cd74	Fzd6	Kit	S100a9	Btk	Il1b
Acox1	Cd83	Gadd45b	Klf4	Sema4a	C5ar1	Il1r1

Adam19	Cd84	Gata3	Lat2	Sema4b	Camp	Il4ra
Adam8	Cdh11	Gata6	Lipa	Sema5a	Casp1	Il6
Adamts1	Cdh13	Gk5	Lpl	Sema6d	Ccl12	Il6ra
Adamts12	Cdh5	Golim4	Lrp5	Serpinb2	Ccl17	Itga4
Adamts14	Ceacam1	Grn	Lrp6	Serpinb6a	Ccl19	Itgal
Adamts17	Ceacam2	H2-Aa	Lst1	Serpinb7	Ccl20	Itgam
Adamts2	Cebpd	H2-D1	Mafb	Serpine1	Ccl22	Itgb2
Adamts3	Cebpg	H2-DMa	Marco	Serpine3	Ccl3	Ltb4r1
Adamts4	Chil3	H2-DMb1	Mcm5	Sesn1	Ccl4	Ltb4r2
Adamts9	Chil4	H2-DMb2	Mertk	Sfrp4	Ccl5	Ly6g
Adgre1	Cldn1	H2-Ea-ps	Met	Siglec1	Ccl8	Mertk
Adgre5	Clec5a	H2-Eb1	Mmp10	Sirpa	Cd44	Mif
Adora3	Clec7a	H2-K1	Mmp12	Ski	Cd99	Mmp8
Aif1	Clec9a	H2-M3	Mmp13	Smad1	Cebpa	Mmp9
Alcam	Col10a1	H2-Ob	Mmp19	Smad2	Cebpb	Mok
Alox15	Col11a1	H2-Q1	Mmp1a	Socs1	Clec1b	Mpo
Alox5	Col12a1	H2-Q10	Mmp9	Socs2	Clec5a	Ms4a1
Alox5ap	Col14a1	H2-Q2	Mob3c	Socs3	Clec7a	Ncf2
Angpt1	Col15a1	H2-T23	Mpeg1	Sphk1	Csf2	Nlrp3
Angpt2	Col1a2	Hbegf	Mrc1	Stab1	Csf2ra	Nod1
Aoah	Col3a1	Hc	Mrc2	Stat1	Csf3	Nod2
Apoe	Col4a1	Hdac6	Msh2	Stat3	Csf3r	Nos2
Areg	Col4a2	Hes1	Mx1	Stat6	Cxcl1	Nox1
Arg1	Csf1r	Hip1r	Mx2	Tek	Cxcl10	Nox3
Arhgef28	Cstb	Hmgb1	Myd88	Terf2ip	Cxcl11	Nox4
Armc1	Ctgf	Hspg2	Nectin1	Tgfb1	Cxcl12	Osm
Batf3	Ctnnb1	Icam1	Nectin2	Tgfbr3	Cxcl16	Pde4a
Birc5	Ctsa	Id3	Nfkb1	Tgm2	Cxcl2	Pdgfrb
Bmp6	Ctsd	Ido1	Nfkbiz	Tigit	Cxcl3	Pf4
Bmp8a	Ctss	Ido2	Nlrp3	Timp3	Cxcl5	Pglyrp1
Btk	Cttnbp2	Ifnar1	Nos2	Tlr2	Cxcl9	Pik3cg
C3	Cx3cr1	Ifnar2	Nr1h3	Tlr3	Cxcr1	Prok2
C3ar1	Cxcl10	Ifnb1	Nr4a1	Tlr7	Cxcr2	Ptafr
C5ar1	Cxcl12	Igf1	Nrip3	Tmem173	Cxcr4	Ptprc
Calr	Cxcl13	Igf2	Oscar	Tnf	Cybb	Ptx3
Casp1	Cxcl14	Ikbke	Pik3cg	Tnfrsf8	Egf	Rgs16
Cav1	Cxcl9	Il10	Plau	Traf1	Elane	Ros1

Ccl1	Cxcr1	Il12a	Plaur	Trem1	F11r	S100a11
Ccl12	Cxcr2	Il12b	Pparg	Trem2	Fas	S100a8
Ccl17	Cxcr3	Il13	Prdx1	Trex1	Fcer1a	S100a9
Ccl2	Cxcr4	Il15ra	Prdx3	Trim9	Fcer2a	Sell
Ccl20	Cxcr5	Il17ra	Pros1	Twistnb	Fcgr1	Selplg
Ccl21a	Cxcr6	Il18	Ptgs1	Txn1	Fcgr2b	Serpinb6a
Ccl22	Cyr61	Il18r1	Ptgs2	Tyrobp	Fcgr3	Syk
Ccl24	Ddr2	Il1a	Ptpn14	Vav1	Fcnb	Tgfa
Ccl25	Dhrs3	Il1b	Ptprb	Vsir	Fgf10	Tgfb1
Ccl27a	Edn1	Il1r1	Ptprc	Yap1	Fgf2	Tlr1
Ccl3	Enpep	Il1r2	Ptprk	Yes1	Fgf7	Tlr2
Ccl4	Ercc1	Il1rap	Pycard	Zmpste24	Fpr1	Tlr4
Ccl5	Erg	Il1rn	Rad51		Fpr2	Tlr5
Ccr1	Ets1	Il21r	Rapgef4		Fpr3	Tlr6
Ccr2	Fabp4	Il22	Rasgrf2		Fpr-rs3	Tlr7
Ccr3	Fasn	Il23a	Rbp1		Fpr-rs4	Tlr8
Ccr4	Fbp1	Il27	Retnla		Fpr-rs5	Tlr9
Ccr5	Fbxl7	Il4i1	Retnlb		Fpr-rs6	Tnf
Ccr9	Fcgr1	Il5ra	Rgl1		Glg1	Tnfrsf11a
Cd14	Fcgr2b	Il6	Rgs1		Hbegf	Tnfrsf1a
Cd163	Fcgr3	Insr	Rgs16		Hgf	Tnfrsf1b
Cd180	Fem1c	Irf1	Rgs6		Hif1a	Tnfsf10
Cd209e	Fgf10	Irf3	Rhoj		Ifna1	Vegfa
Cd247	Fgf18	Irf4	Rictor		Ifng	Zmpste24
Cd36	Fgf7	Irf5	Rin2		Ifngr1	

References

ABRAMSON, S. B. & AMIN, A. 2002. Blocking the effects of IL-1 in rheumatoid arthritis protects bone and cartilage. *Rheumatology (Oxford),* 41**,** 972-80.

ACKERT-BICKNELL, C. L., ANDERSON, L. C., SHEEHAN, S., HILL, W. G., CHANG, B., CHURCHILL, G. A., CHESLER, E. J., KORSTANJE, R. & PETERS, L. L. 2015. Aging Research Using Mouse Models. *Curr Protoc Mouse Biol,* 5**,** 95-133.

AIDA, T., CHIYO, K., USAMI, T., ISHIKUBO, H., IMAHASHI, R., WADA, Y., TANAKA, K. F., SAKUMA, T., YAMAMOTO, T. & TANAKA, K. 2015. Cloning-free CRISPR/Cas system facilitates functional cassette knock-in in mice. *Genome Biol,* 16**,** 87.

AKESON, G. & MALEMUD, C. J. 2017. A Role for Soluble IL-6 Receptor in Osteoarthritis. *J Funct Morphol Kinesiol,* 2.

AKHABIR, L. & SANDFORD, A. 2010. Genetics of interleukin 1 receptor-like 1 in immune and inflammatory diseases. *Curr Genomics,* 11**,** 591-606.

AKUTHOTA, P., WANG, H. B., SPENCER, L. A. & WELLER, P. F. 2008. Immunoregulatory roles of eosinophils: a new look at a familiar cell. *Clin Exp Allergy,* 38**,** 1254-63.

ALEDORT, L. M., HASCHMEYER, R. H. & PETTERSSON, H. 1994. A longitudinal study of orthopaedic outcomes for severe factor-VIII-deficient haemophiliacs. The Orthopaedic Outcome Study Group. *J Intern Med,* 236**,** 391-9.

ALLEGRA, A., INNAO, V., TARTARISCO, G., PIOGGIA, G., CASCIARO, M., MUSOLINO, C. & GANGEMI, S. 2019. The ST2/Interleukin-33 Axis in Hematologic Malignancies: The IL-33 Paradox. *Int J Mol Sci,* 20.

ALLEN, J. E. 2023. IL-4 and IL-13: Regulators and Effectors of Wound Repair. *Annu Rev Immunol*.

ARONSTAM, A., RAINSFORD, S. G. & PAINTER, M. J. 1979. Patterns of bleeding in adolescents with severe haemophilia A. *Br Med J,* 1**,** 469-70.

ASHFORD, S. & WILLIARD, J. 2014. Osteoarthritis: A review. *Nurse Pract,* 39**,** 1-8.

BARNER, M., MOHRS, M., BROMBACHER, F. & KOPF, M. 1998. Differences between IL-4R alpha-deficient and IL-4-deficient mice reveal a role for IL-13 in the regulation of Th2 responses. *Curr Biol,* 8**,** 669-72.

BARNETT, R. 2018. Osteoarthritis. *Lancet,* 391**,** 1985.

BERNTORP, E., FISCHER, K., HART, D. P., MANCUSO, M. E., STEPHENSEN, D., SHAPIRO, A. D. & BLANCHETTE, V. 2021. Haemophilia. *Nat Rev Dis Primers,* 7**,** 45.

BERTLING, A., BRODDE, M. F., VISSER, M., TREFFON, J., FENNEN, M., FENDER, A. C., KELSCH, R. & KEHREL, B. E. 2017. Components in Plasma-Derived Factor VIII, But Not in Recombinant Factor VIII Downregulate Anti-Inflammatory Surface Marker CD163 in Human Macrophages through Release of CXCL4 (Platelet Factor 4). *Transfus Med Hemother,* 44**,** 351-357.

BHARDWAJ, R., RATH, G. & GOYAL, A. K. 2018. Advancement in the treatment of haemophilia. *Int J Biol Macromol,* 118**,** 289-295.

BHAT, V., OLMER, M., JOSHI, S., DURDEN, D. L., CRAMER, T. J., BARNES, R. F., BALL, S. T., HUGHES, T. H., SILVA, M., LUCK, J. V., MOORE, R. E., MOSNIER, L. O. & VON DRYGALSKI, A. 2015. Vascular remodeling underlies rebleeding in hemophilic arthropathy. *Am J Hematol,* 90**,** 1027-35.

BI, L., LAWLER, A. M., ANTONARAKIS, S. E., HIGH, K. A., GEARHART, J. D. & KAZAZIAN, H. H., JR. 1995. Targeted disruption of the mouse factor VIII gene produces a model of haemophilia A. *Nat Genet,* 10**,** 119-21.

BI, L., SARKAR, R., NAAS, T., LAWLER, A. M., PAIN, J., SHUMAKER, S. L., BEDIAN, V. & KAZAZIAN, H. H., JR. 1996. Further characterization of factor VIII-deficient mice created by gene targeting: RNA and protein studies. *Blood,* 88**,** 3446-50.

BLUMBERG, R. S., LILLICRAP, D. & IG, G. F. I. T. G. 2018. Tolerogenic properties of the Fc portion of IgG and its relevance to the treatment and management of hemophilia. *Blood,* 131**,** 2205-2214.

BOLTON-MAGGS, P. H. & PASI, K. J. 2003. Haemophilias A and B. *Lancet,* 361**,** 1801-9.

BRAEM, K., CARTER, S. & LORIES, R. J. 2012. Spontaneous arthritis and ankylosis in male DBA/1 mice: further evidence for a role of behavioral factors in "stress-induced arthritis". *Biol Proced Online,* 14**,** 10.

BRIL, W. S., VAN HELDEN, P. M., HAUSL, C., ZUURVELD, M. G., AHMAD, R. U., HOLLESTELLE, M. J., REITSMA, P. H., FIJNVANDRAAT, K., VAN LIER, R. A., SCHWARZ, H. P., MERTENS, K., REIPERT, B. M. & VOORBERG, J. 2006. Tolerance to factor VIII in a transgenic mouse expressing human factor VIII cDNA carrying an Arg(593) to Cys substitution. *Thromb Haemost,* 95**,** 341-7.

BRYANT, C. D. 2011. The blessings and curses of C57BL/6 substrains in mouse genetic studies. *Ann N Y Acad Sci,* 1245**,** 31-3.

BUCKLEY, C. D. 2019. An immune-cell barrier protects joints. *Nature.*

BUCKLEY, C. D., OSPELT, C., GAY, S. & MIDWOOD, K. S. 2021. Location, location, location: how the tissue microenvironment affects inflammation in RA. *Nat Rev Rheumatol,* 17**,** 195-212.

BURGESS, M., WICKS, K., GARDASEVIC, M. & MACE, K. A. 2019. Cx3CR1 Expression Identifies Distinct Macrophage Populations That Contribute Differentially to Inflammation and Repair. *Immunohorizons,* 3**,** 262-273.

BYRNE, C. 2021. *The Generation and Characterisation of Novel Mouse Models of Haemophilia A.* PhD Thesis, Trinity College Dublin.

CARDONA, A. E., PIORO, E. P., SASSE, M. E., KOSTENKO, V., CARDONA, S. M., DIJKSTRA, I. M., HUANG, D., KIDD, G., DOMBROWSKI, S., DUTTA, R., LEE, J. C., COOK, D. N., JUNG, S., LIRA, S. A., LITTMAN, D. R. & RANSOHOFF, R. M. 2006. Control of microglial neurotoxicity by the fractalkine receptor. *Nat Neurosci,* 9**,** 917-24.

CASTALDO, G., D'ARGENIO, V., NARDIELLO, P., ZARRILLI, F., SANNA, V., ROCINO, A., COPPOLA, A., DI MINNO, G. & SALVATORE, F. 2007. Haemophilia A: molecular insights. *Clin Chem Lab Med,* 45**,** 450-61.

CAYROL, C. & GIRARD, J. P. 2018. Interleukin-33 (IL-33): A nuclear cytokine from the IL-1 family. *Immunol Rev,* 281**,** 154-168.

CHAVALI, V., NANDI, S. S., SINGH, S. R. & MISHRA, P. K. 2014. Generating double knockout mice to model genetic intervention for diabetic cardiomyopathy in humans. *Methods Mol Biol,* 1194**,** 385-400.

CHIN, B., WEE, I., SYN, N. L., O'NEILL, G. K., YAP, E. S. & KOH, P. L. 2022. Surgery for chronic arthropathy in people with haemophilia. *Cochrane Database Syst Rev,* 11**,** CD013634.

CHRISTENSEN, K. R., KJELGAARD-HANSEN, M., NIELSEN, L. N., WIINBERG, B., ALEXANDER ALTHOEHN, F., BLOKSGAARD POULSEN, N., KRYGER VOLS, K., POPP THYME, A., MARIA LOVGREN, K., KORNERUP HANSEN, A. & ROEPSTORFF, K. 2019. Rapid inflammation and early degeneration of bone

and cartilage revealed in a time-course study of induced haemarthrosis in haemophilic rats. *Rheumatology (Oxford),* 58**,** 588-599.
CHU, W. M., HO, H. E., WANG, J. D., CHAN, W. C., LIOU, Y. S., HO, W. C., HU, S. Y. & TSAN, Y. T. 2018. Risk of major comorbidities among workers with hemophilia: A 14-year population-based study. *Medicine (Baltimore),* 97**,** e9803.
CLARK, E. A. & LEDBETTER, J. A. 1989. Structure, function, and genetics of human B cell-associated surface molecules. *Adv Cancer Res,* 52**,** 81-149.
COOKE, E. J., WYSEURE, T., ZHOU, J. Y., GOPAL, S., NASAMRAN, C. A., FISCH, K. M., MANON-JENSEN, T., KARSDAL, M. A., MOSNIER, L. O. & VON DRYGALSKI, A. 2019. Mechanisms of vascular permeability and remodeling associated with hemarthrosis in factor VIII-deficient mice. *J Thromb Haemost,* 17**,** 1815-1826.
COOKE, E. J., ZHOU, J. Y., WYSEURE, T., JOSHI, S., BHAT, V., DURDEN, D. L., MOSNIER, L. O. & VON DRYGALSKI, A. 2018. Vascular Permeability and Remodelling Coincide with Inflammatory and Reparative Processes after Joint Bleeding in Factor VIII-Deficient Mice. *Thromb Haemost,* 118**,** 1036-1047.
COPPOLA, A., DI CAPUA, M., DI MINNO, M. N., DI PALO, M., MARRONE, E., IERANO, P., ARTURO, C., TUFANO, A. & CERBONE, A. M. 2010. Treatment of hemophilia: a review of current advances and ongoing issues. *J Blood Med,* 1**,** 183-95.
CULEMANN, S., GRUNEBOOM, A., NICOLAS-AVILA, J. A., WEIDNER, D., LAMMLE, K. F., ROTHE, T., QUINTANA, J. A., KIRCHNER, P., KRLJANAC, B., EBERHARDT, M., FERRAZZI, F., KRETZSCHMAR, E., SCHICHT, M., FISCHER, K., GELSE, K., FAAS, M., PFEIFLE, R., ACKERMANN, J. A., PACHOWSKY, M., RENNER, N., SIMON, D., HASELOFF, R. F., EKICI, A. B., BAUERLE, T., BLASIG, I. E., VERA, J., VOEHRINGER, D., KLEYER, A., PAULSEN, F., SCHETT, G., HIDALGO, A. & KRONKE, G. 2019. Locally renewing resident synovial macrophages provide a protective barrier for the joint. *Nature,* 572**,** 670-675.
DE LA FUENTE, M., MACDONALD, T. T. & HERMOSO, M. A. 2015. The IL-33/ST2 axis: Role in health and disease. *Cytokine Growth Factor Rev,* 26**,** 615-23.
DE VOOGHT, V., VANOIRBEEK, J. A., LUYTS, K., HAENEN, S., NEMERY, B. & HOET, P. H. 2010. Choice of mouse strain influences the outcome in a mouse model of chemical-induced asthma. *PLoS One,* 5**,** e12581.
DEMYANETS, S., STOJKOVIC, S., HUBER, K. & WOJTA, J. 2021. The Paradigm Change of IL-33 in Vascular Biology. *Int J Mol Sci,* 22.
DONG, C., FU, T., JI, J., LI, Z. & GU, Z. 2018. The role of interleukin-4 in rheumatic diseases. *Clin Exp Pharmacol Physiol,* 45**,** 747-754.
DOSHI, B. S., RANA, J., CASTAMAN, G., SHAHEEN, M. A., KACZMAREK, R., BUTTERFIELD, J. S., MEEKS, S. L., LEISSINGER, C., BISWAS, M. & ARRUDA, V. R. 2021. B cell-activating factor modulates the factor VIII immune response in hemophilia A. *J Clin Invest,* 131.
DULAY, G. S., COOPER, C. & DENNISON, E. M. 2015. Knee pain, knee injury, knee osteoarthritis & work. *Best Pract Res Clin Rheumatol,* 29**,** 454-61.
DUTTA, S. & SENGUPTA, P. 2016. Men and mice: Relating their ages. *Life Sci,* 152**,** 244-8.
EL-MIKKAWY, D. M. E., ELBADAWY, M. A., ABD EL-GHANY, S. M. & SAMAHA, D. 2019. Serum Sclerostin Level and Bone Mineral Density in Pediatric Hemophilic Arthropathy. *Indian J Pediatr,* 86**,** 515-519.

FARRUGIA, M. & BARON, B. 2016. The role of TNF-alpha in rheumatoid arthritis: a focus on regulatory T cells. *J Clin Transl Res,* 2**,** 84-90.
FINKELMAN, F. D., MADDEN, K. B., MORRIS, S. C., HOLMES, J. M., BOIANI, N., KATONA, I. M. & MALISZEWSKI, C. R. 1993. Anti-cytokine antibodies as carrier proteins. Prolongation of in vivo effects of exogenous cytokines by injection of cytokine-anti-cytokine antibody complexes. *J Immunol,* 151**,** 1235-44.
FISCHER, K., BOM, J. G., MAUSER-BUNSCHOTEN, E. P., ROOSENDAAL, G. & BERG, H. M. 2005. Effects of haemophilic arthropathy on health-related quality of life and socio-economic parameters. *Haemophilia,* 11**,** 43-8.
FORNEFETT, J., KRAUSE, J., KLOSE, K., FINGAS, F., HASSERT, R., BENGA, L., GRUNWALD, T., MULLER, U., SCHRODL, W. & BAUMS, C. G. 2018. Comparative analysis of humoral immune responses and pathologies of BALB/c and C57BL/6 wildtype mice experimentally infected with a highly virulent Rodentibacter pneumotropicus (Pasteurella pneumotropica) strain. *BMC Microbiol,* 18**,** 45.
FUKUSHIMA, A., YAMAGUCHI, T., ISHIDA, W., FUKATA, K., TANIGUCHI, T., LIU, F. T. & UENO, H. 2006. Genetic background determines susceptibility to experimental immune-mediated blepharoconjunctivitis: comparison of Balb/c and C57BL/6 mice. *Exp Eye Res,* 82**,** 210-8.
FULKERSON, P. C. & ROTHENBERG, M. E. 2013. Targeting eosinophils in allergy, inflammation and beyond. *Nat Rev Drug Discov,* 12**,** 117-29.
GIBBONS, J. B., LABER, M. & BENNETT, C. L. 2023. Humira: the first $20 billion drug. *Am J Manag Care,* 29**,** 78-80.
GLYN-JONES, S., PALMER, A. J., AGRICOLA, R., PRICE, A. J., VINCENT, T. L., WEINANS, H. & CARR, A. J. 2015. Osteoarthritis. *Lancet,* 386**,** 376-87.
GORDON, E. D., PALANDRA, J., WESOLOWSKA-ANDERSEN, A., RINGEL, L., RIOS, C. L., LACHOWICZ-SCROGGINS, M. E., SHARP, L. Z., EVERMAN, J. L., MACLEOD, H. J., LEE, J. W., MASON, R. J., MATTHAY, M. A., SHELDON, R. T., PETERS, M. C., NOCKA, K. H., FAHY, J. V. & SEIBOLD, M. A. 2016. IL1RL1 asthma risk variants regulate airway type 2 inflammation. *JCI Insight,* 1**,** e87871.
GRALINSKI, L. E., SHEAHAN, T. P., MORRISON, T. E., MENACHERY, V. D., JENSEN, K., LEIST, S. R., WHITMORE, A., HEISE, M. T. & BARIC, R. S. 2018. Complement Activation Contributes to Severe Acute Respiratory Syndrome Coronavirus Pathogenesis. *mBio,* 9.
GRIESENAUER, B. & PACZESNY, S. 2017. The ST2/IL-33 Axis in Immune Cells during Inflammatory Diseases. *Front Immunol,* 8**,** 475.
GRUPPO, R. A., BROWN, D., WILKES, M. M. & NAVICKIS, R. J. 2004. Increased breakthrough bleeding during prophylaxis with B-domain deleted factor VIII--a robust meta-analytic finding. *Haemophilia,* 10**,** 449-51.
GUALTIEROTTI, R., SOLIMENO, L. P. & PEYVANDI, F. 2021. Hemophilic arthropathy: Current knowledge and future perspectives. *J Thromb Haemost,* 19**,** 2112-2121.
GULKESEN, A., AKGOL, G., POYRAZ, A. K., AYDIN, S., DENK, A., YILDIRIM, T. & KAYA, A. 2017. Lipocalin 2 as a clinical significance in rheumatoid arthritis. *Cent Eur J Immunol,* 42**,** 269-273.
GUPTON, M., IMONUGO, O. & TERREBERRY, R. R. 2023. Anatomy, Bony Pelvis and Lower Limb, Knee. *StatPearls.* Treasure Island (FL).

HAKOBYAN, N., ENOCKSON, C., COLE, A. A., SUMNER, D. R. & VALENTINO, L. A. 2008. Experimental haemophilic arthropathy in a mouse model of a massive haemarthrosis: gross, radiological and histological changes. *Haemophilia,* 14**,** 804-9.

HAKOBYAN, N., KAZARIAN, T., JABBAR, A. A., JABBAR, K. J. & VALENTINO, L. A. 2004. Pathobiology of hemophilic synovitis I: overexpression of mdm2 oncogene. *Blood,* 104**,** 2060-4.

HAKOBYAN, N., KAZARIAN, T. & VALENTINO, L. A. 2005. Synovitis in a murine model of human factor VIII deficiency. *Haemophilia,* 11**,** 227-32.

HAKOBYAN, N., VALENTINO, L. A., CONG, L., ENOCKSON, C., SONG, X. Q., DESAI, S., RADTKE, R. & FOGG, L. F. 2016. Haemarthrosis model in mice: BSS - Bleeding Severity Score assessment system. *Haemophilia,* 22**,** 790-8.

HAXAIRE, C., HAKOBYAN, N., PANNELLINI, T., CARBALLO, C., MCILWAIN, D., MAK, T. W., RODEO, S., ACHARYA, S., LI, D., SZYMONIFKA, J., SONG, X., MONETTE, S., SRIVASTAVA, A., SALMON, J. E. & BLOBEL, C. P. 2018. Blood-induced bone loss in murine hemophilic arthropathy is prevented by blocking the iRhom2/ADAM17/TNF-alpha pathway. *Blood,* 132**,** 1064-1074.

HERTWIG, L., HAMANN, I., ROMERO-SUAREZ, S., MILLWARD, J. M., PIETREK, R., CHANVILLARD, C., STUIS, H., POLLOK, K., RANSOHOFF, R. M., CARDONA, A. E. & INFANTE-DUARTE, C. 2016. CX3CR1-dependent recruitment of mature NK cells into the central nervous system contributes to control autoimmune neuroinflammation. *Eur J Immunol,* 46**,** 1984-96.

HO, M., POST, C. M., DONAHUE, L. R., LIDOV, H. G., BRONSON, R. T., GOOLSBY, H., WATKINS, S. C., COX, G. A. & BROWN, R. H., JR. 2004. Disruption of muscle membrane and phenotype divergence in two novel mouse models of dysferlin deficiency. *Hum Mol Genet,* 13**,** 1999-2010.

HOCHBERG, M. C., ALTMAN, R. D., APRIL, K. T., BENKHALTI, M., GUYATT, G., MCGOWAN, J., TOWHEED, T., WELCH, V., WELLS, G., TUGWELL, P. & AMERICAN COLLEGE OF, R. 2012. American College of Rheumatology 2012 recommendations for the use of nonpharmacologic and pharmacologic therapies in osteoarthritis of the hand, hip, and knee. *Arthritis Care Res (Hoboken),* 64**,** 465-74.

HONG, Y. S., MOON, S. J., JOO, Y. B., JEON, C. H., CHO, M. L., JU, J. H., OH, H. J., HEO, Y. J., PARK, S. H., KIM, H. Y. & MIN, J. K. 2011. Measurement of interleukin-33 (IL-33) and IL-33 receptors (sST2 and ST2L) in patients with rheumatoid arthritis. *J Korean Med Sci,* 26**,** 1132-9.

HOOIVELD, M., ROOSENDAAL, G., VIANEN, M., VAN DEN BERG, M., BIJLSMA, J. & LAFEBER, F. 2003a. Blood-induced joint damage: longterm effects in vitro and in vivo. *J Rheumatol,* 30**,** 339-44.

HOOIVELD, M., ROOSENDAAL, G., WENTING, M., VAN DEN BERG, M., BIJLSMA, J. & LAFEBER, F. 2003b. Short-term exposure of cartilage to blood results in chondrocyte apoptosis. *Am J Pathol,* 162**,** 943-51.

HOOIVELD, M. J., ROOSENDAAL, G., VAN DEN BERG, H. M., BIJLSMA, J. W. & LAFEBER, F. P. 2003c. Haemoglobin-derived iron-dependent hydroxyl radical formation in blood-induced joint damage: an in vitro study. *Rheumatology (Oxford),* 42**,** 784-90.

HOOIVELD, M. J., ROOSENDAAL, G., VIANEN, M. E., VAN DEN BERG, H. M., BIJLSMA, J. W. & LAFEBER, F. P. 2003d. Immature articular cartilage is more susceptible to blood-induced damage than mature articular cartilage: an in vivo animal study. *Arthritis Rheum,* 48**,** 396-403.

HOOVER-PLOW, J., SHCHURIN, A., HART, E., SHA, J., HILL, A. E., SINGER, J. B. & NADEAU, J. H. 2006. Genetic background determines response to hemostasis and thrombosis. *BMC Blood Disord,* 6**,** 6.

HUA, B., OLSEN, E. H. N., SUN, S., GUDME, C. N., WANG, L., VANDAHL, B., ROEPSTORFF, K., KJELGAARD-HANSEN, M., SORENSEN, B. B., ZHAO, Y., KARSDAL, M. A. & MANON-JENSEN, T. 2017. Serological biomarkers detect active joint destruction and inflammation in patients with haemophilic arthropathy. *Haemophilia,* 23**,** e294-e300.

IORIO, A., STONEBRAKER, J. S., CHAMBOST, H., MAKRIS, M., COFFIN, D., HERR, C., GERMINI, F., DATA & DEMOGRAPHICS COMMITTEE OF THE WORLD FEDERATION OF, H. 2019. Establishing the Prevalence and Prevalence at Birth of Hemophilia in Males: A Meta-analytic Approach Using National Registries. *Ann Intern Med,* 171**,** 540-546.

JACKSON, S. J., ANDREWS, N., BALL, D., BELLANTUONO, I., GRAY, J., HACHOUMI, L., HOLMES, A., LATCHAM, J., PETRIE, A., POTTER, P., RICE, A., RITCHIE, A., STEWART, M., STREPKA, C., YEOMAN, M. & CHAPMAN, K. 2017. Does age matter? The impact of rodent age on study outcomes. *Lab Anim,* 51**,** 160-169.

JACOB, N., GUO, S., MATHIAN, A., KOSS, M. N., GINDEA, S., PUTTERMAN, C., JACOB, C. O. & STOHL, W. 2011. B Cell and BAFF dependence of IFN-alpha-exaggerated disease in systemic lupus erythematosus-prone NZM 2328 mice. *J Immunol,* 186**,** 4984-93.

JACOBSEN, E. A., HELMERS, R. A., LEE, J. J. & LEE, N. A. 2012. The expanding role(s) of eosinophils in health and disease. *Blood,* 120**,** 3882-90.

JANSEN, N. W., ROOSENDAAL, G., BIJLSMA, J. W., DEGROOT, J. & LAFEBER, F. P. 2007. Exposure of human cartilage tissue to low concentrations of blood for a short period of time leads to prolonged cartilage damage: an in vitro study. *Arthritis Rheum,* 56**,** 199-207.

JENKINS, S. J., RUCKERL, D., COOK, P. C., JONES, L. H., FINKELMAN, F. D., VAN ROOIJEN, N., MACDONALD, A. S. & ALLEN, J. E. 2011. Local macrophage proliferation, rather than recruitment from the blood, is a signature of TH2 inflammation. *Science,* 332**,** 1284-8.

JILKA, R. L. 2013. The relevance of mouse models for investigating age-related bone loss in humans. *J Gerontol A Biol Sci Med Sci,* 68**,** 1209-17.

JOSEPH, R., PADRAIC, G. F. & EMILY, H. 2019. The Pivotal Role of Macrophages in Metabolic Distress. *In:* KHALID HUSSAIN, B. (ed.) *Macrophage Activation.* Rijeka: IntechOpen.

JOSHI, N., YAN, J., LEVY, S., BHAGCHANDANI, S., SLAUGHTER, K. V., SHERMAN, N. E., AMIRAULT, J., WANG, Y., RIEGEL, L., HE, X., RUI, T. S., VALIC, M., VEMULA, P. K., MIRANDA, O. R., LEVY, O., GRAVALLESE, E. M., ALIPRANTIS, A. O., ERMANN, J. & KARP, J. M. 2018. Towards an arthritis flare-responsive drug delivery system. *Nat Commun,* 9**,** 1275.

KAMINSKI, T. W., BRZOSKA, T., TUTUNCUOGLU, E., RAGNI, M. V. & SUNDD, P. 2020. Neutrophil Extracellular Traps Promote Joint Injury in Hemophilia. *Blood,* 136.

KAPOOR, M., MARTEL-PELLETIER, J., LAJEUNESSE, D., PELLETIER, J. P. & FAHMI, H. 2011. Role of proinflammatory cytokines in the pathophysiology of osteoarthritis. *Nat Rev Rheumatol,* 7**,** 33-42.

KAREEM, R., BOTLEROO, R. A., BHANDARI, R., OGEYINGBO, O. D., AHMED, R., GYAWALI, M., VENKATESAN, N. & ELSHAIKH, A. O. 2021. The Impact of

Rheumatoid Arthritis on Bone Loss: Links to Osteoporosis and Osteopenia. *Cureus,* 13**,** e17519.
KARSDAL, M. A., CHRISTIANSEN, C., LADEL, C., HENRIKSEN, K., KRAUS, V. B. & BAY-JENSEN, A. C. 2014. Osteoarthritis--a case for personalized health care? *Osteoarthritis Cartilage,* 22**,** 7-16.
KASHIWAKURA, Y., OHMORI, T., MIMURO, J., YASUMOTO, A., ISHIWATA, A., SAKATA, A., MADOIWA, S., INOUE, M., HASEGAWA, M., OZAWA, K. & SAKATA, Y. 2012. Intra-articular injection of mesenchymal stem cells expressing coagulation factor ameliorates hemophilic arthropathy in factor VIII-deficient mice. *J Thromb Haemost,* 10**,** 1802-13.
KATSIKIS, P. D., CHU, C. Q., BRENNAN, F. M., MAINI, R. N. & FELDMANN, M. 1994. Immunoregulatory role of interleukin 10 in rheumatoid arthritis. *J Exp Med,* 179**,** 1517-27.
KELSEN, S. G., AGACHE, I. O., SOONG, W., ISRAEL, E., CHUPP, G. L., CHEUNG, D. S., THEESS, W., YANG, X., STATON, T. L., CHOY, D. F., FONG, A., DASH, A., DOLTON, M., PAPPU, R. & BRIGHTLING, C. E. 2021. Astegolimab (anti-ST2) efficacy and safety in adults with severe asthma: A randomized clinical trial. *J Allergy Clin Immunol,* 148**,** 790-798.
KEMPTON, C. L., MAKRIS, M. & HOLME, P. A. 2021. Management of comorbidities in haemophilia. *Haemophilia,* 27 Suppl 3**,** 37-45.
KHACHIGIAN, L. M. 2006. Collagen antibody-induced arthritis. *Nat Protoc,* 1**,** 2512-6.
KIIALAINEN, A., NIGGLI, M., KEMPTON, C. L., CASTAMAN, G., CHANG, T., PAZ-PRIEL, I., ADAMKEWICZ, J. I. & LEVY, G. G. 2022. Effect of emicizumab prophylaxis on bone and joint health markers in people with haemophilia A without factor VIII inhibitors in the HAVEN 3 study. *Haemophilia,* 28**,** 1033-1043.
KITCHENS, C. S. 2005. To bleed or not to bleed? Is that the question for the PTT? *J Thromb Haemost,* 3**,** 2607-11.
KNOBE, K. & BERNTORP, E. 2011. Haemophilia and joint disease: pathophysiology, evaluation, and management. *J Comorb,* 1**,** 51-59.
KONKLE, B. A. & NAKAYA FLETCHER, S. 1993. Hemophilia A. *In:* ADAM, M. P., MIRZAA, G. M., PAGON, R. A., WALLACE, S. E., BEAN, L. J. H., GRIPP, K. W. & AMEMIYA, A. (eds.) *GeneReviews((R)).* Seattle (WA).
KOTANI, N., DOLTON, M., SVENSSON, R. J., RIBBING, J., FRIBERG, L. E., VADHAVKAR, S., CHEUNG, D., STATON, T., SPERINDE, G., JIN, J., PUTNAM, W. S. & QUARTINO, A. 2022. Population Pharmacokinetics and Exposure-Response Relationships of Astegolimab in Patients With Severe Asthma. *J Clin Pharmacol,* 62**,** 905-917.
KOTELA, A., WOJDASIEWICZ, P., LEGOSZ, P., SARZYNSKA, S., DRELA, K., PULIK, L., KALETA, B., KNIOTEK, M., BORYSOWSKI, J., PONIATOWSKI, L. A. & KOTELA, I. 2019. Increased serum levels of progranulin (PGRN) in patients with haemophilic arthropathy. *Clin Exp Pharmacol Physiol,* 46**,** 373-379.
LAFEBER, F. P., MIOSSEC, P. & VALENTINO, L. A. 2008. Physiopathology of haemophilic arthropathy. *Haemophilia,* 14 Suppl 4**,** 3-9.
LEE, D. M. & WEINBLATT, M. E. 2001. Rheumatoid arthritis. *Lancet,* 358**,** 903-11.
LEE, M., LEE, Y., SONG, J., LEE, J. & CHANG, S. Y. 2018. Tissue-specific Role of CX3CR1 Expressing Immune Cells and Their Relationships with Human Disease. *Immune Netw,* 18**,** e5.
LEMOINE, A., CHAUVEAU-LE FRIEC, G., LANGA, F. & LOUVET, C. 2016. Generation of a Double KO Mouse by Simultaneous Targeting of the

Neighboring Genes Tmem176a and Tmem176b Using CRISPR/Cas9: Key Steps from Design to Genotyping. *J Genet Genomics,* 43**,** 329-40.
LIEW, F. Y., GIRARD, J. P. & TURNQUIST, H. R. 2016. Interleukin-33 in health and disease. *Nat Rev Immunol,* 16**,** 676-689.
LIMA, I. L., MACARI, S., MADEIRA, M. F., RODRIGUES, L. F., COLAVITE, P. M., GARLET, G. P., SORIANI, F. M., TEIXEIRA, M. M., FUKADA, S. Y. & SILVA, T. A. 2015. Osteoprotective Effects of IL-33/ST2 Link to Osteoclast Apoptosis. *Am J Pathol,* 185**,** 3338-48.
LITWIC, A., EDWARDS, M. H., DENNISON, E. M. & COOPER, C. 2013. Epidemiology and burden of osteoarthritis. *Br Med Bull,* 105**,** 185-99.
LOEF, M., KROON, F. P. B., BERGSTRA, S. A., VAN DER POL, J. A., LEMS, W. F., KERSTENS, P., ALLAART, C. F. & KLOPPENBURG, M. 2018. TNF inhibitor treatment is associated with a lower risk of hand osteoarthritis progression in rheumatoid arthritis patients after 10 years. *Rheumatology (Oxford),* 57**,** 1917-1924.
LOESER, R. F., GOLDRING, S. R., SCANZELLO, C. R. & GOLDRING, M. B. 2012. Osteoarthritis: a disease of the joint as an organ. *Arthritis Rheum,* 64**,** 1697-707.
LUO, P., WANG, P., XU, J., HOU, W., XU, P., XU, K. & LIU, L. 2022. Immunomodulatory role of T helper cells in rheumatoid arthritis : a comprehensive research review. *Bone Joint Res,* 11**,** 426-438.
MANNUCCI, P. M. & TUDDENHAM, E. G. 2001. The hemophilias--from royal genes to gene therapy. *N Engl J Med,* 344**,** 1773-9.
MANON-JENSEN, T., KARSDAL, M. A., NIELSEN, L. N., KJELGAARD-HANSEN, M., VANDAHL, B., OLSEN, E. H., ENOKSSON, M. & ROEPSTORFF, K. 2016. Altered collagen turnover in factor VIII-deficient rats with hemophilic arthropathy identifies potential novel serological biomarkers in hemophilia. *J Thromb Haemost,* 14**,** 2419-2429.
MATARAZZO, L., HERNANDEZ SANTANA, Y. E., WALSH, P. T. & FALLON, P. G. 2022. The IL-1 cytokine family as custodians of barrier immunity. *Cytokine,* 154**,** 155890.
MCINNES, I. B. & SCHETT, G. 2011. The pathogenesis of rheumatoid arthritis. *N Engl J Med,* 365**,** 2205-19.
MEJIA-CARVAJAL, C., HAKOBYAN, N., ENOCKSON, C. & VALENTINO, L. A. 2008. The impact of joint bleeding and synovitis on physical ability and joint function in a murine model of haemophilic synovitis. *Haemophilia,* 14**,** 119-26.
MELCHIORRE, D., MANETTI, M. & MATUCCI-CERINIC, M. 2017. Pathophysiology of Hemophilic Arthropathy. *J Clin Med,* 6.
MESTAS, J. & HUGHES, C. C. 2004. Of mice and not men: differences between mouse and human immunology. *J Immunol,* 172**,** 2731-8.
MILLAR, N. L., O'DONNELL, C., MCINNES, I. B. & BRINT, E. 2017. Wounds that heal and wounds that don't - The role of the IL-33/ST2 pathway in tissue repair and tumorigenesis. *Semin Cell Dev Biol,* 61**,** 41-50.
MILLS, C. D., KINCAID, K., ALT, J. M., HEILMAN, M. J. & HILL, A. M. 2000. M-1/M-2 macrophages and the Th1/Th2 paradigm. *J Immunol,* 164**,** 6166-73.
MISHARIN, A. V., MORALES-NEBREDA, L., MUTLU, G. M., BUDINGER, G. R. & PERLMAN, H. 2013. Flow cytometric analysis of macrophages and dendritic cell subsets in the mouse lung. *Am J Respir Cell Mol Biol,* 49**,** 503-10.
MOHRS, M., SHINKAI, K., MOHRS, K. & LOCKSLEY, R. M. 2001. Analysis of type 2 immunity in vivo with a bicistronic IL-4 reporter. *Immunity,* 15**,** 303-11.

MONTICELLI, L. A., OSBORNE, L. C., NOTI, M., TRAN, S. V., ZAISS, D. M. & ARTIS, D. 2015. IL-33 promotes an innate immune pathway of intestinal tissue protection dependent on amphiregulin-EGFR interactions. *Proc Natl Acad Sci U S A,* 112**,** 10762-7.

MORADI, B., JACKSON, M. T., SHU, C. C., SMITH, S. M., SMITH, M. M., ZAKI, S., PLATZER, H., ROSSHIRT, N., GIANGRECO, D., SCANZELLO, C. R. & LITTLE, C. B. 2019. The role of synovial T-cell infiltration following knee joint injury in symptoms and progression to osteoarthritis. *medRxiv,* 19013227.

MORROW, T. 2018. Hemlibra's Remarkable Efficacy A Beacon For Hemophilia Patients. *Manag Care,* 27**,** 30-32.

MUIRDEN, K. D. & SENATOR, G. B. 1968. Iron in the synovial membrane in rheumatoid arthritis and other joint diseases. *Ann Rheum Dis,* 27**,** 38-48.

MULDER, K. & LLINAS, A. 2004. The target joint. *Haemophilia,* 10 Suppl 4**,** 152-6.

MYERS, L. K., ROSLONIEC, E. F., CREMER, M. A. & KANG, A. H. 1997. Collagen-induced arthritis, an animal model of autoimmunity. *Life Sci,* 61**,** 1861-78.

NACCA, C. R., HARRIS, A. P. & TUTTLE, J. R. 2017. Hemophilic Arthropathy. *Orthopedics,* 40**,** e940-e946.

NAKAGOME, K. & NAGATA, M. 2018. Involvement and Possible Role of Eosinophils in Asthma Exacerbation. *Front Immunol,* 9**,** 2220.

NG, W. H., CHU, W. C., SHING, M. K., LAM, W. W., CHIK, K. W., LI, C. K., LI, C. K. & LING, S. C. 2005. Role of imaging in management of hemophilic patients. *AJR Am J Roentgenol,* 184**,** 1619-23.

NGUYEN, J. K., AUSTIN, E., HUANG, A., MAMALIS, A. & JAGDEO, J. 2020. The IL-4/IL-13 axis in skin fibrosis and scarring: mechanistic concepts and therapeutic targets. *Arch Dermatol Res,* 312**,** 81-92.

NIEUWENHUIZEN, L., SCHUTGENS, R. E., COELEVELD, K., MASTBERGEN, S. C., ROOSENDAAL, G., BIESMA, D. H. & LAFEBER, F. P. 2014. Hemarthrosis in hemophilic mice results in alterations in M1-M2 monocyte/macrophage polarization. *Thromb Res,* 133**,** 390-5.

NIEUWENHUIZEN, L., SCHUTGENS, R. E., VAN ASBECK, B. S., WENTING, M. J., VAN VEGHEL, K., ROOSENDAAL, G., BIESMA, D. H. & LAFEBER, F. P. 2013. Identification and expression of iron regulators in human synovium: evidence for upregulation in haemophilic arthropathy compared to rheumatoid arthritis, osteoarthritis, and healthy controls. *Haemophilia,* 19**,** e218-27.

O'NEIL, L. J., OLIVEIRA, C. B., WANG, X., NAVARRETE, M., BARRERA-VARGAS, A., MERAYO-CHALICO, J., ALJAHDALI, R., AGUIRRE-AGUILAR, E., CARLUCCI, P., KAPLAN, M. J. & CARMONA-RIVERA, C. 2023. Neutrophil extracellular trap-associated carbamylation and histones trigger osteoclast formation in rheumatoid arthritis. *Ann Rheum Dis,* 82**,** 630-638.

OVLISEN, K., KRISTENSEN, A. T., VALENTINO, L. A., HAKOBYAN, N., INGERSLEV, J. & TRANHOLM, M. 2008. Hemostatic effect of recombinant factor VIIa, NN1731 and recombinant factor VIII on needle-induced joint bleeding in hemophilia A mice. *J Thromb Haemost,* 6**,** 969-75.

PEREZ-PUJOL, S., ARAS, O. & ESCOLAR, G. 2012. Factor v leiden and inflammation. *Thrombosis,* 2012**,** 594986.

PETTIT, A. R., JI, H., VON STECHOW, D., MULLER, R., GOLDRING, S. R., CHOI, Y., BENOIST, C. & GRAVALLESE, E. M. 2001. TRANCE/RANKL knockout mice are protected from bone erosion in a serum transfer model of arthritis. *Am J Pathol,* 159**,** 1689-99.

PULLES, A. E., MASTBERGEN, S. C., SCHUTGENS, R. E., LAFEBER, F. P. & VAN VULPEN, L. F. 2017. Pathophysiology of hemophilic arthropathy and potential targets for therapy. *Pharmacol Res,* 115**,** 192-199.

QUADE-LYSSY, P., ABRISS, D., MILANOV, P., UNGERER, C., KONIGS, C., SEIFRIED, E. & SCHUTTRUMPF, J. 2014. Next generation FIX muteins with FVIII-independent activity for alternative treatment of hemophilia A. *J Thromb Haemost,* 12**,** 1861-73.

RAFFINI, L. & MANNO, C. 2007. Modern management of haemophilic arthropathy. *Br J Haematol,* 136**,** 777-87.

REHILL, A. M., MCCLUSKEY, S., O'DONNELL, J. S., DOCKAL, M., PRESTON, R. J. S. & I, P. S. G. 2021. Heterogeneity in Bleeding Tendency and Arthropathy Development in Individuals with Hemophilia. *Semin Thromb Hemost,* 47**,** 183-191.

RODRIGUEZ-MERCHAN, E. C. 1997. Pathogenesis, early diagnosis, and prophylaxis for chronic hemophilic synovitis. *Clin Orthop Relat Res***,** 6-11.

RODRIGUEZ-MERCHAN, E. C. 2012. Prevention of the musculoskeletal complications of hemophilia. *Adv Prev Med,* 2012**,** 201271.

ROOSENDAAL, G. & LAFEBER, F. P. 2003. Blood-induced joint damage in hemophilia. *Semin Thromb Hemost,* 29**,** 37-42.

ROOSENDAAL, G. & LAFEBER, F. P. 2006. Pathogenesis of haemophilic arthropathy. *Haemophilia,* 12 Suppl 3**,** 117-21.

ROOSENDAAL, G., MAUSER-BUNSCHOTEN, E. P., DE KLEIJN, P., HEIJNEN, L., VAN DEN BERG, H. M., VAN RINSUM, A. C., LAFEBER, F. P. & BIJLSMA, J. W. 1998a. Synovium in haemophilic arthropathy. *Haemophilia,* 4**,** 502-5.

ROOSENDAAL, G., VAN RINSUM, A. C., VIANEN, M. E., VAN DEN BERG, H. M., LAFEBER, F. P. & BIJLSMA, J. W. 1999a. Haemophilic arthropathy resembles degenerative rather than inflammatory joint disease. *Histopathology,* 34**,** 144-53.

ROOSENDAAL, G., VIANEN, M. E., MARX, J. J., VAN DEN BERG, H. M., LAFEBER, F. P. & BIJLSMA, J. W. 1999b. Blood-induced joint damage: a human in vitro study. *Arthritis Rheum,* 42**,** 1025-32.

ROOSENDAAL, G., VIANEN, M. E., WENTING, M. J., VAN RINSUM, A. C., VAN DEN BERG, H. M., LAFEBER, F. P. & BIJLSMA, J. W. 1998b. Iron deposits and catabolic properties of synovial tissue from patients with haemophilia. *J Bone Joint Surg Br,* 80**,** 540-5.

ROSALES, C. 2018. Neutrophil: A Cell with Many Roles in Inflammation or Several Cell Types? *Front Physiol,* 9**,** 113.

ROSALES, C. 2020. Neutrophils at the crossroads of innate and adaptive immunity. *J Leukoc Biol,* 108**,** 377-396.

SAUNDERS, S. P., MORAN, T., FLOUDAS, A., WURLOD, F., KASZLIKOWSKA, A., SALIMI, M., QUINN, E. M., OLIPHANT, C. J., NUNEZ, G., MCMANUS, R., HAMS, E., IRVINE, A. D., MCKENZIE, A. N., OGG, G. S. & FALLON, P. G. 2016. Spontaneous atopic dermatitis is mediated by innate immunity, with the secondary lung inflammation of the atopic march requiring adaptive immunity. *J Allergy Clin Immunol,* 137**,** 482-91.

SCHEP, S. J., SCHUTGENS, R. E. G., FISCHER, K. & BOES, M. L. 2018. Review of immune tolerance induction in hemophilia A. *Blood Rev,* 32**,** 326-338.

SCHMITZ, J., OWYANG, A., OLDHAM, E., SONG, Y., MURPHY, E., MCCLANAHAN, T. K., ZURAWSKI, G., MOSHREFI, M., QIN, J., LI, X., GORMAN, D. M., BAZAN, J. F. & KASTELEIN, R. A. 2005. IL-33, an interleukin-1-like cytokine

that signals via the IL-1 receptor-related protein ST2 and induces T helper type 2-associated cytokines. *Immunity,* 23**,** 479-90.
SCHWARTZ, C., O'GRADY, K., LAVELLE, E. C. & FALLON, P. G. 2016. Interleukin 33: an innate alarm for adaptive responses beyond Th2 immunity-emerging roles in obesity, intestinal inflammation, and cancer. *Eur J Immunol,* 46**,** 1091-100.
SCOTT, D. L., WOLFE, F. & HUIZINGA, T. W. 2010. Rheumatoid arthritis. *Lancet,* 376**,** 1094-108.
SCULCO, T. P. 1998. The knee joint in rheumatoid arthritis. *Rheum Dis Clin North Am,* 24**,** 143-56.
SEIDMAN, A. J. & LIMAIEM, F. 2023. Synovial Fluid Analysis. *StatPearls.* Treasure Island (FL).
SELLERS, R. S., CLIFFORD, C. B., TREUTING, P. M. & BRAYTON, C. 2012. Immunological variation between inbred laboratory mouse strains: points to consider in phenotyping genetically immunomodified mice. *Vet Pathol,* 49**,** 32-43.
SHARMA, L. 2021. Osteoarthritis of the Knee. *N Engl J Med,* 384**,** 51-59.
SHI, L. J., LIU, C., LI, J. H., ZHU, X. Y., LI, Y. N. & LI, J. T. 2018. Elevated Levels of Soluble ST2 were Associated with Rheumatoid Arthritis Disease Activity and Ameliorated Inflammation in Synovial Fibroblasts. *Chin Med J (Engl),* 131**,** 316-322.
SHIM, J. H., STAVRE, Z. & GRAVALLESE, E. M. 2018. Bone Loss in Rheumatoid Arthritis: Basic Mechanisms and Clinical Implications. *Calcif Tissue Int,* 102**,** 533-546.
SINDRILARU, A., PETERS, T., WIESCHALKA, S., BAICAN, C., BAICAN, A., PETER, H., HAINZL, A., SCHATZ, S., QI, Y., SCHLECHT, A., WEISS, J. M., WLASCHEK, M., SUNDERKOTTER, C. & SCHARFFETTER-KOCHANEK, K. 2011. An unrestrained proinflammatory M1 macrophage population induced by iron impairs wound healing in humans and mice. *J Clin Invest,* 121**,** 985-97.
SINGH, J. A., INACIO, M. C., NAMBA, R. S. & PAXTON, E. W. 2015. Rheumatoid arthritis is associated with higher ninety-day hospital readmission rates compared to osteoarthritis after hip or knee arthroplasty: a cohort study. *Arthritis Care Res (Hoboken),* 67**,** 718-24.
SINGH, J. A., SAAG, K. G., BRIDGES, S. L., JR., AKL, E. A., BANNURU, R. R., SULLIVAN, M. C., VAYSBROT, E., MCNAUGHTON, C., OSANI, M., SHMERLING, R. H., CURTIS, J. R., FURST, D. E., PARKS, D., KAVANAUGH, A., O'DELL, J., KING, C., LEONG, A., MATTESON, E. L., SCHOUSBOE, J. T., DREVLOW, B., GINSBERG, S., GROBER, J., ST CLAIR, E. W., TINDALL, E., MILLER, A. S. & MCALINDON, T. 2016. 2015 American College of Rheumatology Guideline for the Treatment of Rheumatoid Arthritis. *Arthritis Rheumatol,* 68**,** 1-26.
SINUSAS, K. 2012. Osteoarthritis: diagnosis and treatment. *Am Fam Physician,* 85**,** 49-56.
SMITH, S. A., TRAVERS, R. J. & MORRISSEY, J. H. 2015. How it all starts: Initiation of the clotting cascade. *Crit Rev Biochem Mol Biol,* 50**,** 326-36.
SONG, J., CHEN, D., PAN, Y., SHI, X., LIU, Q., LU, X., XU, X., CHEN, G. & CAI, Y. 2021. Discovery of a Novel MyD88 Inhibitor M20 and Its Protection Against Sepsis-Mediated Acute Lung Injury. *Front Pharmacol,* 12**,** 775117.

SUMMERS, C., RANKIN, S. M., CONDLIFFE, A. M., SINGH, N., PETERS, A. M. & CHILVERS, E. R. 2010. Neutrophil kinetics in health and disease. *Trends Immunol,* 31**,** 318-24.

TANAKA, S. & BABA, Y. 2020. B Cell Receptor Signaling. *Adv Exp Med Biol,* 1254**,** 23-36.

TIEDE, A., ABDUL KARIM, F., JIMENEZ-YUSTE, V., KLAMROTH, R., LEJNIECE, S., SUZUKI, T., GROTH, A. & SANTAGOSTINO, E. 2021. Factor VIII activity and bleeding risk during prophylaxis for severe hemophilia A: a population pharmacokinetic model. *Haematologica,* 106**,** 1902-1909.

TOMINAGA, S. 1989. A putative protein of a growth specific cDNA from BALB/c-3T3 cells is highly similar to the extracellular portion of mouse interleukin 1 receptor. *FEBS Lett,* 258**,** 301-4.

TORANG, A., GUPTA, P. & KLINKE, D. J., 2ND 2019. An elastic-net logistic regression approach to generate classifiers and gene signatures for types of immune cells and T helper cell subsets. *BMC Bioinformatics,* 20**,** 433.

TRAN, C. N., LUNDY, S. K. & FOX, D. A. 2005. Synovial biology and T cells in rheumatoid arthritis. *Pathophysiology,* 12**,** 183-9.

VAIENTI, E., SCITA, G., CECCARELLI, F. & POGLIACOMI, F. 2017. Understanding the human knee and its relationship to total knee replacement. *Acta Biomed,* 88**,** 6-16.

VALENTINO, L. A. 2010. Blood-induced joint disease: the pathophysiology of hemophilic arthropathy. *J Thromb Haemost,* 8**,** 1895-902.

VALENTINO, L. A., HAKOBYAN, N., ENOCKSON, C., SIMPSON, M. L., KAKODKAR, N. C., CONG, L. & SONG, X. 2012. Exploring the biological basis of haemophilic joint disease: experimental studies. *Haemophilia,* 18**,** 310-8.

VALENTINO, L. A., HAKOBYAN, N., KAZARIAN, T., JABBAR, K. J. & JABBAR, A. A. 2004. Experimental haemophilic synovitis: rationale and development of a murine model of human factor VIII deficiency. *Haemophilia,* 10**,** 280-7.

VALENTINO, L. A., HAKOBYAN, N., RODRIGUEZ, N. & HOOTS, W. K. 2007. Pathogenesis of haemophilic synovitis: experimental studies on blood-induced joint damage. *Haemophilia,* 13 Suppl 3**,** 10-3.

VAN LANDUYT, K. B., JONES, E. A., MCGONAGLE, D., LUYTEN, F. P. & LORIES, R. J. 2010. Flow cytometric characterization of freshly isolated and culture expanded human synovial cell populations in patients with chronic arthritis. *Arthritis Res Ther,* 12**,** R15.

VAN MEEGEREN, M. E., ROOSENDAAL, G., JANSEN, N. W., WENTING, M. J., VAN WESEL, A. C., VAN ROON, J. A. & LAFEBER, F. P. 2012. IL-4 alone and in combination with IL-10 protects against blood-induced cartilage damage. *Osteoarthritis Cartilage,* 20**,** 764-72.

VAN VULPEN, L. F., SCHUTGENS, R. E., COELEVELD, K., ALSEMA, E. C., ROOSENDAAL, G., MASTBERGEN, S. C. & LAFEBER, F. P. 2015. IL-1beta, in contrast to TNFalpha, is pivotal in blood-induced cartilage damage and is a potential target for therapy. *Blood,* 126**,** 2239-46.

VEALE, D. J. & FIRESTEIN, G. S. 2017. Chapter 2 - Synovium. *In:* FIRESTEIN, G. S., BUDD, R. C., GABRIEL, S. E., MCINNES, I. B. & O'DELL, J. R. (eds.) *Kelley and Firestein's Textbook of Rheumatology (Tenth Edition).* Elsevier.

VINCENT, T. L. 2019. IL-1 in osteoarthritis: time for a critical review of the literature. *F1000Res,* 8.

VOLS, K. K., KJELGAARD-HANSEN, M., LEY, C. D., HANSEN, A. K. & PETERSEN, M. 2019. Bleed volume of experimental knee haemarthrosis correlates with the subsequent degree of haemophilic arthropathy. *Haemophilia,* 25**,** 324-333.

VOLS, K. K., KJELGAARD-HANSEN, M., LEY, C. D., HANSEN, A. K. & PETERSEN, M. 2020. In vivo fluorescence molecular tomography of induced haemarthrosis in haemophilic mice: link between bleeding characteristics and development of bone pathology. *BMC Musculoskelet Disord,* 21**,** 241.

WASSERMAN, A. M. 2011. Diagnosis and management of rheumatoid arthritis. *Am Fam Physician,* 84**,** 1245-52.

WEAVER, C. M. 2002. Adolescence: the period of dramatic bone growth. *Endocrine,* 17**,** 43-8.

WECHSLER, M. E., MUNITZ, A., ACKERMAN, S. J., DRAKE, M. G., JACKSON, D. J., WARDLAW, A. J., DOUGAN, S. K., BERDNIKOVS, S., SCHLEICH, F., MATUCCI, A., CHANEZ, P., PRAZMA, C. M., HOWARTH, P., WELLER, P. F. & MERKEL, P. A. 2021. Eosinophils in Health and Disease: A State-of-the-Art Review. *Mayo Clin Proc,* 96**,** 2694-2707.

WEITZMANN, M. N., ROSER-PAGE, S., VIKULINA, T., WEISS, D., HAO, L., BALDWIN, W. H., YU, K., DEL MAZO ARBONA, N., MCGEE-LAWRENCE, M. E., MEEKS, S. L. & KEMPTON, C. L. 2019. Reduced bone formation in males and increased bone resorption in females drive bone loss in hemophilia A mice. *Blood Adv,* 3**,** 288-300.

WENG, S. Y., WANG, X., VIJAYAN, S., TANG, Y., KIM, Y. O., PADBERG, K., REGEN, T., MOLOKANOVA, O., CHEN, T., BOPP, T., SCHILD, H., BROMBACHER, F., CROSBY, J. R., MCCALEB, M. L., WAISMAN, A., BOCKAMP, E. & SCHUPPAN, D. 2018. IL-4 Receptor Alpha Signaling through Macrophages Differentially Regulates Liver Fibrosis Progression and Reversal. *EBioMedicine,* 29**,** 92-103.

WOJDASIEWICZ, P., PONIATOWSKI, L. A., NAUMAN, P., MANDAT, T., PARADOWSKA-GORYCKA, A., ROMANOWSKA-PROCHNICKA, K., SZUKIEWICZ, D., KOTELA, A., KUBASZEWSKI, L., KOTELA, I., KURKOWSKA-JASTRZEBSKA, I. & GASIK, R. 2018. Cytokines in the pathogenesis of hemophilic arthropathy. *Cytokine Growth Factor Rev,* 39**,** 71-91.

WYNN, T. A., CHAWLA, A. & POLLARD, J. W. 2013. Macrophage biology in development, homeostasis and disease. *Nature,* 496**,** 445-55.

WYSEURE, T., COOKE, E. J., DECLERCK, P. J., BEHRENDT, N., MEIJERS, J. C. M., VON DRYGALSKI, A. & MOSNIER, L. O. 2018. Defective TAFI activation in hemophilia A mice is a major contributor to joint bleeding. *Blood,* 132**,** 1593-1603.

WYSEURE, T., YANG, T., ZHOU, J. Y., COOKE, E. J., WANKO, B., OLMER, M., AGASHE, R., MORODOMI, Y., BEHRENDT, N., LOTZ, M., MORSER, J., VON DRYGALSKI, A. & MOSNIER, L. O. 2019. TAFI deficiency causes maladaptive vascular remodeling after hemophilic joint bleeding. *JCI Insight,* 4.

XIONG, J., CAWLEY, K., PIEMONTESE, M., FUJIWARA, Y., ZHAO, H., GOELLNER, J. J. & O'BRIEN, C. A. 2018. Soluble RANKL contributes to osteoclast formation in adult mice but not ovariectomy-induced bone loss. *Nat Commun,* 9**,** 2909.

XU, D., JIANG, H. R., LI, Y., PUSHPARAJ, P. N., KUROWSKA-STOLARSKA, M., LEUNG, B. P., MU, R., TAY, H. K., MCKENZIE, A. N., MCINNES, I. B., MELENDEZ, A. J. & LIEW, F. Y. 2010a. IL-33 exacerbates autoantibody-induced arthritis. *J Immunol,* 184**,** 2620-6.

XU, J., GUARDADO, J., HOFFMAN, R., XU, H., NAMAS, R., VODOVOTZ, Y., XU, L., RAMADAN, M., BROWN, J., TURNQUIST, H. R. & BILLIAR, T. R. 2017. IL33-mediated ILC2 activation and neutrophil IL5 production in the lung response after severe trauma: A reverse translation study from a human cohort to a mouse trauma model. *PLoS Med,* 14**,** e1002365.

XU, L., KITANI, A., STUELTEN, C., MCGRADY, G., FUSS, I. & STROBER, W. 2010b. Positive and negative transcriptional regulation of the Foxp3 gene is mediated by access and binding of the Smad3 protein to enhancer I. *Immunity,* 33**,** 313-25.

YAMAKI, K., UCHIDA, H., LI, X., YANAGISAWA, R., TAKANO, H., HAYASHI, H., MORI, Y. & YOSHINO, S. 2005. Effect of varying types of anti-arthritic drugs on Th1 and Th2 immune responses in mice. *Int J Immunopathol Pharmacol,* 18**,** 133-44.

YOUSUF, A. J., MOHAMMED, S., CARR, L., YAVARI RAMSHEH, M., MICIELI, C., MISTRY, V., HALDAR, K., WRIGHT, A., NOVOTNY, P., PARKER, S., GLOVER, S., FINCH, J., QUANN, N., BROOKES, C. L., HOBSON, R., IBRAHIM, W., RUSSELL, R. J., JOHN, C., GRIMBALDESTON, M. A., CHOY, D. F., CHEUNG, D., STEINER, M., GREENING, N. J. & BRIGHTLING, C. E. 2022. Astegolimab, an anti-ST2, in chronic obstructive pulmonary disease (COPD-ST2OP): a phase 2a, placebo-controlled trial. *Lancet Respir Med,* 10**,** 469-477.

ZHANG, L., YUAN, Y., XU, Q., JIANG, Z. & CHU, C. Q. 2019. Contribution of neutrophils in the pathogenesis of rheumatoid arthritis. *J Biomed Res,* 34**,** 86-93.

ZHANG, S., LU, C., YING, J., WANG, P., XU, T., CHEN, D., JIN, H. & TONG, P. 2015. Inflammatory focal bone destruction in femoral heads with end-stage haemophilic arthropathy: a study on clinic samples with micro-CT and histological analyses. *Haemophilia,* 21**,** e472-8.

ZHONG, C., SZOLLOSI, D., SUN, J., HUA, B., GHONEIM, O., BILL, A., ZHUANG, Y. & EDAFIOGHO, I. 2019. Novel Piperazino-Enaminones Decrease Pro-inflammatory Cytokines Following Hemarthrosis in a Hemophilia Mouse Model. *Inflammation,* 42**,** 1719-1729.